Interferometry with atomic- and molecular matter waves

Håkon Bjørgen

Thesis submitted for the degree of Master of Science

Department of Physics
University of Oslo

May 2010

Abstract

The thesis is twofold. The first part is an introduction to atom interferometers based on light-atom interactions. The mechanical effect on atoms, induced by light is discussed. Certain combinations of light pulses can make atoms interfere. Two atom interferometer designs are explained in some detail. Finally, applications are discussed.

The second part concerns one of the applications of atomic interferometry: the index of refraction of gases for matter waves. This is an optical property which microscopic effect is the collision between the atoms of the waves and the atoms of the gas. Three different systems have been investigated, including atomic- and molecular waves. Calculations are based on the interparticle potentials along with an averaging effect due to the thermal motion of the gas. All the systems are characterized by a low temperature.

Takk til

En stor takk rettes til den norske stat som gjennom sine finansielle ordninger tilrettelegger for utdanning. Takk til Marius Lysebo hvis hjelp har vært til stor nytte de siste to årene. En stor takk går også til min veileder Leif Veseth, som har akseptert meg som sin student og introdusert meg for dette emnet.

Håkon Bjørgen
Oslo, mai 2010

Contents

Part I

Atom interferometry

Outline

Interferometers make use of the interference pattern caused by two or more interacting waves to extract information. In atom interferometers matter-waves are being manipulated. This new field of research stem from de Broglie who postulated that matter can exhibit wavelike behaviour in certain situations. The atom interferometer is a physical device subject to physical limitations, and because the de Broglie wavelengths are of the order 10^{-12}m for thermal- and 10^{-6}m for ultracold atoms, advanced technology is needed.

It is not until recently that atom interferometers have been realized in laboratories. The first experiment in 1991 [36] used nanostructures as diffraction gratings. Later, light has been employed to spatially manipulate atoms and molecules. This is largely due to laser technology which opens up for new ways to manipulate atoms and molecules.

This first part gives an introduction to atom interferometry. The chapters contain the following:

- Chapter 1: The basic ideas are presented. The terms used to describe the atom interferometer are explained. Matter waves are discussed briefly and some numbers are presented to display the length scales involved.

- Chapter 2: Certain mechanical effects on atoms can be induced by light-atom interactions. The atom interferometers discussed here applies light in order to spatially manipulate the atoms. This chapter explains how light-atom interactions can induce processes similar to mirrors and beam splitters from classical optics.

- Chapter 3: Combinations of light-atom interactions can make atom interferometers. This chapter presents atom interferometers in a general way. Two specific interferometer designs are discussed in detail. This chapter also explains how to access the information from an atom interferometer experiment.

- Chapter 4 : This chapter presents some applications. Some information is only accessible through an atom interferometer experiment. An atom interferometer also proves to be a very precise instrument, with possible applications to fundamental physics.

Chapter 1

Introduction

Atom interferometers make use of the wave particle duality of matter. This is a quantum mechanical effect and the interfering objects are particles with mass.

Matter waves are briefly discussed and relations to other fundamental physical quantities like momentum and temperature is introduced.

1.1 Interferometry

To describe an interferometer, words like coherence and phase is used. In Webster's new world dictionary the word coherent is explained as follows: *To cohere is 1: to stick together or 2: to be connected naturally or logically.* Coherent is an adjective and coherence is the property of being coherent. Coherence is a collective property and describes a relationship. This relationship can be quantified with a so called phase. The word phase is a noun and a physical property. If two objects have a constant relative phase, the two objects are said to be coherent.

Phenomena in nature do not always have a well defined behaviour, one example is the wave particle duality. This behaviour is provided for in the formalism of quantum mechanics. An abstract state contains all possible information about a system. For a two-level quantum mechanical system the most general state can be represented as a *coherent* superposition of the basis states

$$|\psi\rangle = c_1 |1\rangle + c_2 |2\rangle . \tag{1.1}$$

The coefficients $c_{1,2}$ are the amplitudes which connected to a measurement would result in the outcomes $\{|1\rangle, |2\rangle\}$ with probabilities $|c_1|^2$ and $|c_2|^2$. A classical analogy is[1] an ensemble of N_0 two-level systems where N_1 are occupying state $|1\rangle$ and N_2 are occupying state $|2\rangle$. Selecting a single system at random the probabilities would be $|c_1|^2 = N_1/N_0$ and $|c_2|^2 = N_2/N_0$. This is not so different from quantum mechanics, but the word coherent makes no sense in this classical connection. The quantum mechanical state $|\psi\rangle$ in equation (1.1) is coherent in the sense that a single system, prior to a measurement, is in *both* states.

The classical ensemble above excludes any interference effect. Coherence is a collective property and interference may occur even for a single atom. Consider

[1] This argument is taken from Fox [21].

an operator with eigenvector $|\varphi\rangle$ and eigenvalue φ. If the atom is represented by the state $|\psi\rangle$ as in equation (1.1), the probability that a measurement would produce φ is

$$\begin{aligned} P(\varphi) &= |\langle\varphi|\psi\rangle|^2 \\ &= |c_1\langle\varphi|1\rangle + c_2\langle\varphi|2\rangle|^2 \\ &= |c_1|^2|\langle\varphi|1\rangle|^2 + |c_2|^2|\langle\varphi|2\rangle|^2 \\ &\quad + c_1c_2^*\langle\varphi|1\rangle\langle 2|\varphi\rangle + c_1^*c_2\langle 1|\varphi\rangle\langle\varphi|2\rangle . \end{aligned} \tag{1.2}$$

The last two terms include interference and displays the connection between coherence and the *phase*. Only the relative phase of c_1 and c_2 affects the outcome. A global phase would not alter any physical properties.

Interferometry makes use of the interference between coherent waves. An incident wave is split into several coherent components, each travelling separate paths denoted arms, before being recombined. The resulting interference pattern contains information concerning the paths. The idea behind the atom interferometer is illustrated in figure 1.1. Traversing atoms are subject to light

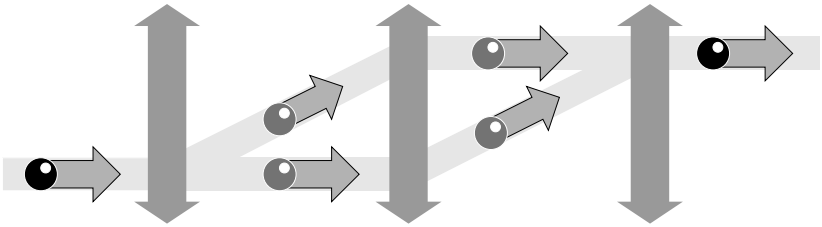

Figure 1.1: Illustration of the basic idea behind the atom interferometer. The vertical arrows indicates light interacting with the traversing atoms. The atom is in a coherent superposition as it travels the separated arms.

pulses or standing light waves whose purpose is to give an angular spread in the momentum distribution. In this case the atom is only allowed to exist in two states like in equation (1.1), each corresponding to the possible momenta. Although coherence is a collective property a single atom is in a coherent superposition as it travels the separate arms and will interfere with itself when recombined.

1.2 Matter waves

According to the state representation of physical phenomena, wavelike or particle-like behaviour may be observed, depending on the physical situation. In 1925 de Broglie postulated that the momentum p of an object and the corresponding de Broglie wavelength λ_{dB} was related via Planck's constant h

$$\lambda_{\mathrm{dB}} = \frac{h}{p}. \tag{1.3}$$

For a complex system the de Broglie wavelength is defined by the total mass and velocity of the center-of-mass. An example demonstrates the order of magnitude: The most probable speed for atoms with a Maxwell speed distribution

is $v = \sqrt{2k_BT/m}$ where T is the temperature, m is the mass and k_B is the Boltzmann constant. The de Broglie wavelength relates to the temperature as

$$\lambda_{\mathrm{dB}} \sim \frac{1}{\sqrt{mT}}. \tag{1.4}$$

Sodium atoms at room temperature $T = 300$ K has a wavelength $\lambda_{\mathrm{dB}} \sim 10^{-11}$ m. Sodium atoms cooled to 10^{-4} K has a wavelength $\lambda_{\mathrm{dB}} \sim 10^{-8}$ m. Less massive lithium atoms cooled to $\sim 10^{-6}$K (ultracold) has a wavelength $\lambda_{\mathrm{dB}} \sim 10^{-6}$ m.

Diffraction experiments illustrates the wavelike behaviour of physical objects considered particles. Electrons traversing a pair of slits behave as waves for the unobserved propagation, revealing a diffraction pattern on a detector screen positioned after the slits. Experiments using C_{60} [42] and C_{70} [9] fullerene molecules have been carried out. Using an ensemble of these molecules clearly display interference. The internal structures are complex with many rotational and vibrational modes (174 for C_{60}) in addition to excitations, therefore two molecules are unlikely to be in the same state. Interference only occur between indistinguishable states therefore the interference pattern is due solely to single particle interference.

Chapter 2

Manipulating atoms with light

Conventional mirrors and beam splitters used for light rays are not suitable for atom interferometers. Material nano gratings can be applied to construct a grating interferometer, but the gratings block a portion of the atoms and they may get clogged up. Instead light plays the role as mirror and beam splitter in a sort of reversed world compared to classical light interferometers. Atoms have internal structure which is utilised through the interaction with an external electromagnetic- or radiation field. Electric fields carry momentum which is transferred to the atoms and in this way the motion of the atom can be controlled. The electric field is treated like a classical field while the atom is treated with quantum mechanics. Three different methods to coherently manipulate atoms are discussed: Rabi oscillations, Raman transitions and Bragg diffraction.

2.1 The atoms

Atoms are complex structures composed of a nucleus and electrons. They can be described in terms of stationary states corresponding to an energy. These states depends on the internal structure of the atom and they are described by the time independent Schrödinger equation. The light is treated as a classical radiation field described by Maxwell's equations. When an atom is subject to radiation the atomic state generally change. The light transfers energy that may rearrange the internal atomic state. In addition light transfers momentum that changes the motion of the atom. The time evolution of the internal state of the atom is described by the time dependent Schrödinger equation. The radiation is treated as a time dependent perturbation and the internal state Schrödinger equation is, see Bransden [8],

$$i\hbar\frac{\partial}{\partial t}\left|\Psi\right\rangle = \left(H_0 + V(t)\right)\left|\Psi\right\rangle, \tag{2.1}$$

where H_0 is the time-independent Hamiltonian for an atom in the absence of radiation and $V(t)$ is the interaction Hamiltonian when the radiation field is present. The unperturbed Hamiltonian H_0 describes the nucleus, electrons and

their mutual interactions. The internal states of the atom are solutions $|n\rangle$ of the time-independent Schrödinger equation

$$H_0 |n\rangle = E_n |n\rangle , \tag{2.2}$$

where E_n is the energy corresponding to the state $|n\rangle$ for $n = 1, 2, \ldots$. Exact solutions or wave functions can only be obtained for hydrogen-like atoms, but there is no need to reveal the detailed form of the wave functions in this case. This is because one is only interested in transitions between different internal states and how these transitions affect the external state of the system. The external state describes the motion of the center of mass of the atom. The internal transitions are induced by the light interaction and one assumes that only a finite number of internal states are accessible.

General discrete system

The general solution of the time-dependent Schrödinger equation without any interaction, is a superposition of the energy eigenkets

$$|\Psi_0(t)\rangle = \sum_n c_n(0) e^{-iE_n t/\hbar} |n\rangle , \tag{2.3}$$

where $c_n(0)$ are constants determined by the initial conditions and the subscript zero indicates that the total Hamiltonian is only the internal Hamiltonian H_0 in equation (2.1). In the act of measurement the outcome will be one of the eigenvalues or energies E_n with probability $|c_n|^2$. The coefficients has to be normalised $\sum |c_n|^2 = 1$, which is just summing all the probabilities in the sample space.

In connection with radiation, a time-dependent perturbation $V(t)$ is applied as in equation (2.1). The general state is still a superposition of the energy eigenkets, but the coefficients c_n become time dependent. If the initial state is

$$|\Psi(t = 0)\rangle = \sum_n c_n(0) |n\rangle , \tag{2.4}$$

then the general state at later times is

$$|\Psi(t)\rangle = \sum_n c_n(t) e^{-iE_n t/\hbar} |n\rangle , \tag{2.5}$$

where the coefficient $c_n(t)$ are dependent on time. The probability amplitudes $|c_n(t)|^2$ will therefore depend on time. The time evolution factor $e^{-iE_n t/\hbar}$ is separated from the coefficient c_n. This way only the time dependence from the interaction potential is included in the coefficients. The time evolution of this state is described by the time-dependent Schrödinger equation. Inserting $|\Psi(t)\rangle$ in the Schrödinger equation (2.1) and using equation (2.2) gives

$$i\hbar \sum_n \dot{c}_n(t) e^{-iE_n t/\hbar} |n\rangle = \sum_n c_n(t) e^{-iE_n t/\hbar} V |n\rangle , \tag{2.6}$$

where the dot indicates derivation with respect to time. The inner product between the internal states becomes

$$i\hbar \sum_n \dot{c}_n(t) e^{-iE_n t/\hbar} \langle m|n\rangle = \sum_n c_n(t) \langle m| e^{-iE_n t/\hbar} V |n\rangle . \tag{2.7}$$

Using the fact that the internal states are orthonormal, one gets the following set of coupled differential equations

$$i\hbar\dot{c}_m(t) = \sum_n \langle m| V |n\rangle e^{i(E_m - E_n)t/\hbar} c_n(t). \tag{2.8}$$

The above equation can be written in terms of the Bohr angular frequency defined as

$$\omega_{mn} = \frac{E_m - E_n}{\hbar}, \tag{2.9}$$

see e.g. Bransden [8]. The time-dependent Schrödinger equation (2.1) is rewritten as a set of coupled differential equations

$$\dot{c}_m(t) = (i\hbar)^{-1} \sum_n \langle m| V |n\rangle e^{i\omega_{mn}t} c_n(t). \tag{2.10}$$

In order to obtain the dynamics of the system one needs to solve these equations. This is done in section 2.2 in order to describe Rabi oscillations.

Atomic structure

The atomic state can be a coherent superposition of different excited states, as in equation (2.5). Excited states can spontaneously emit a photon. This way the coherence is lost because the atom may reveal its position. If the atom was travelling through an atom interferometer, spontaneously emitted photons would reveal information concerning which way the atom went. This will obstruct the wave like behaviour. Actually the photons do not have to reach a detector. Information left in the surroundings is enough to break the superposition [15]. An excited state decays spontaneously at time t with probability

$$P(t) = \Gamma e^{-\Gamma t}, \tag{2.11}$$

where Γ is the spontaneous emission rate. The mean time the system stays in the excited state is

$$\langle t\rangle = \int_0^\infty tP(t)dt = \frac{1}{\Gamma} = \tau. \tag{2.12}$$

This is defined as the lifetime and is a characterisation of the instability of the state.

Due to their internal structure atoms can be prepared, so that within an approximation they contain only a finite number of allowed states due to selection rules. Using a polarized laser beam an atom can be prepared to effectively become a two-level system. This is called optical pumping, see Foot [20]. The two level system has two basis states $\{|1\rangle, |2\rangle\}$. These can be the solutions of the time independent Schrödinger equation (2.2). The rate of spontaneous emission between level $|2\rangle$ and $|1\rangle$ is quantitatively described by the Einstein A coefficient [8]

$$A_{21} = \frac{4\alpha}{3c^2} |\mathbf{D}_{12}|^2 \cdot \omega_0^3, \tag{2.13}$$

where α is the fine-structure constant and c is the speed of light. The Einstein A coefficient is related to the mean life time as $A = 1/\Gamma$. The vector $\mathbf{D}_{12}$

$$\mathbf{D}_{12} = \langle 1| \mathbf{r} |2\rangle = \int \psi_1^* \mathbf{r} \psi_2 d\mathbf{r}, \tag{2.14}$$

is an integral over the atomic wave functions. Accordingly the Einstein A coefficient is an atomic property. The lifetime of the excited level is $\tau = 1/A_{21}$. A small energy difference correspond to lower frequency and ensures longer lifetimes

$$\tau \propto \frac{1}{\omega_0^3}. \tag{2.15}$$

Typically one employs hyperfine levels for two-level realization. Consider the ground state of sodium $^2S_{1/2}$. This has two hyperfine levels with $F = 2$ and $F = 1$. The Einstein coefficient is calculated in [22] to be $A = 8.35 \cdot 10^{-15}\mathrm{s}^{-1}$, corresponding to lifetime $\sim 10^{14}$s.

The relation above assumes a two level system with only one allowed transition. In any realistic experiment the excited level may decay to other levels as well. More general the lifetime is given by

$$\tau = \frac{1}{A_1 + A_2 + A_3 + \ldots}, \tag{2.16}$$

where A_i is the transition rate to level i, Griffiths [24]. States with a long lifetime are called metastable. The lifetimes of some metastable states are given in table 2.1.

Atom	State	$\tau[s]$	Reference
Argon*	[Ne]$3p^5 4s, {}^3P_0$	≥ 30 s	[32]
Argon*	[Ne]$3p^5 4s, {}^3P_2$	≥ 30 s	[32]
Helium	2^3S_1	~ 8000 s	[2]

Table 2.1: Lifetime of some metastable states used in atom interferometers.

2.2 Rabi oscillations

Two-level atoms subject to radiation can oscillate between the different internal states. This behaviour is called Rabi oscillations. The two internal states are the energy eigenkets: $|1\rangle$ and $|2\rangle$, the solutions of equation (2.2). The general internal atomic wave function is at all times, a coherent superposition of the two internal states

$$|\Psi\rangle = c_1 |1\rangle + c_2 |2\rangle , \tag{2.17}$$

where the time dependence is included in the coefficients. The radiation field is produced by a laser that is coherent and monochromatic. Only the electric part of the radiation field contributes. The magnetic part is insignificant since the magnitudes are related by $|\mathbf{E}_0| = c|\mathbf{B}_0|$, where c is the speed of light. The light is therefore an oscillating electric field

$$\mathbf{E} = \mathbf{E}_0 \mathrm{Re}[e^{i(\mathbf{k}\cdot\mathbf{r} - \omega t)}], \tag{2.18}$$

where ω is the angular frequency and $\mathbf{E}_0$ is the amplitude and the direction of the field, $\mathbf{k}$ is the wave vector and $\mathbf{r}$ is the spatial coordinates of the field. The wavelengths λ of the radiation field is usually much larger than the size of the atom $\lambda \gg a_0$. The size of an atom is approximately one Bohr-radius a_0. This

means that the electric field has an almost uniform amplitude over the spatial atomic wave function. Therefore one makes the so-called dipole approximation, where the spatial part of the phase is neglected $\exp(i\mathbf{k}\cdot\mathbf{r}) \approx 1$ since $\mathbf{k}\cdot\mathbf{r} \ll 1$, see e.g. Bransden [8]. The electric field in the dipole approximation becomes

$$\mathbf{E} = \mathbf{E}_0 \cos(\omega t). \tag{2.19}$$

The interaction potential in equation (2.1) is given by, see Bransden [8],

$$V(t) = -\mathbf{D}\cdot\mathbf{E}, \tag{2.20}$$

where $\mathbf{D}$ is the electric dipole moment operator. For an atom with N electrons, the electric dipole moment operator is

$$\mathbf{D} = \sum_{i=1}^{N}(-e)\mathbf{r}_i = -e\mathbf{R}, \tag{2.21}$$

where $-e$ is the charge of the electron and

$$\mathbf{R} = \sum_{i=1}^{N}\mathbf{r}_i, \tag{2.22}$$

is the sum over all the electronic coordinates. The interaction potential becomes

$$V(t) = e\mathbf{R}\cdot\mathbf{E}_0 \cos(\omega t). \tag{2.23}$$

This interaction potential couples the different internal states and induces transitions between them. It is assumed that the light only couples different internal states. In terms of the inner product between the two internal states the interaction potential is

$$\begin{aligned} \langle 1|\, V\, |1\rangle &= \langle 2|\, V\, |2\rangle = 0 \\ \langle 1|\, V\, |2\rangle &= \langle 2|\, V\, |1\rangle^* = \hbar\Omega\cos(\omega t), \end{aligned} \tag{2.24}$$

where Ω is called the Rabi frequency. It is defined as, see Foot [20],

$$\Omega = \frac{\langle 1|\, e\mathbf{R}\cdot\mathbf{E}_0\, |2\rangle}{\hbar} = \frac{e}{\hbar}\int \psi_1^*\mathbf{R}\cdot\mathbf{E}_0\psi_2 d\mathbf{R}, \tag{2.25}$$

where the integral is taken over all the electronic coordinates. The Rabi frequency is a measure of how strongly the radiation field couples the light field and the transition between the internal states. The integral is specified by the system, but Ω is assumed to be real in this case. Another important quantity is the atomic resonance frequency

$$\omega_0 = \frac{E_2 - E_1}{\hbar}. \tag{2.26}$$

Using the general relation in equation (2.10) one obtains a pair of coupled differential equations

$$\begin{aligned} i\dot{c}_1 &= \frac{\Omega}{2}\left\{e^{i(\omega-\omega_0)t} + e^{-i(\omega+\omega_0)t}\right\}c_2 \\ i\dot{c}_2 &= \frac{\Omega}{2}\left\{e^{i(\omega+\omega_0)t} + e^{-i(\omega-\omega_0)t}\right\}c_1. \end{aligned}$$

These equations have an analytical solution within the so called rotating wave approximation. In this approximation one assumes that the terms with $\omega + \omega_0$ averages to zero during any realistic interaction time. The equations then reduce to

$$\begin{aligned} i\dot{c}_1 &= \frac{\Omega}{2} e^{i\Delta t} c_2 \\ i\dot{c}_2 &= \frac{\Omega^*}{2} e^{-i\Delta t} c_1, \end{aligned} \tag{2.27}$$

where $\Delta = \omega - \omega_0$ is the detuning of the laser. The general solution is given in [59]

$$\begin{aligned} c_1(t) &= e^{i\Delta t/2} \Big\{ \frac{(\Delta - W)}{\Omega} A e^{iWt/2} + \frac{(\Delta + W)}{\Omega} B e^{-iWt/2} \Big\} \\ c_2(t) &= e^{-i\Delta t/2} \big\{ A e^{iWt/2} + B e^{-iWt/2} \big\}, \end{aligned} \tag{2.28}$$

where $W = \sqrt{\Omega^2 + \Delta^2}$ is the generalised Rabi frequency. A and B are constants determined by initial conditions. If the system is prepared at time $t = 0$ so that $c_1(0) = 1$ and $c_2(0) = 0$ and $A = -B = -\Omega/2W$. Then the probability of observing the different internal states are given by

$$\begin{aligned} |c_1(t)|^2 &= \Big(\frac{W}{\Omega}\Big)^2 \cos^2\Big(\frac{Wt}{2}\Big) \\ |c_2(t)|^2 &= \Big(\frac{\Omega}{W}\Big)^2 \sin^2\Big(\frac{Wt}{2}\Big). \end{aligned} \tag{2.29}$$

For monochromatic radiation with angular frequency tuned to the atomic resonance $\omega = \omega_0$, the detuning Δ becomes zero. The probabilities in equations (2.29) becomes

$$\begin{aligned} |c_1(t)|^2 &= \cos^2\Big(\frac{\Omega t}{2}\Big) \\ |c_2(t)|^2 &= \sin^2\Big(\frac{\Omega t}{2}\Big). \end{aligned} \tag{2.30}$$

While exposed to the light the atom experience Rabi oscillations between the internal states, see figure 2.1. These Rabi oscillations imply that the probabilities of measuring the different internal states oscillates. Physically this means that the electrons oscillate between occupying the excited state or occupying the ground state.

Subject to radiation the internal atomic state can be rearranged. The light field has a momentum according to the de Broglie relation $\mathbf{p} = \hbar\mathbf{k}$, where $\mathbf{k}$ is the wave vector of the light. An atom initially in the state $|1\rangle$ subject to light that induces a transition to the excited state $|2\rangle$, changes external state. This means that the motion of the atom is affected due to conservation of momentum. Consider an atom in the internal ground state $|1\rangle$ that has a initial momentum $\mathbf{p}$. The light has a wave vector $\mathbf{k}$ and transfers an amount of momentum $\mathbf{p} = \hbar\mathbf{k}$. Because of the quantized internal energy levels the transferred momenta is quantized as well. The corresponding internal and external states would be

$$\{|1, \mathbf{p}\rangle, |2, \mathbf{p} + \hbar\mathbf{k}\rangle\}, \tag{2.31}$$

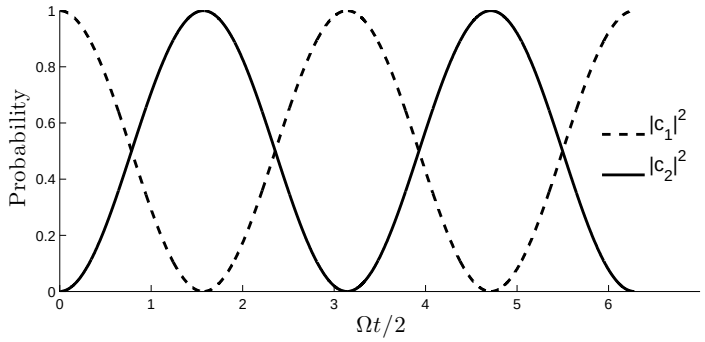

Figure 2.1: The probabilities to measure either of the internal states, when the atom is subject to strong radiation. The oscillating behaviour is called Rabi oscillations.

where the ket is labelled $|\text{internal state}, \text{external state}\rangle$. When undergoing Rabi oscillations of the internal states the atom also undergo momentum oscillations of the external states. If the difference between the energy levels is small the photon momentum implies a minor difference in the external states. In the next section Raman transitions are discussed. These transitions transfer a larger amount of momentum to the atom.

2.3 Raman transitions

Atoms subject to two counter propagating lasers can experience so called Raman transitions. These transitions involve the simultaneous absorption and stimulated emission of a photon. The situation is illustrated in figure 2.2. Three

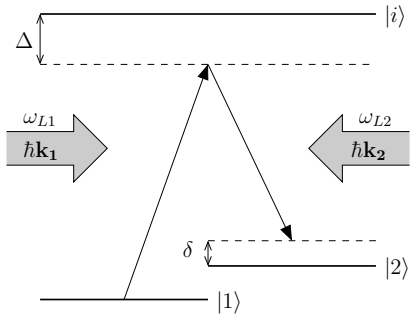

Figure 2.2: A Raman transition is a transition between internal level $|1\rangle$ and $|2\rangle$ involving a third intermediate level $|i\rangle$. Two counter propagating lasers induces a two-photon process involving simultaneously absorption and stimulated emission of two photons via a virtual level, the dashed line below $|i\rangle$. The momentum associated with level $|1\rangle$ is $\mathbf{p}$ and with level $|2\rangle$ is $\mathbf{p} + 2h\mathbf{k}$.

atomic states are involved: The ground state $|1\rangle$, an excited state $|2\rangle$ and a third intermediate state $|i\rangle$. The states $|1\rangle$ and $|2\rangle$ can be the hyperfine split-

tings of the ground state with resonance frequency

$$\omega_{21} = \frac{E_2 - E_1}{\hbar}, \tag{2.32}$$

where E_2 is the energy of level $|2\rangle$ and E_1 is the energy of level $|1\rangle$. Employing hyperfine levels ensures a long lifetime of the excited state according to equation (2.15). The third level $|i\rangle$ involved can be some higher excited state of the atom, and the energies assigned to the levels are related by

$$E_i \gg E_2 > E_1, \tag{2.33}$$

where E_i is the energy of the intermediate level $|i\rangle$. Raman transitions are second order processes, called two-photon processes since it involves simultaneous absorption and stimulated emission of two photons via a virtual level. The level is virtual in the sense that the atom is never excited to this level.

In order to achieve Raman transitions the difference in laser frequencies $\omega_{L1} - \omega_{L2}$ must be very close or equal the resonance frequency for the ground state splitting ω_{21}. The difference in laser frequencies must be controlled precisely and the detuning from exact resonance is given by

$$\delta = \omega_{L1} - \omega_{L2} - \omega_{21}. \tag{2.34}$$

This detuning arises from the Doppler shift caused by the atomic motion. This makes Raman transitions sensitive to the speed of the atoms and is a complicating factor. Since a Raman transition is a second order process the radiation field must be intense. Therefore first order processes must be far off resonance, since these are more easily induced. In this case the transitions between $|1\rangle \leftrightarrow |i\rangle$ and $|i\rangle \leftrightarrow |2\rangle$ are first order processes. The radiation field coupling these are detuned from the intermediate level $|i\rangle$ an amount Δ which is large to avoid excitation to level $|i\rangle$.

Each laser transfer momentum to the atom. The energy difference between $|1\rangle$ and $|2\rangle$ is small so each laser transfer approximately equal amount of momentum. The direction of propagation is opposite so that $\hbar\mathbf{k}_1 \approx -\hbar\mathbf{k}_2 = \hbar\mathbf{k}$, see figure 2.2. A photon is simultaneously absorbed from the first laser and the second laser induces stimulated emission of a photon in the opposite direction. Therefore the external state for the excited state differs from the first with an extra momentum of $\hbar\mathbf{k}_1 - \hbar\mathbf{k}_2 = 2\hbar\mathbf{k}$. If the atom is in the ground state $|1\rangle$ with momentum $\mathbf{p}$, the corresponding internal and external states would be

$$\{|1, \mathbf{p}\rangle, |2, \mathbf{p} + 2h\mathbf{k}\rangle\}. \tag{2.35}$$

Raman transitions can induce Rabi oscillations between the internal states $|1\rangle$ and $|2\rangle$. This is favourable compared to the 'ordinary' Rabi oscillations because the excited atom has more momentum added to the external state from each laser. In addition spontaneous emission from the excited level $|2\rangle$ is negligible.

The total electric field from the two counter propagating lasers with frequency ω_{L1} and ω_{L2}, is given by

$$\mathbf{E} = \mathbf{E}_1 \cos(\omega_{L1} t) + \mathbf{E}_2 \cos(\omega_{L2} t), \tag{2.36}$$

where the first term couples the levels $1 \leftrightarrow i$ and the second term couples the levels $i \leftrightarrow 2$. There is no direct coupling between level $|1\rangle$ and $|2\rangle$. Each of the

transitions is assigned a Rabi frequency. These are defined as in equation (2.25) and given by

$$\begin{aligned}\Omega_{i1} &= \frac{\langle i| e\mathbf{R}\cdot\mathbf{E}_1 |1\rangle}{\hbar} \\ \Omega_{2i} &= \frac{\langle 2| e\mathbf{R}\cdot\mathbf{E}_2 |i\rangle}{\hbar},\end{aligned} \tag{2.37}$$

where e is the electron charge and $\mathbf{R}$ is given in equation (2.22). The Rabi frequencies are assumed to be real. For the transition between $|1\rangle$ and $|2\rangle$, one defines an effective Rabi frequency given by [20]

$$\Omega_{\text{eff}} = \frac{\Omega_{2i}\Omega_{i1}}{2\Delta} = \frac{\langle 2| e\mathbf{R}\cdot\mathbf{E}_2 |i\rangle \langle i| e\mathbf{R}\cdot\mathbf{E}_1 |1\rangle}{2\hbar^2\Delta}, \tag{2.38}$$

where Δ is the detuning from the intermediate state. In terms of the angular frequencies, this can be written as $\Delta = \omega_{i1} - \omega_{L1}$, where

$$\omega_{i1} = \frac{E_i - E_1}{\hbar}. \tag{2.39}$$

To calculate the effective Rabi frequency for real atoms, one must consider the hyperfine structure of the intermediate level. Therefore several intermediate states are possible. In that case the effective Rabi frequency is a sum over all the intermediate levels [35]

$$\Omega_{\text{eff}} = \sum_i \frac{\Omega_{2i}\Omega_{i1}}{2\Delta_i}. \tag{2.40}$$

For a strong field all the population oscillates between $1 \leftrightarrow 2$ with the effective Rabi flopping frequency Ω_{eff}, see e.g. Foot [20]. The atom experience Rabi oscillations between level $|1\rangle$ and $|2\rangle$ and the probabilities for measuring the different states are given by

$$\begin{aligned}|c_1(t)|^2 &= \cos^2\left(\frac{\Omega_{\text{eff}}t}{2}\right) \\ |c_2(t)|^2 &= \sin^2\left(\frac{\Omega_{\text{eff}}t}{2}\right).\end{aligned} \tag{2.41}$$

By adjusting the duration of the light-interaction one can use Raman transitions to put an atom into a coherent superposition of level $|1\rangle$ and $|2\rangle$. If these are the ground state hyperfine splittings, the lifetime of the superposition has a long lifetime according to equation (2.15).

Raman transitions for sodium

Sodium atoms are suitable for Raman transitions between the hyperfine splittings of the ground state: $3S_{1/2}$ with $F = 1$, $m_F = 0$ and $F = 2$, $m_F = 0$. The first excited state $3P_{3/2}$ is used as the intermediate level, see figure 2.3. Since the relative energy difference between the excited level and both hyperfine splittings are almost equal, one can assume the two counter propagating lasers to have similar wavelengths $\lambda \sim 590$nm.

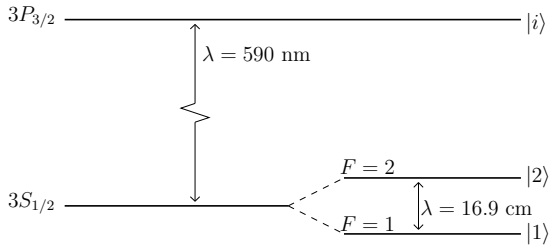

Figure 2.3: The first excited state and the hyperfine splittings of the ground state for sodium.

Each of the two counter propagating laser beams transfer momentum to the atom. The total momentum from the lasers is given by

$$\Delta p \approx 2\hbar k = \frac{2h}{\lambda}. \tag{2.42}$$

Consider the situation as a collision between the photons and the atom, where the atoms receives a momentum kick from two photons. The momentum is conserved and the velocity of the atom will change an amount given by

$$v_{\text{rec}} = \frac{\Delta p}{M} = \frac{2h}{M\lambda}. \tag{2.43}$$

This is called the photon recoil velocity and is the change in the atomic velocity due to emission or absorption of photons.

For a sodium atom with mass $M = 3.8 \cdot 10^{-26}$ kg and wavelength $\lambda = 590$nm, the recoil speed becomes $v_{\text{rec}} \approx 0.06$ m/s. One can induce a Raman transition so that the atom is put in a coherent state of spatially separate components. The momentum from the light is perpendicular to the atomic velocity and the different components is separated in two directions. After 1 second this separation would be 6 cm. Kasevich and Chu [34] have applied Raman transitions between the hyperfine splittings of the ground state of sodium (see figure 2.3). The recoil velocity was 0.06 m/s.

Consider some typical speeds of atoms used in atom interferometers. The speed component v_x is related to the temperature T via the equipartition theorem

$$\frac{1}{2}Mv_x^2 = \frac{1}{2}k_{\text{B}}T, \tag{2.44}$$

where k_{B} is the Boltzmann constant. One is often interested in cold atoms in atom interferometers. If the atoms are cooled down to 1K the speed is $v_x = \sqrt{k_{\text{B}}T/M} \approx 19$m/s. If the Raman lasers are perpendicular to the speed of the atoms, the scattering angle is

$$\theta = \arctan\frac{0.06}{27} = 0.18^\circ. \tag{2.45}$$

For ultracold sodium atoms with $T = 1$ mK the speed is $v \approx 1$ m/s. The scattering angle then becomes $\theta = 0.4^\circ$. If the atoms travel with $v \approx 1$ m/s then a 1 meter long interferometer would give a spatial separation of 6 cm between the components. Formation of cold atom involve some sophisticated technology

like laser cooling and magneto-optical traps MOT's. In atom interferometers the scattering angles induced by the beam splitters are small. Applying some interaction to only one of the separated components one must employ advanced technology because of the small scales involved.

Velocity dependence for Raman transitions

The probability for Raman transitions is sensitive to the velocity of the atoms, due to the Doppler shift of the employed frequencies, see equation (2.34). The velocity range is related to the interaction time [20]

$$\Delta v = \frac{\lambda}{t_{\text{pulse}}}, \tag{2.46}$$

where t_{pulse} is the duration of a light-pulse. For the case of the π-pulse (discussed in section 2.5) $t_\pi \approx 10\,\mu$s the velocity range is $\Delta v \approx 6$ cm/s. This is the maximum deviation for transverse velocity. For shorter pulses the velocity range can be larger.

2.4 Diffraction of atoms by light

To make atoms undergo Raman transitions two counter propagating laser beams with slightly different frequencies are used. If these frequencies are the same the two counter propagating lasers makes a standing wave. This standing wave sets up a periodic potential. For traversing atoms this potential can act as a diffraction grating, so that incident atoms are scattered in different directions. Depending on the characterization of the optical gratings several types of diffraction can occur. This discussion is an overview of Bragg diffraction which is characterized by a thick grating with a low intensity. A more detailed discussion is found in [17].

In classical optics light incident upon a diffraction grating is scattered into different directions. Bragg diffraction occur for light incident upon a crystal. The light has wavelength λ, and the condition for Bragg diffraction into order n is

$$2l \sin\theta = n\lambda, \tag{2.47}$$

where θ is the angle of inclination, l is the distance between crystal planes and n is an integer denoting order of diffraction.

An analog condition exists for matter waves. Consider atoms with longitudinal momentum p at an incident angle θ upon a standing wave of light, see figure 2.4. The transverse component of the momentum is $p_z = p\sin\theta$. According to the de Broglie relation the momentum is assigned a wavelength

$$p = \frac{h}{\lambda_{\text{dB}}} = \hbar k, \tag{2.48}$$

where the k is the wave vector of the light. The standing wave of light makes an optical grating with grating period $\lambda/2$, where λ is the wavelength of the light. Equation (2.47) for matter waves becomes

$$\lambda \sin\theta = n\lambda_{\text{dB}}. \tag{2.49}$$

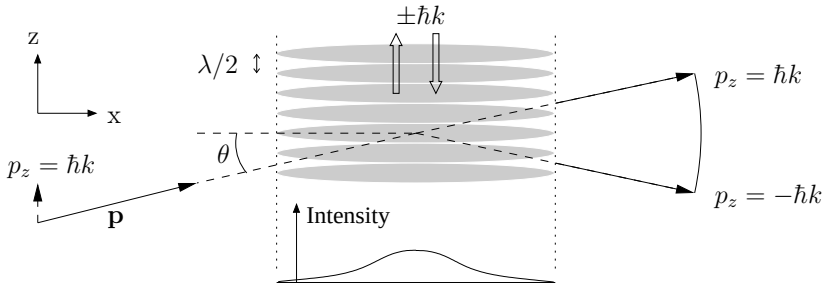

Figure 2.4: Atoms satisfying the Bragg condition $p_z = p\sin\theta = n\hbar k$ are diffracted, photons transfer momenta to the atom in multiples of $2\hbar k$. The intensity profile of the beam in the transverse direction is Gaussian and the traversing atoms emerge out of the light field with the same internal state.

In terms of the transverse momentum the Bragg condition for matter waves is given by

$$p_z = n\hbar k, \tag{2.50}$$

where n is an integer. This means that the incident atoms must have a well defined momentum with a traverse component satisfying equation (2.50) in order to be diffracted.

The light-atom interaction can be interpreted as a two-photon process involving simultaneous absorption and stimulated emission of a photon. One laser beam excites the atom giving it a momentum kick from one photon, the other laser beam stimulates emission and the atom receives a momentum kick in the opposite direction.

Consider incident atoms with transverse momentum $\hbar k$, so that equation (2.50) is satisfied for $n = 1$. Receiving momentum from two photons the transverse momentum becomes $-\hbar k$. This is illustrated in figure 2.4. The situation where the external state becomes $3\hbar k$ or $-3\hbar k$ are higher order processes. Since the intensity is low for Bragg diffraction these processes are unlikely to occur. Therefore the incident atom has two possible momentum states after traversing the grating. The atom can either transmit the grating receiving no momentum from the light, or it can be reflected by receiving a momentum kick from two photons. The probabilities for reflection and transmission can be varied experimentally. The intensity of the light, denoted χ, can be adjusted or the interaction time τ can be adjusted. The interaction region is finite and the interaction time is determined by the speed of the traversing atoms. For first order diffraction the atom is reflected or transmitted with probabilities [17]

$$\begin{aligned} |t|^2 &= \cos^2(\chi\tau) \\ |r|^2 &= \sin^2(\chi\tau), \end{aligned} \tag{2.51}$$

where $|t|^2$ is the transmission probability and $|r|^2$ is the reflection probability. The different external states have an oscillating behaviour similar to the Rabi oscillations discussed in section 2.2. The Bragg diffraction of atoms has some similarities with Raman transitions discussed in the preceding section. For Raman transitions the atom ends up in a different internal state while for Bragg

diffraction the internal state is the same for both momentum states. No spontaneous emission occur for Bragg diffraction and the process is coherent. An atom can be put in a coherent superposition of two momentum states, but with the same internal states. This is different from Raman transitions where the atom ends up in different internal states.

2.5 π- and π/2-pulses

Strong monochromatic radiation affects the populations of the atomic levels. Raman transitions and Bragg diffraction are suitable ways to manipulate atoms in atom interferometers, since the photons transfer enough momenta to spatially manipulate the atoms.

For an atom subject to a resonant Raman pulse with duration $t_\pi = \pi/\Omega_{\text{eff}}$, the state ket changes as

$$c_1 |1\rangle + c_2 |2\rangle \xrightarrow{\pi-\text{pulse}} -i(c_2 |1\rangle + c_1 |2\rangle). \tag{2.52}$$

A light-atom interaction with this duration is called a π-pulse. In particular an atom in the state $|1\rangle$ ends up in $|2\rangle$, but with an factor $-i$ in front:

$$|1\rangle \xrightarrow{\pi-\text{pulse}} -i |2\rangle . \tag{2.53}$$

Applying two successive π-pulses on the state $|1\rangle$ gives $-|1\rangle$, and the identity-operation requires a 4π-pulse

$$\hat{\pi}\hat{\pi}\hat{\pi}\hat{\pi} = \mathbb{1}. \tag{2.54}$$

The π-pulse is an operator. The matrix representation of this operator in the basis $\{|1\rangle, |2\rangle\}$, is given by

$$\hat{\pi} = \begin{bmatrix} 0 & -ie^{i\phi(t)} \\ -ie^{-i\phi(t)} & 0 \end{bmatrix}, \tag{2.55}$$

where $\phi(t)$ is the phase of the light. For Raman transitions this phase is the difference in the arbitrary phase of each counter propagating beam evaluated at the interaction point. The phase $\phi(t)$ is transferred to the atom, and is $+\phi(t)$ for absorption and $-\phi(t)$ for emission of a photon, see Godun [23]. This phase can be adjusted experimentally and this is done in an atom interferometer to determine phase shifts, see section 3.4. Applying the field a period $t_{\pi/2} = \pi/(2\Omega_{\text{eff}})$ puts an atom initially in the ground state $|1\rangle$ in a coherent superposition of the ground state and the excited state:

$$|1\rangle \xrightarrow{\pi/2-\text{pulse}} \frac{1}{\sqrt{2}}(|1\rangle - i |2\rangle). \tag{2.56}$$

This is a called π/2-pulse and the matrix representation is given by

$$\frac{\hat{\pi}}{2} = \frac{1}{\sqrt{2}} \begin{bmatrix} 1 & -ie^{i\phi(t)} \\ -ie^{-i\phi(t)} & 1 \end{bmatrix}, \tag{2.57}$$

where $\phi(t)$ is the phase of the laser beam. Both the π- and π/2 matrices have unitary properties which means that the probability is conserved.

The concept of π- and $\pi/2$-pulses also holds for Bragg diffracted atoms. The interaction times is found from equation (2.51) and is given by

$$t_\pi = \pi/(2\chi), \quad t_{\pi/2} = \pi/(4\chi). \tag{2.58}$$

In analogy to optics the $\pi/2$-pulse acts as a 50-50 beam-splitter and a π-pulse acts as a mirror. It is worthwhile to notice that this is ideal situations. The duration of the laser light must last exactly the right amount of time and this can be difficult to realize experimentally. In table 2.2 some realistic values of

	π-pulse	$\pi/2$-pulse	Reference
Bragg diffraction (Rb)	90 μs	45 μs	[17]
Raman transitions (Na)	10 μs	5 μs	[20]

Table 2.2: Duration of light pulses.

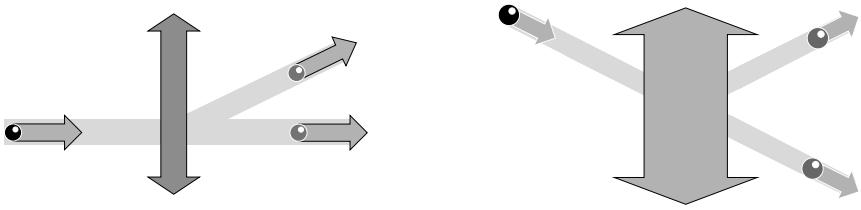

Figure 2.5: An incident atom in the ground state is subject to a $\pi/2$-pulse and ends up in a coherent superposition of two momentum states. The $\pi/2$-pulse acts as a beam-splitter for an incident beam of atoms. The figure on the left illustrates a $\pi/2$-pulse for a Raman transition. The figure on the right illustrates a $\pi/2$-pulse for Bragg diffraction. The Bragg beam splitter is drawn with a wide arrow to indicate a wide intensity profile.

the duration time for π- and $\pi/2$-pulses are listed. Figure 2.5 illustrates what happens when an atom in the ground state is subject to a $\pi/2$-pulse. The same situation is shown for both a Raman transition and Bragg diffraction. In both cases the atom ends up in a coherent superposition of spatially separated states. The grey color on the atoms is meant to illustrate this.

Chapter 3

Atom interferometry

Light can be used to put an atom in a coherent superposition of spatially different states. Combinations of light-pulses or standing light waves can guide atoms along certain paths. A spatial separation of the components enables the possibility to apply different interactions to the different components of the same atom. Depending on the purpose, different architectures are applied to set up an interferometer. The physical property being the subject of investigation is related to a phase or amplitude which are the two quantities measured with atom interferometers. The source prepares an ensemble of single systems: atoms or molecules. According to the statistical interpretation, repeated measurements of identical single systems should reproduce the single system wave function. In order to observe interference fringes the atomic state must stay coherent during its way through the interferometer. Random phases between components will wash out any interference fringes because the detection process averages over the ensemble of atoms. Direct applications are discussed in chapter 4 while this chapter presents a more general discussion.

3.1 Atomic motion

In the absence of any interactions the atom is (approximately) a free particle with a well defined energy

$$E = \hbar\omega = \frac{\hbar^2\mathbf{k}^2}{2m}. \tag{3.1}$$

The free particle wave function is a plane wave with a uniform probability distribution throughout space. Upon measurement the particle can be localised everywhere. In any realistic experiment the atomic wave function is a superposition of many plane waves which adds up to a wave packet with non-uniform probability density. This wave packet has a translatory movement and can be assigned a speed in the classical sense. The classical speed v is equal the group velocity of the wave packet defined as

$$v = \frac{d}{dk}\omega(k) \tag{3.2}$$

The dispersion relation $\omega(k)$ for a non-relativistic free particle, is found from equation (3.1), $\omega(k) = \hbar k^2/2m$. The classical speed or the ratio of movement

for the probability distribution is

$$v = \frac{d}{dk}\Big(\frac{\hbar k^2}{2m}\Big) = \frac{\hbar k}{m}. \tag{3.3}$$

The de Broglie relation $p = h/\lambda_{\mathrm{dB}} = \hbar k$ relates the classical speed and the momentum

$$v = \frac{p}{m}. \tag{3.4}$$

The notion of speed together with the lifetime of the excited level can be combined to define a coherence length

$$L = \tau v. \tag{3.5}$$

This is the maximum distance the atom can stay in the coherent superposition and the length of an atom interferometer is limited by this. The lifetime of the states must exceed the transit time. If the atoms has a speed ~ 20m/s see table 3.1 and lifetimes ~ 30s the coherence length is ~ 600m.

3.2 The source

The source produces an ensemble of atoms characterised by a momentum distribution. Different types of sources give different flux reaching the detector. In this context the flux is the number of atoms counted in the interferometer region and is denoted with counts per second. A higher flux is advantageous as it gives better signal-to-noise ratio and therefore may increase the precision of the measurement. The two main types of sources are atom beams and samples of cold atoms that can be moved by lasers. The choice of source is largely dependent on the purpose. Atom beams are produced by emitting thermal atoms from an oven. Collimating slits allow only atoms within a certain momentum range to escape out of the oven and into the interferometer. Thermal beams basically exhibit a Boltzmann distribution of velocities while supersonic beams produces Gaussian velocity distributions with a narrower width [57].

Spontaneous emission is utilised to cool atoms into samples with narrow momentum distributions. A magneto-optical trap MOT, see Foot [20], can contain a sample of ultra cold atoms. The cold atomic sample is moved by lasers or simply accelerated by gravity and sent into the interferometer. The detected flux is usually lower than for thermal atomic beams, see table 3.1. Both

Source	Thermal atom beam [26]	Cold atomic sample [41]
Atom	Cs	^{87}Rb
Measured flux	10^{11} atoms/s	10^{10} atoms/s
Most prob. speed	290 m/s	20 m/s
Transverse spread	$\pm$0.10 m/s	$\pm$0.6 mm/s

Table 3.1: Physical properties of the two main types of sources.

types of sources produce an incoherent collection of atoms in the sense that each atom is mutually independent. Nevertheless interference occur because every atom interferes with itself as stated in section 1.1. The detector measures an

ensemble of atoms and averaging gives the single particle wave function. The atom-light interactions discussed in chapter 2 are dependent on the form of the momentum distribution. The Bragg condition in equation (2.50) requires a narrow momentum distribution. Raman transitions are also more likely to occur within a given velocity range, see equation (2.46). For an open interferometer design discussed in section 3.4 the speed distribution also affects the fringe pattern.

3.3 The phase shift

The phase of the atomic states is important in atom interferometry. For a single oscillating object the phase is the offset from a given reference point as illustrated in figure 3.1. According to this figure the phase of a single oscillating object

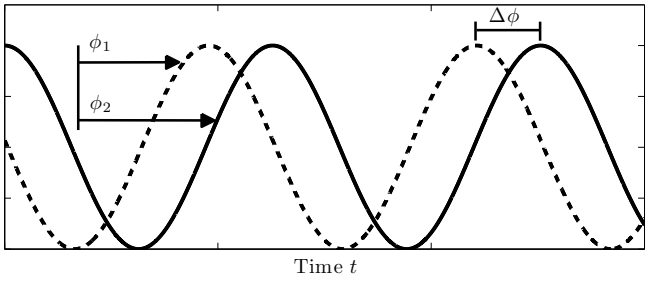

Figure 3.1: Two oscillating objects propagating in time. Each accumulates a phase ϕ_1 and ϕ_2 relative to a reference line. The relative phase $\Delta\phi$ describes the relationship. If this is constant the two objects are coherent.

is of no physical importance since the reference point can be placed arbitrary. When a multiple of oscillating objects are present one can assign a relative phase describing the relationship between them. This relative phase, denoted $\Delta\phi$ in figure 3.1, can have certain physical implications. If $\Delta\phi$ is constant the objects are coherent.

Atoms exhibit wave-like behaviour and can be assigned a phase. In atom interferometers the atomic state is split into two spatially separated components. Each of these components is assigned a phase and there is a relative phase between the components. This phase relationship can be revealed through an interference pattern. In atom interferometers the atoms either propagate freely, interact with light pulses or are subject to some interaction under investigation, the phase changes either way. Inertial effects like rotations and acceleration affects the whole interferometer. Atomic and molecular properties can be examined by local interactions along one of the arms of the interferometer. One way of investigating atomic and molecular properties is to apply a time independent potential along one arm. This potential affects the traversing atoms and connects physical properties to a phase (this is discussed in chapter 4). The Schrödinger equation is

$$i\hbar\frac{\partial}{\partial t}\Psi(\mathbf{r},t) = H\Psi(\mathbf{r},t). \tag{3.6}$$

The Hamiltonian is time independent since the interaction potential is. There exists separable solutions of the form $\Psi(\mathbf{r},t) = \psi(\mathbf{r})\chi(t)$, so that

$$\frac{i\hbar}{\chi(t)}\frac{d\chi(t)}{dt} = \frac{H\psi(\mathbf{r})}{\psi(\mathbf{r})}. \tag{3.7}$$

This is true only if both sides is equal a constant E, interpreted as the energy. The time-part has the solution

$$\chi(t) = e^{-iEt/\hbar}. \tag{3.8}$$

The spatial part must fulfill the time independent Schrödinger equation

$$-\frac{\hbar^2}{2m}\nabla^2\psi(\mathbf{r}) + V(\mathbf{r})\psi(\mathbf{r}) = E\psi(\mathbf{r}). \tag{3.9}$$

The time dependent solution is

$$\Psi(\mathbf{r},t) = \psi(\mathbf{r})e^{-iEt/\hbar}. \tag{3.10}$$

The Hamiltonian is time independent and the solutions have a well defined energy $E = \hbar\omega$. Consider the plane wave solution of the Schrödinger equation

$$\begin{aligned}\Psi(\mathbf{r},t) &= Ae^{i(\mathbf{k}\cdot\mathbf{r}-Et/\hbar)} \\ &= \psi(\mathbf{r})e^{-iEt/\hbar},\end{aligned} \tag{3.11}$$

where $E = \hbar\omega$ is the energy and A is a normalisation constant. These plane waves can represent the travelling atoms.

An alternative representation of the accumulated phase is by line integrals. Denote the classical path the atoms travel $x(t)$. The accumulated phase along this path $x(t)$ can be expressed in terms of the classical action. The action is a characterisation of the dynamics of a physical system and is defined [38]

$$S[x(t)] = \int_{t_0}^{t} L(x,\dot{x})dt, \tag{3.12}$$

where the Lagrangian L is the difference between kinetic and potential energy. This is a line integral along the path $x(t)$ starting at time t_0 until t. For a particle propagating freely along $x(t)$, the wave function is [58]

$$\Psi(\mathbf{r},t) = \psi(\mathbf{r})e^{iS[x(t)]/\hbar}. \tag{3.13}$$

In atom interferometers the multiple waves travel along separate arms and accumulates a phase corresponding to the path. The action along arm i is $S_i = S[x_i(t)]$ for $i = 1, 2$. The total wave function is

$$\begin{aligned}\Psi(\mathbf{r},t) &= \psi_1(\mathbf{r})e^{iS_1/\hbar} + \psi_2(\mathbf{r})e^{iS_2/\hbar} \\ &= e^{iS_1/\hbar}[\psi_1(\mathbf{r}) + e^{-i\Delta\phi}\psi_2(\mathbf{r})]\end{aligned} \tag{3.14}$$

The object of interest is the relative phase between the components. Expressed in terms of action along arm 1 and 2 the relative phase shift is

$$\Delta\phi = \frac{1}{\hbar}(S_1 - S_2). \tag{3.15}$$

The phase shift can be split into two parts. One depending on the geometry of the interferometer and one part due to the difference in interactions along the way

$$\Delta\phi = \phi_{\text{geometry}} + \Delta\phi_{\text{int}}. \tag{3.16}$$

In this case geometry means the position of the light-atom interactions or the phase of the light-atom interactions. The geometric phase can be varied experimentally. If the interaction can be turned on or off the interaction phase shift can be determined. Two interferometers are discussed below.

3.4 Raman type interferometers

Raman transitions spatially manipulates the two components of the wave function. Momentum transferred from the light interaction is used to separate atomic states. This enables the possibility for the different components to undergo different interactions. An atom in the ground state $|1\rangle$ enters the interferometer region with momentum $\mathbf{p}$. A Raman transition to the excited state $|2\rangle$, gives an extra momentum $2\hbar\mathbf{k}$ to the external state. The momentum from the photons is perpendicular to the initial atomic momentum: $\mathbf{p} \perp \mathbf{k}$. The external momentum states differ an amount $2\hbar\mathbf{k}$, and is connected to the internal states:

$$\begin{aligned} |1\rangle &= |1, \mathbf{p}\rangle \\ |2\rangle &= |2, \mathbf{p} + 2\hbar\mathbf{k}\rangle\,, \end{aligned} \tag{3.17}$$

where the ket denotes $|\text{internal state}, \text{momentum state}\rangle$. Since the external and internal states has a one-to-one correspondence, the momentum notation is suppressed. The general atomic state for an interferometer using Raman transitions can therefore be written as

$$|\Psi\rangle = c_1\,|1\rangle + c_2\,|2\rangle\,, \tag{3.18}$$

where the time dependence is included in the coefficients. The relevant light-atom interactions are the π-pulse given in equation (2.55), and the $\pi/2$-pulse given in equation (2.57). The evolution of the states between the light-pulses is described by the time-evolution operator

$$|\Psi(t_0 + t)\rangle = U(t, t_0)\,|\Psi(t_0)\rangle\,. \tag{3.19}$$

Between the pulses the atoms propagate freely or is subject to some interaction. This interaction is assumed to be diagonal in the internal state basis so no transitions occur. Therefore the evolution of the wave function is given by the time evolution operator:

$$U(t, t_0)\,|\Psi\rangle = c_1\,|1\rangle\,e^{i\alpha(t-t_0)} + c_2\,|2\rangle\,e^{i\beta(t-t_0)}, \tag{3.20}$$

where α and β are the accumulated phase shifts. The phase accumulated for the free propagation can be found using equation (3.12). Following the matrix representations of the light-pulses, the time evolution operator can be written on matrix form:

$$U(t) = \begin{bmatrix} e^{i\alpha(t)} & 0 \\ 0 & e^{i\beta(t)} \end{bmatrix}. \tag{3.21}$$

The physics is thus described by such matrices. The wave function for different interferometers can be determined by matrix multiplication.

The open $\pi/2$ - $\pi/2$ interferometer

An incident atom beam subject to two $\pi/2$-pulses separated by a time T_0 makes an open atom interferometer. Open means that the paths are not recombined at the end of the interferometer. The interferometer is illustrated in figure 3.2. The atomic state is represented by the superposition in equation (3.18). The

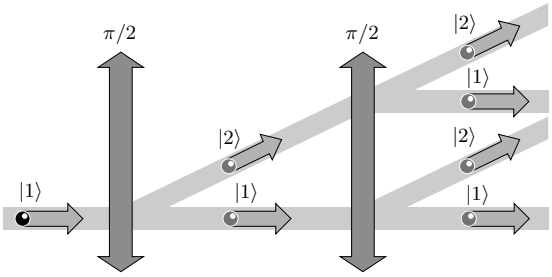

Figure 3.2: A $\pi/2$- $\pi/2$ interferometer with open paths. The incident atom is in the ground state $|1\rangle$. The grey color of the atoms is meant to display the coherent superposition of spatially different states.

first $\pi/2$-pulse is applied at the time $t = t_1$, and acts as a beam splitter for the incident atomic state. Then there is free propagation a time T_0 before a second $\pi/2$-pulse is applied at $t = t_2$. Both light-atom interactions acts as beam splitters. The laser beams shifts the phase of the atomic state by an amount $\phi(t_i) = \phi_i$ for $i = 1, 2$, where $\phi(t)$ was introduced in equation (2.57). The final state is obtained by using the operators in the following order:

$$|\Psi_{\text{final}}\rangle = \frac{\hat{\pi}}{2}(t_2)\hat{U}(T_0)\frac{\hat{\pi}}{2}(t_1)\,|\Psi_{\text{init}}\rangle\,, \tag{3.22}$$

where the $\pi/2$-pulse is given in equation (2.57) and $U(T_0)$ is given in equation (3.21). The final state is found by multiplying the matrices representing the different operations. The initial state at $t = 0$ is the ground state $|1\rangle$, so the final state is given by

$$\begin{aligned}
|\Psi_{\text{final}}\rangle &= \frac{1}{\sqrt{2}}\begin{bmatrix} 1 & -ie^{i\phi_2} \\ -ie^{-i\phi_2} & 1 \end{bmatrix} \times \begin{bmatrix} e^{i\alpha} & 0 \\ 0 & e^{i\beta} \end{bmatrix} \\
&\quad \times \frac{1}{\sqrt{2}}\begin{bmatrix} 1 & -ie^{i\phi_1} \\ -ie^{-i\phi_1} & 1 \end{bmatrix}\begin{bmatrix} 1 \\ 0 \end{bmatrix} \\
&= \frac{1}{2}\begin{bmatrix} e^{i\alpha}(1 - e^{i(\phi_2-\phi_1+\beta-\alpha)}) \\ -ie^{i(\alpha-\phi_2)}(1 + e^{i(\phi_2-\phi_1+\beta-\alpha)}) \end{bmatrix} \\
&= \frac{1}{2}\begin{bmatrix} e^{i\alpha}(1 - e^{i\Phi}) \\ -ie^{i(\alpha-\phi_2)}(1 + e^{i\Phi}) \end{bmatrix}.
\end{aligned} \tag{3.23}$$

The phase shift is denoted Φ, and is given by

$$\Phi = \phi_2 - \phi_1 + \beta - \alpha. \tag{3.24}$$

Since the matrices in equation (3.23) are unitary the probability is conserved and the final state is normalised so that $|c_1|^2 + |c_2|^2 = 1$. The probability of

measuring the ground state is

$$\begin{aligned} |c_1|^2 = |\langle 1|\Psi_{\text{final}}\rangle|^2 &= \left|\frac{1}{2}e^{i\alpha}(1-e^{i\Phi})\right|^2 \\ &= \frac{1}{4}(1-e^{i\Phi})(1-e^{-i\Phi}) \\ &= \frac{1}{2}[1-\cos\Phi]. \end{aligned} \tag{3.25}$$

A similar calculation gives the probability for the excited state. Performing an internal state measurement, the outcomes occur with probabilities

$$\begin{aligned} |c_1|^2 = |\langle 1|\Psi_{\text{final}}\rangle|^2 &= \frac{1}{2}[1-\cos\Phi] \\ |c_2|^2 = |\langle 2|\Psi_{\text{final}}\rangle|^2 &= \frac{1}{2}[1+\cos\Phi]. \end{aligned} \tag{3.26}$$

Between the light-pulses the atomic state propagate freely. Each component $|1\rangle$ and $|2\rangle$ of the atomic state moves with a classical velocity $\mathbf{v}_1$ and $\mathbf{v}_2$. According to equation (3.13) the accumulated phase during the free propagation is the action along the classical path. Only the kinetic energy contributes and the action for the ground state $|1\rangle$ is

$$S = \int_0^{T_0} \frac{1}{2}m\mathbf{v}_1 dt = \frac{1}{2}m\mathbf{v}_1^2 T_0, \tag{3.27}$$

where m is the mass of the atom. The phase shift in terms of the velocities is given by:

$$\begin{aligned} \alpha(T_0) &= -\frac{1}{2}m\mathbf{v}_1^2 T_0/\hbar \\ \beta(T_0) &= -\frac{1}{2}m\mathbf{v}_2^2 T_0/\hbar. \end{aligned} \tag{3.28}$$

Rewriting the phase shift from equation (3.24) in terms of the velocities, see [11], one has for Φ:

$$\begin{aligned} \Phi &= \phi_2 - \phi_1 + \frac{mT_0}{2\hbar}(\mathbf{v}_1^2 - \mathbf{v}_2^2) \\ &= \varphi + \frac{mT_0}{\hbar}\left(\frac{\mathbf{v}_1+\mathbf{v}_2}{2}\right)\cdot(\mathbf{v}_1-\mathbf{v}_2). \end{aligned} \tag{3.29}$$

The first term is the phase shift from the light-atom interaction $\varphi = \phi_2 - \phi_1$. The second term is dependent on the velocity of the atoms and the difference in speed is the photon recoil velocity $|\mathbf{v}_1 - \mathbf{v}_2| = 2\hbar k/m$. The mean velocity of the atoms is

$$v = \left|\frac{\mathbf{v}_2+\mathbf{v}_1}{2}\right|. \tag{3.30}$$

In terms of the mean velocity the phase shift is

$$\Phi = \varphi + 2kT_0 v. \tag{3.31}$$

The phase shift is dependent on the speed of the atoms. For an open interferometer design this is generally the case. Consider the case where the velocities

of the atoms have a normal probability distribution. The fraction of atoms with velocity in the range between v and $v + dv$ is

$$f_v(v)dv = \frac{1}{\sqrt{2\pi}\sigma_v} e^{-v^2/(2\sigma_v^2)} dv, \tag{3.32}$$

where σ_v^2 is the variance. This depends on the temperature T of the atoms and is given by

$$\sigma_v^2 = \frac{k_\mathrm{B} T}{m}, \tag{3.33}$$

where k_B is Boltzmann's constant and m is the mass of one atom. The width of the distribution is dependent on the temperature of the atomic sample. If the sample has a high temperature the distribution becomes wide. A colder sample would correspond to a more narrow distribution. Figure 3.3 shows the velocity distribution at three different temperatures. The probability density function

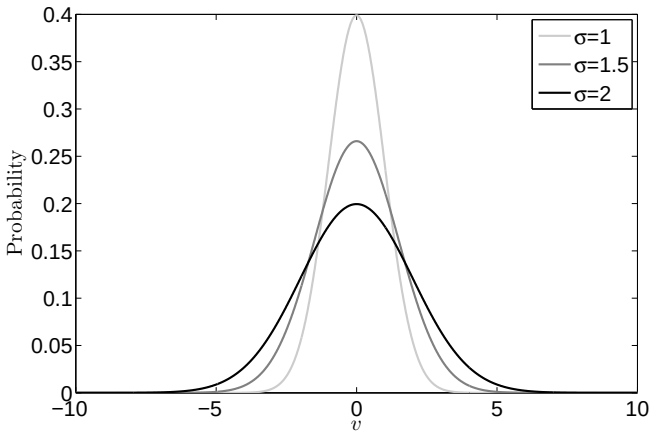

Figure 3.3: Distribution functions $f_v(v)$ of atomic velocities. Three different standard deviations are included corresponding to three different temperatures. A higher temperature gives a wider distribution of the atomic velocities. The black curve has the highest temperature.

$f_\Phi(\Phi)$ of the phase shift is found by transforming the random variable from v to Φ. Since the relationship in equation (3.31) is linear $f_\Phi(\Phi)$ is also a normal distribution

$$f_\Phi(\Phi) = \frac{1}{\sqrt{2\pi}\sigma_\Phi} e^{-(\Phi-\varphi)^2/(2\sigma_\Phi^2)}, \tag{3.34}$$

where the variance is

$$\sigma_\Phi^2 = \left(2kT_0\right)^2 \cdot \frac{k_\mathrm{B} T}{m}. \tag{3.35}$$

Internal state measurements are performed by counting the number of excited atoms while the phase shift from the light φ is varied experimentally. Since the probability in equation (3.26) not only depends on φ but on Φ from equation (3.29), the probability has a distribution as well. The expected value of $|c_2|^2$ is

found by integrating over the distribution $f_\Phi(\Phi)$

$$\begin{aligned}\langle |c_2|^2 \rangle &= \frac{1}{2}\int_{-\infty}^{+\infty} f_\Phi(\Phi)(1+\cos\Phi)d\Phi \\ &= \frac{1}{2\sqrt{2\pi}\sigma_\Phi}\int_{-\infty}^{+\infty} e^{-(\Phi-\varphi)^2/(2\sigma_\Phi^2)}(1+\cos\Phi)d\Phi \\ &= \frac{1}{2\sqrt{2\pi}\sigma_\Phi}\big[\sqrt{2\pi}\sigma_\Phi + \int_{-\infty}^{+\infty} e^{-u^2/(2\sigma_\Phi^2)}\cos(u+\varphi)du\big] \\ &= \frac{1}{2}\big[1+\frac{1}{2\sqrt{2\pi}\sigma_\Phi}\int_{-\infty}^{+\infty} e^{-u^2/(2\sigma_\Phi^2)}(e^{i(u+\varphi)}+e^{-i(u+\varphi)})du\big] \\ &= \frac{1}{2}(1+e^{-\sigma_\Phi^2/2}\cos\varphi).\end{aligned} \tag{3.36}$$

Repeated measurements should produce fringes as shown in figure 3.4. The line

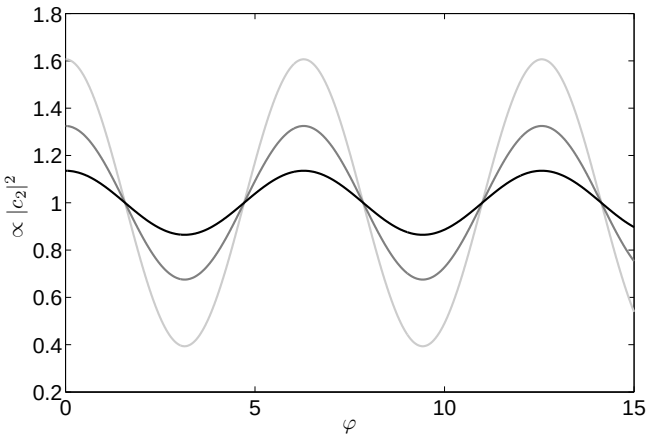

Figure 3.4: The visibility of the interference fringes decreases with increasing temperature T of the atomic sample. Colder atoms can therefore increase the precision of the measurement. The different shades of grey corresponds to figure 3.3.

style corresponds to figure 3.3. A higher temperature on the atoms results in less difference between the maximum and minimum probabilities. This difference displays how visible the fringes are. A normalised quantity is the visibility of the fringes

$$V = \frac{I_{\max} - I_{\min}}{I_{\max} + I_{\min}}, \tag{3.37}$$

where $I_{\max/\min}$ denotes the max/min intensity recorded by a detector. The intensity is proportional to the population $|c_2|^2$ in figure 3.4. In this case $I_{\max} \propto (1+e^{-\sigma_\Phi^2/2})$ and $I_{\min} \propto (1-e^{-\sigma_\Phi^2/2})$ since the cosine varies between 1 and -1. According to equation (3.37) the visibility is

$$\begin{aligned}V &= \frac{1+e^{-\sigma_\Phi^2/2}-1+e^{-\sigma_\Phi^2/2}}{1+e^{-\sigma_\Phi^2/2}+1-e^{-\sigma_\Phi^2/2}} \\ &= e^{-\sigma_\Phi^2/2}.\end{aligned} \tag{3.38}$$

The visibility decreases with increasing width of the speed distribution. As seen from equation (3.35) the variance is proportional to the temperature. A high temperature will give a wide speed distribution that will wash out the fringe pattern shown in figure 3.4. It may therefore be advantageous to use cold atoms in this type of interferometer since this makes it easier to determine the fringe pattern. In addition more massive atoms gives a better visibility due to the $1/m$ behaviour of the variance in equation (3.35). The time T_0 of free propagation is an experimental parameter and from equation (3.35), it seems that this should be as short as possible. Note that this assumes an ideal experiment. In a real experiment other systematic effects may contribute to further reduce the visibility. An open interferometer design can be used to measure the fine structure constant. This is discussed in chapter 4.

The closed $\pi/2$ - π - $\pi/2$ interferometer

Incident atoms subject to $\pi/2$ - π - $\pi/2$ light-pulses makes a closed interferometer. Closed means that the paths are recombined by the last light-pulse. As for the $\pi/2$-$\pi/2$ interferometer the atomic wave function accumulates a phase from the light interactions and during the propagation between the pulses. The interferometer is illustrated in figure 3.5. The atoms are drawn with a grey color between the light-pulses to indicate that each atom travel both paths.

An incident atom in the ground state $|1\rangle$ is put in a coherent superposition of spatially different states by the first $\pi/2$-pulse. Then it propagates freely before it is subject to a π-pulse that swaps the internal states and the momentum changes accordingly. The path of the atom changes and it propagates freely before a $\pi/2$-pulse recombines the internal states. In the last period of free propagation a box is drawn in the upper path. This can be some interaction that shifts the phase of the traversing atoms. This phase shift is only measurable with an atom interferometer. The wave function after the last $\pi/2$-pulse is

$$|\Psi_{\text{final}}\rangle = \frac{\hat{\pi}}{2}(t_3)U(T_2)\hat{\pi}(t_2)U(T_1)\frac{\hat{\pi}}{2}(t_1)\,|\Psi_{\text{init}}\rangle\,. \tag{3.39}$$

The free propagation is described by the matrix in equation (3.21) and the light-pulses by the matrices in equations (2.55) and (2.57). The laser interaction is applied at three different times and shifts the phase by an amount $\phi(t_i) = \phi_i$ for $i = 1, 2, 3$. The atom propagates freely for two periods T_1 and T_2, denoted $\alpha(T_i) = \alpha_i$ and $\beta(T_i) = \beta_i$ for $i = 1, 2$, according to equation (3.21). If the initial state is $|1\rangle$ the final state can be found by matrix multiplication:

$$\begin{aligned}
|\Psi_{\text{final}}\rangle &= \frac{1}{\sqrt{2}}\begin{bmatrix} 1 & -ie^{i\phi_3} \\ -ie^{-i\phi_3} & 1 \end{bmatrix}\begin{bmatrix} e^{i\alpha_2} & 0 \\ 0 & e^{i\beta_2} \end{bmatrix}\begin{bmatrix} 0 & -ie^{i\phi_2} \\ -ie^{-i\phi_2} & 0 \end{bmatrix} \\
&\quad \times \begin{bmatrix} e^{i\alpha_1} & 0 \\ 0 & e^{i\beta_1} \end{bmatrix} \times \frac{1}{\sqrt{2}}\begin{bmatrix} 1 & -ie^{i\phi_1} \\ -ie^{-i\phi_1} & 1 \end{bmatrix}\begin{bmatrix} 1 \\ 0 \end{bmatrix} \\
&= \frac{1}{2}\begin{bmatrix} -e^{i(-\phi_1+\beta_1+\phi_2+\alpha_2)} - e^{i(\alpha_1-\phi_2+\beta_2+\phi_3)} \\ ie^{i(-\phi_1+\beta_1+\phi_2+\alpha_2-\phi_3)} - ie^{i(\alpha_1-\phi_2+\beta_2)} \end{bmatrix} \\
&= \frac{1}{2}\begin{bmatrix} -e^{i(-\phi_1+\beta_1+\phi_2+\alpha_2)}(1 + e^{i(\phi_1-2\phi_2+\phi_3+\beta_2-\beta_1-\alpha_2+\alpha_1)}) \\ ie^{i(-\phi_1+\beta_1+\phi_2+\alpha_2-\phi_3)}(1 - e^{i(\phi_1-2\phi_2+\phi_3+\beta_2-\beta_1-\alpha_2+\alpha_1)}) \end{bmatrix} \\
&= \frac{1}{2}\begin{bmatrix} -e^{i(-\phi_1+\beta_1+\phi_2+\alpha_2)}(1 + e^{i\Phi}) \\ ie^{i(-\phi_1+\beta_1+\phi_2+\alpha_2-\phi_3)}(1 - e^{i\Phi}) \end{bmatrix}.
\end{aligned} \tag{3.40}$$

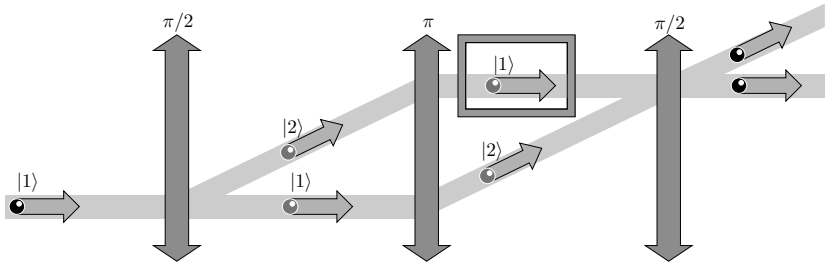

Figure 3.5: A $\pi/2$ - π - $\pi/2$ combination of light-pulses makes a closed interferometer. The box along the upper path illustrates a local interaction applied to the passing atomic components. The grey color of the atoms is meant to display the lack of information concerning which path the atom travels, if it were measured.

The phase shift is denoted Φ, and is divided in two parts

$$\Phi = \varphi + \phi_{\text{prop}}, \tag{3.41}$$

where the first term is the phase acquired from the light-pulses $\varphi = \phi_1 - 2\phi_2 + \phi_3$. The second term is the phase accumulated during the propagation between the pulses

$$\phi_{\text{prop}} = \beta_2 - \beta_1 - (\alpha_2 - \alpha_1). \tag{3.42}$$

For the open interferometer discussed above the phase shift was dependent on the speed of the atoms, see equation (3.31). A closed interferometer design gives a phase shift independent of the velocity of the atoms. To see that this is the case, consider the velocity of the atoms. The translatory motion of the atoms can be described with a probability current or probability flux defined as

$$\mathbf{j} = -\frac{i\hbar}{2m}[\Psi^*\nabla\Psi - (\nabla\Psi^*)\Psi]. \tag{3.43}$$

This is related to the probability density $\rho = |\Psi(\mathbf{r}, t)|^2$ by the continuity equation

$$\frac{\partial\rho}{\partial t} + \nabla\cdot\mathbf{j} = 0. \tag{3.44}$$

The travelling atoms in the interferometer can approximately be represented as plane waves given in equation (3.11)

$$\Psi = Ae^{i(\mathbf{k}\cdot\mathbf{r} - Et/\hbar)} \tag{3.45}$$

where A is a normalisation constant. The probability current becomes

$$\begin{aligned}\mathbf{j} &= -\frac{i\hbar}{2m}[i\mathbf{k}|\Psi|^2 + i\mathbf{k}|\Psi|^2] \\ &= -\frac{i\hbar}{2m}2i\mathbf{k}|A|^2 \\ &= |A|^2\mathbf{v},\end{aligned} \tag{3.46}$$

where $\mathbf{v}$ is the group velocity defined in equation (3.3). The probability density $\rho = |\psi(\mathbf{r})|^2$ is time independent for stationary solutions, and the continuity equation gives

$$\nabla\cdot\mathbf{j} = 0. \tag{3.47}$$

Assume the atomic movement is directed along the x-axis so that $\mathbf{j} = (|A|^2 v_x, 0, 0)$. Then equation (3.47) gives

$$\begin{aligned} \nabla \cdot \mathbf{j} = |A|^2 \frac{dv_x}{dx} = 0 \\ \Rightarrow v_x = \text{constant.} \end{aligned} \tag{3.48}$$

The speed of the atom is constant during the free propagation. Even if there is an interaction along the way, the speed is constant because the probability is conserved. In terms of the speed, the phase shift for the free propagation is

$$\begin{aligned} \alpha_1 = -\frac{1}{2} m \mathbf{v}_1^2 T_1/\hbar, \quad \alpha_2 = -\frac{1}{2} m \mathbf{v}_1^2 T_2/\hbar \\ \beta_1 = -\frac{1}{2} m \mathbf{v}_2^2 T_1/\hbar, \quad \beta_2 = -\frac{1}{2} m \mathbf{v}_2^2 T_2/\hbar, \end{aligned} \tag{3.49}$$

where $\mathbf{v}_i$ denotes the speed of the atomic state $|i\rangle$ for $i = 1, 2$. Equation (3.42) becomes

$$\phi_{\text{prop}} = -\frac{m}{2\hbar}(\mathbf{v}_2^2 - \mathbf{v}_1^2)(T_2 - T_1). \tag{3.50}$$

For the paths to be closed the propagation times is equal $T_1 = T_2$ and the propagation phase shift becomes zero. The visibility of the interference fringes is therefore not dependent on the speed distribution of the atomic ensemble.

In the absence of any interactions the atoms propagate freely between the pulses. Then $\alpha_1 = \alpha_2 = \alpha$ and $\beta_1 = \beta_2 = \beta$ because of the symmetry. The propagation phase shift is zero and $\Phi = \varphi$. The probabilities for measuring the ground state $|1\rangle$ or excited state $|2\rangle$ are only dependent on the light-interaction phase, and is given by

$$\begin{aligned} |c_1|^2 = |\langle 1|\Psi_{\text{final}}\rangle|^2 = \frac{1}{2}[1 + \cos\varphi] \\ |c_2|^2 = |\langle 2|\Psi_{\text{final}}\rangle|^2 = \frac{1}{2}[1 - \cos\varphi]. \end{aligned} \tag{3.51}$$

Consider what happens if one of the components of the wave function is subject to an interaction along its path. This interaction is illustrated with a box in the upper path before the last $\pi/2$-pulse in figure 3.5. The box may be filled with a gas or an electromagnetic field and the interaction with the traversing atom is effectively summarized in a phase shift. This phase shift denoted α_2 is generally different from the phase α_1 acquired along the lower arm after the first $\pi/2$-pulse. The phase shifts $\beta_1 = \beta_2$. Denote the interaction phase shift $\Delta\phi = \alpha_2 - \alpha_1$ so the total phase shift is $\Phi = \varphi + \Delta\phi$. The modified probabilities for measuring the different states is found from equation (3.40)

$$\begin{aligned} |c_1|^2 = |\langle 1|\Psi_{\text{final}}\rangle|^2 = \frac{1}{2}[1 + \cos(\varphi + \Delta\phi)] \\ |c_2|^2 = |\langle 2|\Psi_{\text{final}}\rangle|^2 = \frac{1}{2}[1 - \cos(\varphi + \Delta\phi)]. \end{aligned} \tag{3.52}$$

If the paths between the light-pulses are different, the phase may change. To observe the phase shift $\Delta\phi$, the interference fringes are recorded with and without the interaction. See the following section.

3.5 Detection

The purpose of the detection process is to determine the phase shift and possibly the attenuation of the atomic wave function. This is done by measuring some property dependent on the phase shift. According to equations (3.26), (3.51) and (3.52), an internal state measurement is sufficient. The atoms are fluorescent which is the property of emitting light when acted upon by radiation. A probe laser sweeps over the ensemble of atoms emerging from the interferometer, as illustrated in figure 3.6. The probe laser is resonant with either the excited

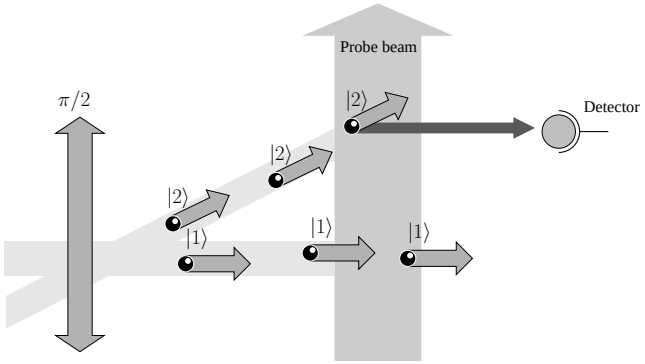

Figure 3.6: Counting number of atoms in the exited state $|2\rangle$ by sweeping the whole ensemble with a probe laser beam. Atoms in the excited state scatter photons which is counted by the detector.

state or the ground state and makes only atoms in the relevant state scatter light. These fluorescence photons are counted by a detector and the relative population is recorded. For a normalised signal the relative populations of both internal states are observed.

If the interaction is absent the internal state populations are given by equation (3.51). Variation of the light-pulse phase shift φ, while measuring the excited state, gives a reference fringe pattern. If the interaction is present the populations are given by equation (3.52). In this case, variation of φ gives a fringe pattern that deviates from the reference fringes. To determine the phase shift $\Delta\phi$, measure the deviation. This is illustrated in figure 3.7. If the interaction implies a reduction of the fringe amplitudes, the reference pattern will yield the amount of reduction.

The phase shift can be measured other ways as well. Assume the wave function is of the form (and for simplicity assume $c_1 = c_2 = 1/\sqrt{2}$)

$$|\psi_{\text{final}}\rangle = \frac{1}{\sqrt{2}}\big\{\,|1\rangle + e^{i\Phi}\,|2\rangle\,\big\} \tag{3.53}$$

where Φ is the relative phase between the two components. This phase shift is divided into two parts, $\Phi = \varphi + \Delta\phi$ where the first terms is an experimental adjustable phase and the second term is the interaction phase shift. The detection process consists of measuring some observable A. This observable is projected on the internal state basis. The amplitudes are $A_i = \langle A|i\rangle$ and it is assumed

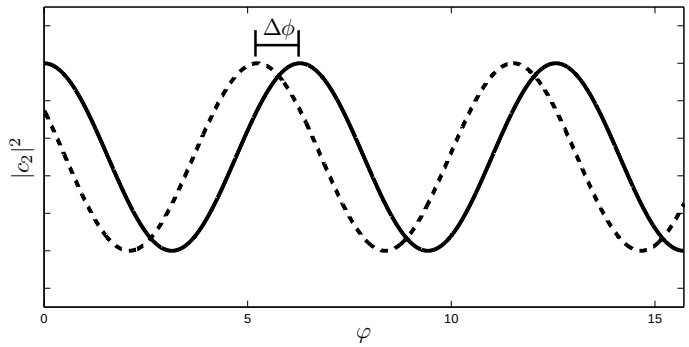

Figure 3.7: Interference fringes recorded by a detector. Uniform variation of the phase acquired inside the atom interferometer gives a uniform variation of the relative population. The phase shift $\Delta\phi$ is determined by measuring the deviation from the solid reference line (no interaction) and the dashed line. For a normalised signal the number of atoms in both states are counted.

$A_i = A_i^* \neq 0$ for $i = 1, 2$. The probability of measuring A is

$$P(A) = |\langle A|\psi_{\text{final}}\rangle|^2. \tag{3.54}$$

This probability depends on the phase shift as

$$\begin{aligned} P(A) &\propto |\langle A|1\rangle + e^{i\Phi}\langle A|2\rangle|^2 \\ &\propto (A_1^2 + A_2^2 + 2A_1A_2\cos\Phi) \\ &\propto (1 + V\cos\Phi), \end{aligned} \tag{3.55}$$

where V is the visibility. The visibility was introduced in equation (3.37). This can also be written on the form

$$V = \frac{2A_1A_2}{A_1^2 + A_2^2}. \tag{3.56}$$

This term applies to all fringe patterns not only for the open design interferometer discussed in the last section. To determine the interaction phase shift, record the probability $P(A)$ with the interaction present and absent. The fringe pattern would be of the same form as the one shown in figure 3.7, where the interaction phase shift can be determined.

Chapter 4

Applications

The atom interferometer can measure the phase shift of atoms directly. This phase shift which is accessible only through atom interferometer experiments, can provide insight into certain physical processes. As a measuring tool, the atom interferometer is very precise and may provide accurate determination of fundamental physical constants. In addition inertial displacements can be measured very precisely. The atom interferometer is also a valuable tool for studying fundamental quantum mechanical phenomena.

Three main types of applications are discussed: investigation of atomic and molecular properties, inertial forces and studies of more fundamental type.

4.1 Atomic and molecular properties

Investigation of atomic and molecular properties is in particular feasible with the interferometer design shown in figure 3.5 in chapter 3. The separated paths allow different interactions to be applied to the different components of the wave function. In this way the phase shift can give information regarding different properties under investigation. Common for the interactions discussed here is that the overall effect from the potential can be described as a constant scalar potential. That is, the interference pattern is effectively explained as if some constant potential is applied along one arm. From equation (3.15) in section 3.3 one has the general relation for the phase shift

$$\Delta\phi = \frac{1}{\hbar}(S_1 - S_2). \tag{4.1}$$

This can be written in terms of the wave vectors [49]

$$\Delta\phi = \int_\Gamma [k - k_0]dx, \tag{4.2}$$

where k_0 is the wave vector if the interaction is absent, and k is the wave vector if the interaction is present. The integral is taken along the classical path through the interaction region. If the the interaction is absent, the free particle Schrödinger equation describes the situation. This is given by

$$\left[\nabla^2 + k_0^2\right]\psi(r) = 0, \tag{4.3}$$

where k_0 is the wave vector and $\psi(r)$ is the wave function. This is related to the mass m and the energy E by the usual expression:

$$k_0^2 = \frac{2mE}{\hbar^2} \tag{4.4}$$

The overall effect for a potential confined to some region, is described as a constant potential V. The modified Schrödinger equation is

$$\left[\nabla^2 + \frac{2m}{\hbar^2}(E - V)\right]\psi(r) = 0, \tag{4.5}$$

where the wave vector can be written as

$$k^2 = \frac{2m(E - V)}{\hbar^2}. \tag{4.6}$$

Assume the energy of the atom is much smaller than the interaction energy $E = \hbar^2 k^2/2m \ll V$. In that case the difference between the wave vectors can be written

$$\begin{aligned} k - k_0 &= \frac{\sqrt{2mE}}{\hbar}(\sqrt{1 - V/E} - 1) \\ &\approx -\sqrt{\frac{m}{2E}}\frac{V}{\hbar} \\ &= -\frac{V}{\hbar v}, \end{aligned} \tag{4.7}$$

where v is the classical speed of the particle. The phase shift as a function of the potential V is given by

$$\Delta\phi = -\frac{1}{\hbar v}\int V(x)dx. \tag{4.8}$$

This relates a potential interaction along one arm to a phase shift that can be measured.

4.1.1 Polarizability

Polarizability is an atomic and a molecular property. Atoms subject to an external electric field experience a relative displacement of the atomic charge distribution. The electrons are pushed along the direction of the field and the nuclei is pushed in the opposite direction. The net effect is a polarized atom with a small dipole moment directed along the electric field. The dipole moment is proportional to the electric field

$$\mathbf{d} = \alpha\mathbf{E}, \tag{4.9}$$

where α is the *polarizability* that quantifies the polarization of the atom. For an atom the polarizability is just a number or scalar quantity. For molecules the polarizability is more complex due to the molecular structure. A scalar quantity is not enough to describe the relation between $\mathbf{d}$ and $\mathbf{E}$. In that case a matrix is used or more formally a nine component tensor, see e.g. Griffiths [25].

Many important physical properties depends on the polarizability: The dielectric constant and the refractive index (in classical optics). It is also important for calculating the index of refraction for matter waves traversing a gas (Part II). Knowledge about the polarizability can predict the outcome of quantum mechanical collision processes more precisely. In quantum collisions one is interested in the potential interaction between the involved particles. The long range interaction are determined from the so called van der Waals coefficients which depends on the polarizability (see chapter 7 in part II).

Atom interferometers are suitable for measuring polarizabilities. The atom interferometer must have separated arms, like the $\pi/2$-π-$\pi/2$ interferometer discussed in the previous chapter. To measure the polarizability apply an electric field along one arm. The box shown along with the interferometer in figure 3.5 could represent an electric field. This electric field causes a phase shift for the passing atoms which is related to the amount of polarization. The atom be-

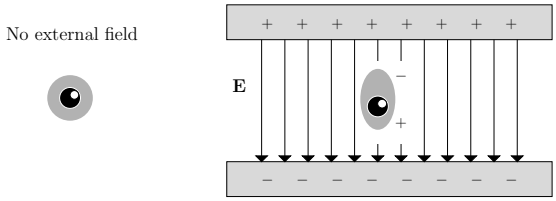

Figure 4.1: Measuring polarizability with an atom interferometer. The interferometer in figure 3.5 is drawn with a box along the upper arm. The box can represent an electric field, like the one illustrated here.

comes a dipole when traversing the electric field, see figure 4.1. To see how this is related to the phase shift, consider the potential energy U for an infinitesimal dipole in an electric field E given by

$$dU = -\alpha E dE. \tag{4.10}$$

The total potential energy is

$$U = -\int_0^E \alpha E' dE' = -\frac{1}{2}\alpha E^2. \tag{4.11}$$

The electric field is produced by two metal plates separated by a distance D, which makes a capacitor. The potential difference (applied voltage) is V and the field is applied over a length L. The electric field is $E = V/D$. For a constant field the phase shift is given by equation (4.8)

$$\begin{aligned} \Delta\varphi &= \frac{\alpha}{2\hbar v}\int_0^L E^2(x)dx \\ &= \frac{\alpha}{2\hbar v}E_0^2 L \\ &= \frac{\alpha}{2\hbar v}\frac{V^2}{D^2}L. \end{aligned} \tag{4.12}$$

where α is the polarizability. Notice how the phase shift depends on the velocity v of the passing atoms. Precise measurements requires precise determination of this velocity.

The polarizabilities for single atoms, is difficult to measure. Measurements usually rely on macroscopic quantities like the refractive index (in classical optics) or on electric deflection of a beam [39]. In 1974 Molof *et al.* [40] measured polarizabilities for some alkali atoms using the so called E-H gradient balance technique: A beam of atoms passes through a strong electric field, and experiences a dipole moment that depends on the polarizability. By measuring the deviation of the beam due to the electric field, the polarizability can be determined. Ground state polarizabilites for some atoms were measured by [40]. The numbers are given in table 4.1.

Ekstrom *et al.* [18] measured the polarizability for sodium atoms with an atom interferometer in 1995. In that experiment mechanical nanogratings were employed. They measured the ground state polarizability for sodium atoms and the value they found is given in table 4.1. Later in 2010 Holmgren *et al.* [28] measured the polarizability for several alkali atoms including sodium, see table 4.1, they also used mechanical nanogratings. In 2008 Miffre *et al.* [39] measured the polarizability for lithium using an atom interferometer with gratings of light. The main limitation on the precision were the uncertainty on the mean atomic velocity, see equation (4.12).

Atom	Method	Polarizability α	reference (year)
Li	E-H balance	24.3 ± 0.5	[40] (1974)
Li	Atom int.	24.33 ± 0.16	[39] (2008)
Rb	E-H balance	47.3 ± 0.9	[40] (1974)
Rb	Atom int.	47.24(21)	[28] (2010)
K	E-H balance	43.4 ± 0.9	[40] (1974)
K	Atom int.	43.06(21)	[28] (2010)
Na	Atom int.	24.11(6)	[18] (1995)
Na	Atom int.	24.11(8)	[28] (2010)

Table 4.1: Ground state polarizabilities for some atoms in units of $10^{-30}\mathrm{m}^3$

4.1.2 Index of refraction

The index of refraction for matter waves is an atomic property that was inaccessible to measurements before the construction of atom interferometers. The experiment consists of sending atoms through a gas and measure the modification of the physical properties due to the presence of the gas. The attenuation of the beam can be measured other ways, but the phase shift is only measurable with an atom interferometer. A detailed discussion of the origin of the refractive index is devoted to part II which concerns theoretical studies on three different systems.

The interferometer setup is equal to the setup for measuring polarizability. The box shown along with the interferometer in figure 3.5 could represent a container filled with a gas sample. The interference fringes contains information about the phase shift and the attenuation which relates to the index of refraction for the matter waves through the gas.

The first index of refraction measurement was reported by Schmiedmayer *et al.* [55] in 1995. They measured the index of refraction for sodium matter waves

through various noble gases. Their experiment was performed using an atom interferometer with mechanical nanogratings. In 2007 the first measurements of lithium matter waves through various noble gases were reported by Jacquey *et al.* [30]. They used gratings of light in their interferometer.

Measurements if the index of refraction can provide information about the interaction between the particles in the gas and the beam particles. This is discussed in depth in part II.

4.2 Inertial forces

Matter wave interferometers have the potential for being very sensitive to inertial forces. Interferometers using light are very precise measurement tools. The difference in speed of light compared to the speed of atoms is large. Consider a rotating interferometer measuring rotation where the light waves and matter waves travel the same distance. Then the ratio of the measured phase shift is [23]

$$\frac{\varphi_{\text{atom}}}{\varphi_{\text{light}}} = \frac{mc^2}{\hbar\omega}. \tag{4.13}$$

This large ratio, up to 10^{11}, suggests a higher resolution for a measurement using atoms in place of light. In addition atom interferometers can measure gravitational effects, because atoms and molecules have mass.

4.2.1 Measuring the gravitational acceleration

The $\pi/2$-π-$\pi/2$ interferometer discussed in section 3.4 is sometimes called the gravimeter. This is because this type of design can measure the gravitational constant g. The first experiment was demonstrated by Kasevich and Chu in 1992 [35]. They measured g with a resolution of $3 \cdot 10^{-8} g$. Their interferometer applied Raman transitions to manipulate the atoms.

The measured phase shift is related to the gravitational acceleration. To see the origin of this, one must consider the Raman pulses applied to the different atomic states. Before the Raman pulse the atom is (approximately) a free particle traveling along the z-axis. The wave function is given by

$$\Psi_0(z,t) = Ae^{ik'z}e^{-iEt/\hbar}, \tag{4.14}$$

where A is a normalization constant, k' is the wave vector and E is the energy of the atomic state. Depending on the internal state, the atomic momentum may change. An atom in the ground state receives a momentum $\hbar k$ from the Raman transition, where k is the effective wave vector directed along the z-axis. The Raman transition involves simultaneous absorption and emission of a photon, but the situation is described as a collision: A photon with energy $\hbar\omega$ and momentum $\hbar k$ collides with an atom. The energy and the momentum is conserved and the wave function after the light interaction is given by

$$\begin{aligned} \Psi(z,t) &= Ae^{i(k'z+kz)}e^{-i(E+\hbar\omega)t/\hbar}e^{-i\phi} \\ &= \Psi_0(z,t)e^{i(kz-\omega t-\phi)} \end{aligned} \tag{4.15}$$

where ϕ is the arbitrary phase of the lasers. The momentum transfer causes a phase shift of the atomic state. After the Raman transition the atomic state is

still a free particle. The energy is given by the Schrödinger equation

$$H\Psi(z,t) = \Big(\frac{\hbar^2 k'^2}{2m} + \frac{\hbar^2 k^2}{2m}\Big)\Psi(z,t), \tag{4.16}$$

where the energy from the light is $\hbar\omega = \hbar^2 k^2/2m$. This corresponds to a (group) velocity $v = \hbar k/m$, which is the photon recoil velocity defined in equation (2.43). If the atom is in the excited state, the momentum changes from $p + \hbar k \to p$. In that case the phase shift has the opposite sign.

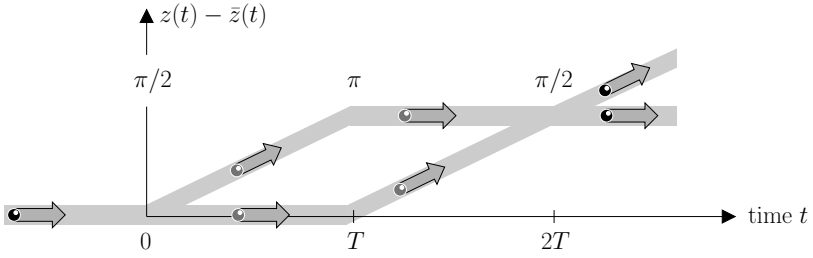

Figure 4.2: Measuring gravitational acceleration with an atom interferometer. In the gravitational field the atoms fall freely (along the z-axis). The vertical axes show the position after subtracting the free-fall trajectory $\bar{z}(t)$. The applied light pulses compensate for the Doppler shift due to the speed of the atoms.

A gravimeter is illustrated in figure 4.2. Atoms fall freely along the z-axis in the gravitational field. The vertical position $\bar{z}(t)$ in a gravitational field is given by

$$\bar{z}(t) = -\frac{1}{2}gt^2 + v_0 t + z_0, \tag{4.17}$$

where v_0 is the initial speed and z_0 is the initial position. Raman pulses along the z-axis, parallel to the atom's velocity, are applied to the falling atoms and the momentum changes accordingly. The pulse-sequence is $\pi/2$-π-$\pi/2$ and the time between the pulses is T. The vertical position after the free fall trajectory has been subtracted is shown in figure 4.2.

Since the atoms fall freely, the change in speed varies linearly in time:

$$\bar{v}(t) = v_0 - gt. \tag{4.18}$$

The atomic speed gives rise to a Doppler shift that also varies in time. Raman transitions are very sensitive to the speed of the atoms, see equation (2.34). The difference in the laser frequencies must be tuned to the resonance frequency ω_0 for the transition. Therefore the effective laser frequency is varied linearly in time (just as for the speed of the atoms) [19]:

$$\omega_{\text{eff}}(t) = \omega_0 - \gamma t, \tag{4.19}$$

where γ is adjusted to compensate for the Doppler shift of the falling atoms.

For a Raman transition applied at position $z(t)$ at time t, the phase shift is given by [19]

$$\phi_{\text{eff}}(z,t) = kz(t) - \int_0^t \omega_{\text{eff}}(\tau)d\tau - \phi(t), \tag{4.20}$$

where kz is due to the momentum change at position z, the second term corresponds to the energy absorbed from the field and $\phi(t)$ is externally adjustable. This is the same ϕ as in equation (4.15). The effective frequency varies in time and is therefore integrated over. The phase of the atom is shifted an amount $+\phi_{\text{eff}}$ when the momentum changes as $(p \to p + \hbar k)$, and $-\phi_{\text{eff}}$ when the momentum changes as $(p + \hbar k \to p)$.

Between the light pulses the acquired phase is the same for the upper and the lower path[1]. Thus the acquired phase is only due to the light pulses and is given by equation (3.41):

$$\begin{aligned}\varphi_{\text{light}} &= \phi_{\text{eff}}(z(0),0) - 2\phi_{\text{eff}}(z(T),T) + \phi_{\text{eff}}(z(2T),2T) \\ &= k[z(0) - 2z(T) + z(2T)] + 2\int_0^T \omega_{\text{eff}}(\tau)d\tau - \int_0^{2T} \omega_{\text{eff}}(\tau)d\tau \\ &\quad - \phi(0) + 2\phi(T) - \phi(2T).\end{aligned} \tag{4.21}$$

where $z(t)$ is the position at time t and the variation in the effective wave vector is neglected. At time $t = T$ (π-pulse) the vertical position is different for the two atomic states, but the phase shift from the light is the same for both. Using equation (4.17) one obtains

$$\begin{aligned}z(0) - 2z(T) + z(2T) &= z_0 + gT^2 - 2v_0T - 2z_0 - 2gT^2 + 2v_0T + z_0 \\ &= -gT^2.\end{aligned} \tag{4.22}$$

Note that this is not dependent on the initial speed v_0 of the atoms. Integration over the effective frequency gives

$$2\int_0^T (\omega_0 - \gamma\tau)d\tau - \int_0^{2T} (\omega_0 - \gamma\tau)d\tau = \gamma T^2. \tag{4.23}$$

Inserting the above into equation (4.21), one obtains the expression for the phase shift:

$$\varphi_{\text{light}} = (\gamma - kg)T^2 - \phi(0) + 2\phi(T) - \phi(2T), \tag{4.24}$$

where γ and the last three terms can be varied experimentally. To measure the phase shift, an internal state measurement is performed (discussed in section 3.5). Measure either state with a uniform variation of the phase with γ constant, to obtain a reference pattern. Then vary γ and measure the phase shift. The relation between the phase shift and g is $\Delta\varphi = (\gamma - kg)T^2$, where all but g is known.

The sensitivity can be improved by increasing the time T between light pulses. This can be achieved by using a so called atomic fountain. In an atomic fountain the atoms are launched up into the air instead of just being released. This way the atoms can fall freely for twice as long. Peters *et al.* [44] haves used an atomic fountain to measure g. They reported a resolution of $\Delta g/g = 3 \cdot 10^{-9}$.

[1]Elevation variation of 1 cm changes g by an amount $3 \cdot 10^{-9}g$ [15]. Gravity gradients become important when the accuracy becomes $10^{-9}g$. In this case the gravity field is uniform.

4.2.2 Measuring the Newtonian gravitational constant

The Newtonian gravitational constant G is the least accurately known fundamental physical constant. The constant G can be measured with an atom interferometer. One adds a well known so called source mass nearby a gravimeter, and measures by which amount the vertical acceleration varies due to its presence.

To measure G Fattori *et al.* [19] have proposed to use two atom interferometers. The two identical atom interferometers, placed upon each other, are separated by a height. Two atomic clouds are launched upward to make two atomic fountains. The Raman pulses acts on both clouds simultaneously, creating two interferometers. A source mass is placed somewhere between the atom interferometers. The source mass affects the atoms in the upper interferometer so that their acceleration is $g \rightarrow (-g - a)$, and the down most atoms so that $g \rightarrow (-g + a)$, where a is the acceleration caused by the source mass. The two interferometers produces fringes that is shifted by an amount $\Delta\phi \propto 2a$. The phase shift is insensitive to spatially homogeneous variations of g (like tidal effects), but the gravity gradient must be taken into account.

A source mass of 1 ton is able to affect the acceleration by an amount $10^{-7}g$ [19]. The experiment is repeated with the source mass at different positions. Taking the mass distribution into account one is able to predict a value for G. Fattori *et al.* [19] have proposed a targeted accuracy of $\Delta G/G \propto 100$ ppm, using atom interferometers. The recommended value of G has an uncertainty of 1500 ppm [19]

4.3 Fundamental studies

Atom interferometers can measure fundamental constants precisely, with possible implications for certain theories. The Newtonian gravitational constant appears in fundamental equations, and the fine structure constant, discussed below, is important for adjusting other physical constants. Atom interferometers can also probe the limit between classical mechanics and quantum mechanics by examining how large a object can exhibit quantum mechanical behaviour.

4.3.1 The fine structure constant

The fine structure constant α is a fundamental physical constant. It is a dimensionless quantity that determines the strength of the electromagnetic field. Atom interferometers can provide precise measurements and maybe increase the accuracy on the fine structure constant. In addition it may provide knowledge whether the fine structure constant changes over time.

The fine structure constant α is related to other physical constants:

$$\alpha^2 = \frac{2R_\infty}{c} \cdot \frac{h}{m_e}, \tag{4.25}$$

where c is the speed of light, m_e is the mass of the electron and R_∞ is the Rydberg constant. The fine structure constant can be written in terms of the atomic mass m_X [11]:

$$\alpha^2 = \frac{2R_\infty}{c} \frac{A_r(X)}{A_r(e)} \frac{h}{m_X}, \tag{4.26}$$

where $A_r(e)$ is the relative atomic mass of the electron and $A_r(X)$ is the relative atomic mass of the particle X with mass m_X. In this expression the only factor limiting the accuracy is the ratio h/m_X [11]. An atom interferometer can measure this ratio. Consider the photon recoil velocity introduced in equation (2.43):

$$v_{\text{rec}} = \frac{\hbar k}{m}, \tag{4.27}$$

where v_{rec} is the recoil speed of an atom with mass m, due to absorption or emission of a photon with wave vector k. In this relation the ratio $\hbar/m$ enters.

Cadoret *et al.* [11] have determined the ratio h/m by measuring the recoil velocity for ^{87}Rb atoms. Their atom interferometer consisted of two successive pairs of $\pi/2$-pulses. This corresponds to the $\pi/2$-$\pi/2$ interferometer (see section 3.4) applied twice to the same atoms. The coherent evolution of the atomic state holds precise information about the recoil velocity. The atoms were cooled to about 3μK using the optical molasses technique. The discussion in section 3.4 showed that colder atoms increase the visibility of the interference fringes. The result had an relative uncertainty of $4.7 \cdot 10^{-9}$ on α. The recommended value has an uncertainty of $3.7 \cdot 10^{-10}$ [11]. Further progress involves reducing sources of error, accomplished by further cooling of atoms.

4.3.2 How large a particle can interfere?

In principle there is no restriction on the size of a particle that can show interference effects. Considering material gratings, the limitations are practical: The propagation time through the interferometer and the grating dimensions. The particles must be able to pass through the openings. For a single slit the diffraction angle is given by

$$\theta_{\text{diff}} \approx \frac{\lambda_{\text{dB}}}{d}, \tag{4.28}$$

where d is the width of the slit and λ_{dB} is the de Broglie wave length of the respective particle. The particles evolves coherently from the first grating to a second grating. Denote the length between the gratings L. At the second grating the width of the wave function must span over at least two slits so that $L\theta_{\text{diff}} > d$. The length between the gratings must fulfill

$$L > \frac{d}{\theta_{\text{diff}}} = \frac{d^2}{\lambda_{\text{dB}}} > \frac{s^2}{\lambda_{\text{dB}}}, \tag{4.29}$$

where s is the diameter of the particle, that must be smaller than the width of the slits. The particle has mass density ρ. If the particle is spherical the mass is given by

$$m = \rho \cdot \frac{4}{3}\pi\left(\frac{s}{2}\right)^3 = \frac{1}{6}\pi\rho s^3. \tag{4.30}$$

The time it takes the particle to travel between the slits is $t = L/v$, where v is the speed of the particle. This relates to the de Broglie wavelength as

$$v\lambda_{\text{dB}} = \frac{h}{m} = \frac{6h}{\pi\rho s^3}, \tag{4.31}$$

where h is Planck's constant. The condition in equation (4.29) in terms of the travel time is

$$t > \frac{s^2}{v\lambda_{\text{dB}}}. \tag{4.32}$$

For a particle with mass density ρ, the time it takes to traverse the gratings, is given by

$$t > \frac{\rho \pi s^5}{6h}. \tag{4.33}$$

This is the time it would take to perform an interference experiment. A cluster of about one million sodium atoms has a size $\sim$ 30nm and mass $\sim 10^{-20}$kg [15]. This corresponds to a flight time of about 0.01 seconds. A large bacterium has diameter $\sim 2\mu$m and mass $\sim 10^{-15}$ kg. To observe interference fringes the transit time would be in the order of years [50].

The above limitations are due to mechanical gratings. Solid nanostructures has the advantage of being largely independent on the internal structure of the diffracted object. But diffraction gratings made of light omit some of the practical limitations caused by material gratings. The transmission is higher and the gratings cannot be destroyed by the diffracting particles. Nairz *et al.* [43] have used gratings of light to diffract C_{60} and C_{70} molecules. They report that conceptually, light gratings can diffract particles with a size comparable to the grating constant (the distance between the slits).

Part II

Index of refraction for matter waves through cold noble gases

Outline

The index of refraction provides an effective description of the situation when matter waves travels through a gas. The study of this process may add understanding to atomic and molecular properties. This part focuses on matter waves through cold noble gases and is meant to explain in some detail, the physics behind it and how to perform calculations. Calculations have been performed on three systems: Lithium atoms through a helium gas, lithium atoms through an argon gas and diatomic sodium molecules through a helium gas. The processes takes place in the low temperature region where certain physical properties are more evident. Measurements are only accessible through atom interferometry and in this low energy regime little experimental data exist. But for the lithium-argon system a recent (2007) experiment [30] shows consistency with the theoretical predictions.

- Chapter 5: The situation of atoms traversing a gas is illustrated and described in simple terms. The effect of the gas on the wave propagation is summarized in the index of refraction. Beer's law describing the attenuation is presented. Snell's law for matter waves is briefly discussed.
- Chapter 6: This chapter gives an overview on the quantum theory of collisions. Typical collision properties are discussed using a simple model collision. This has certain resemblances with the more realistic situations. For the latter, the collision properties is obtained numerically. The algorithm is discussed.
- Chapter 7: The gas atoms and the matter waves interact. This interaction is expressed in terms of potentials. One way of obtaining these is described. The special case of lithium-helium is discussed, along with the potential interaction between a diatomic sodium molecule and a helium atom.
- Chapter 8: The behaviour of the index of refraction can give information about the interaction potentials. A computer program calculates the number of bound states for two potentials. This calculation shows consistency with the other results.
- Chapter 9: The complex interactions taking place between the gas and the atomic waves are related to the index of refraction. A formula for the index of refraction is presented. This chapter motivates the reason and explains why studying the refractive index can provide valuable information.
- Chapter 10: The index of refraction for three systems is discussed: Lithium atoms through a helium gas, lithium atoms through an argon gas and diatomic sodium molecules through a helium gas.

Chapter 5

Index of refraction

The systems under consideration all consists of a beam of atoms or molecules passing through a noble gas medium confined to some region of space, i.e. a box, see figure 5.1. A beam of matter waves traversing a gas (medium) is generally attenuated and the phase of the matter wave is shifted. The process is described with an index of refraction. The index of refraction is a macroscopic concept

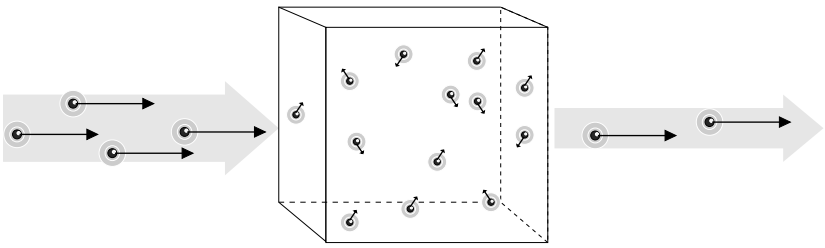

Figure 5.1: Part 2 concerns matter waves traversing a gas of noble atoms. The gas modifies the physical properties of the traversing matter wave. These can be measured with an atom interferometer. This particular situation can be identified with the box shown in figure 3.5.

which microscopic origin is atomic collisions. Atomic collisions are discussed in chapter 6. This chapter discusses the wave function with the refractive index as a macroscopic concept. The attenuation is described by Beer's law in section 5.2. In addition an analogy from optics is included: Snell's law for matter waves.

5.1 Wavelike propagation through a medium

A beam of atoms passing through a dilute gas can be described in terms of a matter wave traversing a medium with an index of refraction. Consider a beam of particles incident upon a medium with an index of refraction n. The incident particles are assumed to be described by plane waves, with a well defined energy, propagating along the x-axis. The wave function is given by

$$\psi_0 = A_0 e^{ikx}, \tag{5.1}$$

where A_0 is a normalisation constant and k is the wave vector. In the media the wave vector becomes nk, as illustrated in figure 5.2. Generally n is complex

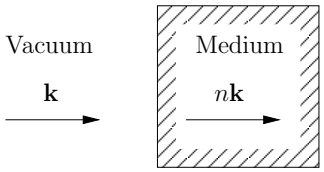

Figure 5.2: A wave propagating in vacuum is represented with a wave vector $\mathbf{k}$. The same wave propagating through a media has wave vector $n\mathbf{k}$ where n is the index of refraction.

$n = \mathrm{Re}(n) + i\mathrm{Im}(n)$. If the media has an effective length L, the wave function for the transmitted wave is given by

$$\begin{aligned}\psi_{\text{medium}} &= A_0 e^{ink\cdot L} = e^{i(n-1)k\cdot L}\psi_0 \\ &= \underbrace{e^{-\mathrm{Im}[n-1]k\cdot L}}_{\text{Attenuation}} \cdot \underbrace{e^{i\mathrm{Re}[n-1]k\cdot L}}_{\text{Phase change}} \psi_0,\end{aligned} \tag{5.2}$$

where ψ_0 is the wave function if the medium were absent. The imaginary part of the index of refraction attenuates the wave and the real part shifts the phase of the wave. Note that this summarize the net effect of many identical atoms passing through the medium. If the medium is a gas then a single atom will not reproduce the wave function. It is the net effect on an ensemble of identically prepared systems that will reproduce the wave function. The relations discussed here holds for both matter waves and light waves.

5.2 Beer's law

Consider atoms travelling through a gas confined to some region. The gas consist of noble-gas atoms that is unlikely to react with the traversing atoms. Assume the gas extends over a length denoted L. The situation is shown in figure 5.3. Some of the incident atoms does not get through the gas. They collide with

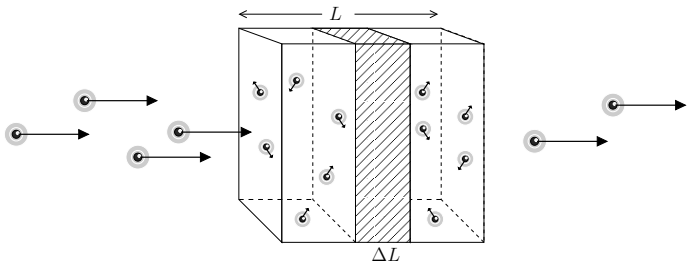

Figure 5.3: Atoms traversing a gas is scattered off due to atomic collisions.

the atoms in the gas and some of these collisions force the traversing atoms to scatter into different directions. These collision processes are complex in

nature, a detailed discussion is found in chapter 6. But the overall effect can be described in simple terms. The incident atoms is described by a flux I defined as the number of atoms per unit area incident upon the gas region. Assume the incident atomic flux has an uniform distribution over the area A that is the extension of the gas region as "seen" from the incident atoms, see figure 5.4. The flux emerging out of the gas region is generally less than the incident

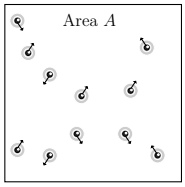

Figure 5.4: The gas as seen from the incident atoms. The probability for an incident atom to scatter off is the fraction of target area A covered by atoms.

flux. The attenuation depends on the density of the gas and the length of the gas region. Every atom in the gas makes an effective cross section denoted σ_{eff}. This effective cross section depends on the interaction between the incident atoms and the gas atoms, but is effectively described as a hard sphere area σ_{eff}. The fraction of area covered equals the probability for incident atoms to scatter off. Consider a slab of the gas with thickness ΔL. Assume the gas is dilute so that atoms in front do not overlap those behind. The density of the gas is ρ so the fraction of the area covered by atoms is $\rho\sigma_{\text{eff}}\Delta L$. Therefore the lost flux, denoted ΔI, is given by

$$\Delta I = -\rho\sigma_{\text{eff}}\Delta L I. \tag{5.3}$$

In the limit $\Delta L \to 0$ one obtains a first order differential equation:

$$\frac{dI}{dL} = -\rho\sigma_{\text{eff}} I. \tag{5.4}$$

For a gas container with length L and incident flux I_0 the solution is given by

$$I(L) = I_0 e^{-\rho\sigma_{\text{eff}}L}. \tag{5.5}$$

The fraction of lost flux becomes

$$\frac{I(L)}{I_0} = e^{-\rho\sigma_{\text{eff}}L}. \tag{5.6}$$

This relation known as Beer's law or the Beer-Lambert law. The atomic flux is attenuated. The amount of reduction depends on the density of the gas ρ, the length of the gas container L and the effective cross section σ_{eff}.

Relation to the index of refraction

Following the preceding section the attenuation of the amplitude for the wave function traveling through a media with index of refraction n was related to the imaginary part of the index of refraction. The attenuation of the transmitted intensity is the square of the wave function given by

$$\frac{I(L)}{I_0} = |e^{-\text{Im}[n-1]k\cdot L}|^2 = e^{-2\text{Im}[n-1]k\cdot L}. \tag{5.7}$$

This is equal to the fraction of lost flux described with Beer's law equation (5.6). Combining these two expressions gives an expression for the imaginary part for the index of refraction:

$$\mathrm{Im}[n-1] = \frac{\rho\sigma_{\mathrm{eff}}}{2k}. \tag{5.8}$$

The effective cross section σ_{eff} can be related to certain collision properties on an atomic scale. This is discussed in the next chapter.

5.3 Snell's law for matter waves

The index of refraction is usually encountered in relation with Snell's law from optics. This law describes the wave propagation from one media to another and is derived from Maxwell's equations with appropriate boundary conditions, see e.g. Griffiths [25]. A similar Snell's law for matter waves exists. The situation is illustrated in figure 5.5. A plane wave is incident with an angle θ upon an interface between media with a potential difference V. The incident plane wave

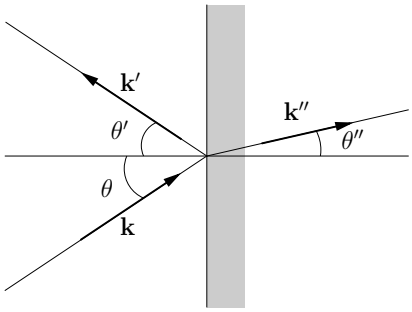

Figure 5.5: Snell's law for matter waves at oblique incidence upon a potential V for $z > 0$. The z-axis points to the right, and the x-axis points upwards.

is partially reflected and refracted at $z = 0$. The incident particles are assumed to be plane waves with a well defined energy

$$E = \frac{\hbar^2|\mathbf{k}|^2}{2m}. \tag{5.9}$$

where $|\mathbf{k}|$ is the incident wave number and m is the mass of the particle. The classical speed, see equation (3.2), for the incident and reflected wave must be equal, so that

$$|\mathbf{k}| = |\mathbf{k}'| = k. \tag{5.10}$$

The wave function consist of an incident wave, a reflected wave and an refracted wave:

$$\Psi(\mathbf{r},t) = \begin{cases} Ae^{i(\mathbf{k}\cdot\mathbf{r}-\omega t)} + A'e^{i(\mathbf{k}'\cdot\mathbf{r}-\omega t)}, & \text{if } z \le 0, \\ A''e^{i(\mathbf{k}''\cdot\mathbf{r}-\omega t)}, & \text{if } z > 0. \end{cases} \tag{5.11}$$

where A, A', A'' are constants and

$$k''^2 = \frac{2m(E-V)}{\hbar^2}. \tag{5.12}$$

The index of refraction is defined as

$$n^2 = \frac{k''^2}{k^2}. \tag{5.13}$$

In terms of the index of refraction, the time independent Schrödinger equation is given by

$$[\nabla^2 + k^2]\Psi(\mathbf{r}, t) = 0 \quad \text{for } z \leq 0, \tag{5.14}$$

$$[\nabla^2 + n^2k^2]\Psi(\mathbf{r}, t) = 0 \quad \text{for } z > 0. \tag{5.15}$$

The wave function must be continuous everywhere. At the interface the continuity requirement is

$$\left(Ae^{i(\mathbf{k}\cdot\mathbf{r}-\omega t)} + A'e^{i(\mathbf{k}'\cdot\mathbf{r}-\omega t)}\right)\Big|_{z=0} = A''e^{i(\mathbf{k}''\cdot\mathbf{r}-\omega t)}\Big|_{z=0}. \tag{5.16}$$

This must hold for all x and y. The coefficients must obey

$$A + A' = A'', \tag{5.17}$$

and the exponential factors

$$\mathbf{k}\cdot\mathbf{r} = \mathbf{k}'\cdot\mathbf{r} = \mathbf{k}''\cdot\mathbf{r}, \quad \text{at } z = 0. \tag{5.18}$$

Choosing $y = 0$ at the interface, the x-component gives

$$k\sin\theta = k''\sin\theta''. \tag{5.19}$$

This can be written in terms of the refractive index as

$$\sin\theta = n\sin\theta'', \tag{5.20}$$

which is similar to Snell's law in classical optics. The continuity condition on the derivative implies

$$A\mathbf{k} + A'\mathbf{k}' = A''\mathbf{k}'', \tag{5.21}$$

which indicates momentum conservation.

Experiments with a neutron beam refracted through a magnetic prism [33] and an iron prism [56] has been performed, see figure 5.6. For the magnetic prism the angle of refraction was measured. Data: $\theta_0 = 30^\circ$ and $n - 1 = 2.12 \cdot 10^{-6}$.

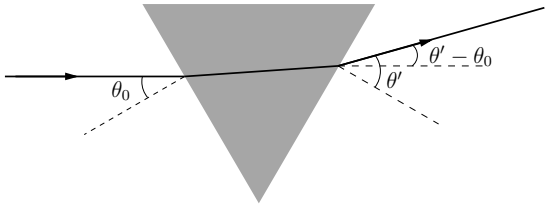

Figure 5.6: Equilateral magnetic prism used in a neutron beam experiment [33]. Snell's law predicts the direction of the refracted beam and fits the experimental data.

The angle using Snell's law for matter waves equation (5.20) is

$$\theta' - \theta_0 = 1.403 \cdot 10^{-4\circ} = 0.50508\text{arcsec}. \tag{5.22}$$

The measured angular separation is between $(0.5 - 0.9)$ arcsec [33]. Neutrons are particles without internal structure. Atoms are more complex, but Snell's law also hold for atoms. Scmiedmayer *et al.* [51] have measured the index of refraction for sodium atoms through various gases. Their results shows that the index of refraction differ from unity by a few parts per 10^{10}. Measuring refracting angles is therefore not experimentally feasible, since they will be too small. It may also be difficult to define the angle of inclination upon a medium.

Chapter 6

Atomic collisions

Atoms and molecules are systems with internal structure. Collisions involving these are complex physical processes. One separates between atom-atom and atom-molecule collisions. The latter is more complex. The typical atomic collision process consist of an incident beam of atoms colliding with some target atoms. The collision experiment is a scattering process as illustrated in figure 6.1. Interactions between the colliding atoms generally leads to a deviation in the trajectories of the incident atoms. The interaction is assumed to be confined

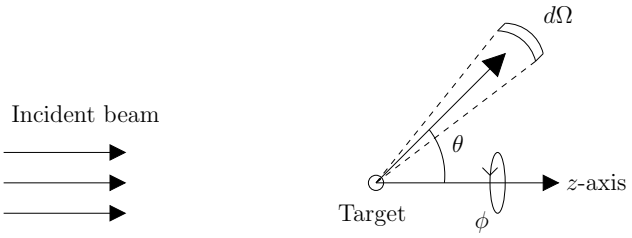

Figure 6.1: Typical collision process with an incident beam of particles with a well defined momenta. The target particles scatter the incident particles forcing it to deviate from its original path. The situation is symmetric about the z-axis.

to a region defined by the distance between them. Outside of this region the atoms do not feel the presence of each other. It is in this region that measurements are performed by measuring some quantity of interest. If the colliding particles are identical the Pauli exclusion principle comes into play. This complicates the process. Therefore only collisions between different types of particles are considered here.

Collision properties are usually expressed in terms of the so called differential cross section. The differential cross section is denoted $d\sigma/d\Omega$ and is defined as the number of states scattered in the direction (θ, ϕ) per unit solid angle per unit incident flux. All relevant information about the collision is contained in the differential cross section.

There are two types of collisions: *Elastic collisions* where the internal state of the particles are the same before and after the collision. Internal state means the atomic wave function describing the internal structure of the particles, like

spatial states of the electrons, spin etc. These can be expressed with quantum numbers. None of the collision energy affects the internal structure, therefore elastic collisions only affects the motion of the particles. The other type is *inelastic collisions* where the internal states changes in addition to motion. Some of the kinetic energy involved is transformed into rearranging the internal states. Inelastic collisions also include reactions where particles may combine to make new ones, or split up.

In order to describe a collision process the term *channel* is used. A channel is the internal quantum mechanical state of the composite system far away from the interaction region. One separates between initial and final channel. The initial channel is the internal state of the system infinitely long before the collision. The final channel is the state infinitely long after the collision. A channel is either open or closed. If the known conservation laws of physics are satisfied for a certain channel, it is open. Otherwise it is closed. The channels can be expressed in terms of quantum numbers.

6.1 Basic equations

The temperature of the colliding systems influence the outcome. The temperature T is related to the energy via the equipartition theorem

$$E = \frac{3}{2} k_{\mathrm{B}} T, \tag{6.1}$$

where k_{B} is the Boltzmann constant. If the temperature is low $\sim$mK the collision is cold. Cold collisions involves smaller velocities because the temperature relates to the speed v of the particles via

$$\frac{3}{2} k_{\mathrm{B}} T = \frac{1}{2} m v^2, \tag{6.2}$$

where m is the mass. In the low temperature regime it is convenient to use the so called partial wave expansion to express the relevant quantities. This is a series expansion of the wave function describing the system, that converges for low energies[1]. One still has to solve the Schrödinger equation, but the solutions are connected directly to the so called scattering amplitude that relates to certain physical properties, like the differential cross section.

Center of mass frame

The relevant calculations are performed in the center of mass frame for the two atoms. In this frame the collision is described as an effective one-particle potential scattering process. Incident atoms are called projectile atoms. These collide with the target atoms. The target atoms can be a gas that is assumed to be dilute. In this way the collision only involves interaction between two atoms. The projectile atoms are denoted with a subscript letter p and the target atoms are denoted with a subscript letter t. Ignoring any internal structure the two-particle Hamiltonian is given by

$$H = \frac{\mathbf{p}_p^2}{2m_p} + \frac{\mathbf{p}_t^2}{2m_t} + V(\mathbf{r}_p - \mathbf{r}_t), \tag{6.3}$$

[1] Only the fundamental relations are given, for a comprehensive treatment see e.g. Bransden [8].

where m_t is the mass of the target atoms and m_p is the mass of projectile atoms. Introducing new coordinates:

$$\mathbf{R} = \frac{m_p\mathbf{r}_p + m_t\mathbf{r}_t}{m_p + m_t}, \quad \mathbf{r} = \mathbf{r}_p - \mathbf{r}_t, \tag{6.4}$$

where $\mathbf{R}$ is the center of mass coordinate and $\mathbf{r}$ is the relative coordinate for the two atoms. Rewriting the original coordinates in terms of these:

$$\mathbf{r}_p = \mathbf{R} - \frac{m_t}{m_p + m_t}\mathbf{r}, \quad \mathbf{r}_t = \mathbf{R} + \frac{m_p}{m_p + m_t}\mathbf{r}. \tag{6.5}$$

In the center of mass frame $\mathbf{R} = 0$. To find the Hamiltonian operator in the new coordinates, first rewrite the classical kinetic energy Hamiltonian T. Then rewrite the new function in terms of operators, see e.g. Hemmer [27]. The kinetic energy function in the new coordinates becomes:

$$\begin{aligned} T &= \frac{1}{2}m_p\dot{\mathbf{r}}_p^2 + \frac{1}{2}m_t\dot{\mathbf{r}}_t^2 \\ &= \frac{1}{2}m_p\left(\frac{m_t}{m_p + m_t}\right)^2\dot{\mathbf{r}}^2 + \frac{1}{2}m_t\left(\frac{m_p}{m_p + m_t}\right)^2\dot{\mathbf{r}}^2 \\ &= \frac{1}{2}\frac{1}{(m_p + m_t)^2}(m_p m_t^2 + m_p^2 m_t)\dot{\mathbf{r}}^2 \\ &= \frac{1}{2}\frac{m_p m_t}{(m_p + m_t)^2}(m_p + m_t)\dot{\mathbf{r}}^2 = \frac{1}{2}\mu\dot{\mathbf{r}}^2, \end{aligned} \tag{6.6}$$

where the reduced mass is defined

$$\mu = \frac{m_p m_t}{m_p + m_t}. \tag{6.7}$$

The potential is only dependent on the relative coordinate and the Hamiltonian operator in the center of mass frame is given by

$$H = \frac{\mathbf{p}^2}{2\mu} + V(\mathbf{r}). \tag{6.8}$$

The projectile atoms are represented by plane waves with a well defined energy and a corresponding wave vector. In the lab frame this wave vector is denoted k_p and is related to the energy $k_p^2 = 2m_pE_p/\hbar^2$ where E_p is the energy in the lab frame. There are the fundamental relations given by

$$p_p = \hbar k_p = m_p v_p, \tag{6.9}$$

where v_p is the speed of the particle in the lab frame. The relation to the center of mass frame is given by

$$k = \frac{\mu}{\hbar}|v_p - v_t|, \tag{6.10}$$

where k is the wave vector describing the motion in the center of mass frame.

Partial wave expansion

Assume the incident beam has a well defined energy. One is therefore interested in the stationary solutions of the Schrödinger equation. In the center of mass frame the Schrödinger equation is given by

$$\Big[-\frac{\hbar^2}{2\mu}\nabla^2 + V(\mathbf{r})\Big]\psi(\mathbf{r}) = E\psi(\mathbf{r}), \tag{6.11}$$

where E is the energy. The collision energy is related to the wave vector k:

$$E = \frac{\hbar^2 k^2}{2\mu}. \tag{6.12}$$

For atom-atom collisions the potential between the colliding particles is spherical symmetric so that $V(\mathbf{r}) = V(r)$. This potential describes the energy between the atoms as a function of the distance between the nuclei. It is called the interatomic potential curve and is discussed further in chapter 7. The coordinate system is placed so that the incident particles have a well defined momentum along the z-axis. These are plane waves e^{ikz} symmetric about the z-axis with no ϕ-dependence. Because the interaction potential is spherical symmetric no process during the collision can induce any ϕ-dependence on the final state. Therefore the magnetic quantum number $m = 0$, and the physical properties are cylinder symmetric about the z-axis[2].

Any wave function describing the system can be written as a superposition of energy eigenfunctions. The energy eigenfunctions are superpositions of radial functions and the spherical harmonics. Since $m = 0$ the spherical harmonics are proportional to the Legendre polynomials

$$Y_l^0 \propto P_l(\cos\theta). \tag{6.13}$$

The Legendre polynomials P_l form a complete set for arguments between 1 and -1. The general wave function can therefore be written as

$$\psi(r,\theta) = \sum_{l=0}^{\infty} C_l \frac{\psi_l(r)}{r} P_l(\cos\theta), \tag{6.14}$$

where C_l are constants, $\psi_l(r)$ are called *partial waves* and the sum is over the orbital angular momentum quantum numbers l. This way of writing the wave function is called the partial wave expansion. There is one partial wave $\psi_l(r)$ for each l. They are the solutions of the radial Schrödinger equation given by

$$\Big[\frac{d^2}{dr^2} - \frac{l(l+1)}{r^2} - U(r) + k^2\Big]\psi_l(r) = 0, \tag{6.15}$$

where

$$k^2 = \frac{2\mu E}{\hbar^2}, \quad U(r) = \frac{2\mu V(r)}{\hbar^2}. \tag{6.16}$$

There are special cases for the wave function given in equation (6.14). If the distance $r \to \infty$ the potential is zero and the second term in equation (6.15)

[2] A formal calculation showing that $m = 0$ is done in Sakurai [47].

vanishes. Then the radial Schrödinger equation describes a free particle. In this far away region the solution takes the form

$$\begin{aligned}\psi(r,\theta) &\approx A\Big[e^{ikz} + f(k,\theta)\frac{e^{ikr}}{r}\Big] \\ &= \psi_{\text{inc}} + \psi_{\text{sc}}.\end{aligned} \tag{6.17}$$

where A is a normalisation constant and $f(k,\theta)$ is called the scattering amplitude. The first term represents an incident beam of particles and the second term represents an outgoing scattered spherical wave. This is called the asymptotic solution and is illustrated in figure 6.2. The scattering amplitude $f(k,\theta)$

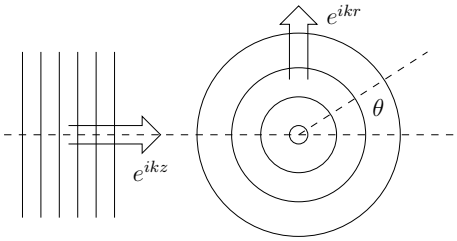

Figure 6.2: Illustration of the asymptotic solution. Incident plane waves and scattered spherical waves.

determines the spatial distribution of the outgoing waves.

The object for a collision process is to calculate the scattering amplitude $f(k,\theta)$ defined by the asymptotic solution. This is in principle possible if the interaction between the atoms is known. It is convenient to express $f(k,\theta)$ in terms of Legendre polynomials

$$f(k,\theta) = \sum_{l=0}^{\infty} f_l(k) P_l(\cos\theta), \tag{6.18}$$

where $f_l(k)$ is called the partial wave amplitudes. Notice that the angular dependence is contained in the Legendre polynomials. The partial wave amplitudes can be expressed in terms of the so called phase shifts $\delta_l(k)$ [8]

$$f_l(k) = \frac{2l+1}{2ik}\{e^{2i\delta_l(k)} - 1\} = \frac{2l+1}{k} e^{i\delta_l(k)} \sin\delta_l(k). \tag{6.19}$$

Only the phase shift is unknown so the problem is reduced to finding the phase shifts for each orbital quantum number l.

The scattering amplitude is related to the differential cross section. This can be shown by considering the probability flux for the incident and the scattered states. A good explanation is given in Hemmer [27]. The result is

$$\frac{d\sigma}{d\Omega} = |f(k,\theta)|^2. \tag{6.20}$$

From this expression one obtains the total cross section:

$$\begin{aligned}\sigma_{\text{tot}} &= \int |f(k,\theta)|^2 d\Omega \\ &= \frac{4\pi}{k^2} \sum_{l=0}^{\infty} (2l+1) \sin^2\delta_l(k).\end{aligned} \tag{6.21}$$

Determining the phase shift

To determine the phase shifts one must solve the Schrödinger equation for all r. For all collision processes discussed here, it is assumed that the potential has a finite range denoted a, where the potential becomes zero. The interaction region can be divided into an interior region and an exterior region where the range a is the intersection between the two. In the interior region the potential is generally not zero, while in the exterior region it is zero. If one is to find the phase shifts, they must enter the solutions somehow. For the exterior region, the radial part of the wave function can be written as [8]

$$R_l(k,r) = \frac{\psi_l(k,r)}{r} = B_l(k)[j_l(kr) - \tan(\delta_l(k))n_l(kr)], \quad r > a \tag{6.22}$$

where $j_l(kr)$ ($n_l(kr)$) are the Bessel (Neumann) functions of order l and B_l is some constant. Bessel functions are regular at the origin (they do not diverge as $kr \to 0$). Neumann functions has a pole of order $(kr)^l$ as $kr \to 0$. Note that if $\delta_l(k) = 0$ only the Bessel functions contribute to the solution. These makes up the solution if the potential were absent. Therefore the phase shift displays the influence of the interaction potential. The exterior solution is given but the phase shift is still not determined. One is left with the interior region. One solves the internal radial equation and this solution is joined to the exterior solution at the intersection $r = a$. The wave function and its derivative must be continuous everywhere. This is summarised in the logarithmic derivative. For the interior solution one defines

$$\gamma_l(k) = \frac{dR_l/dr}{R_l}\Big|_{r=a}. \tag{6.23}$$

This is joined to the exterior solution and the phase shift can be written

$$\tan[\delta_l(k)] = \frac{kj_l'(ka) - \gamma_l(k)j_l(ka)}{kn_l'(ka) - \gamma_l(k)n_l(ka)}, \tag{6.24}$$

where

$$j_l'(ka) = \frac{dj_l(\rho)}{d\rho}\Big|_{\rho=ka}, \quad n_l'(ka) = \frac{dn_l(\rho)}{d\rho}\Big|_{\rho=ka}. \tag{6.25}$$

To summarize, solve the radial Schrödinger equation where the potential is present. Then use the boundary conditions to relate it to the phase shifts, equation (6.24). Once the phase shifts are obtained the partial waves is found using equation (6.19). Repeat this for all relevant l to finally obtain the scattering amplitude (equation (6.18)) which is the object of interest.

6.2 A simple model

A simple model potential gives insight regarding the main features of cold atomic collisions. The process is an elastic collision between two spinless, structureless and distinguishable atoms. In terms of channels only one channel is considered. Infinitely long before the collision, the internal state for the composite system is the same as for infinitely long after. The interaction between the two atoms

is described with a simple spherical square well potential, given by

$$U(r) = \begin{cases} \infty, & r < L_0 \\ -U_0, & L_0 \leq r \leq a \\ 0, & r > a \end{cases}, \tag{6.26}$$

where U_0 is the potential depth and L_0 and a defines the range. In figure 6.7 the potential curve is drawn along with some wave functions. These wave functions are discussed later in this section. The Schrödinger equation is solved in each region. If the appropriate boundary conditions are satisfied one obtains a possible wave function for the system.

A semiclassical argument can estimate the number of partial waves that contributes. The classical relative angular momentum between two colliding particles with reduced mass μ, are given by

$$L = b\mu v \tag{6.27}$$

where v is the relative speed and b is the so called impact parameter. This is the perpendicular distance from the center of the potential (or z-axis), as illustrated in figure 6.3. The quantum mechanical angular momentum is found

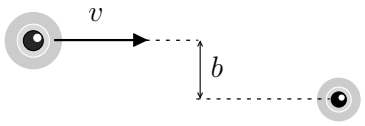

Figure 6.3: Collision between a target and projectile atom with relative speed v and impact parameter b.

by using the operator $\mathbf{L}^2$ on the angular parts of the wave function. The angular part is proportional to the Legendre polynomials because the magnetic quantum number $m = 0$. These are eigenfunctions for the total angular momentum and one has

$$\mathbf{L}^2 P_l(\cos\theta) = \hbar^2 l(l+1) P_l(\cos\theta). \tag{6.28}$$

The quantum mechanical angular momentum is $L \approx \hbar l$. Both the classical and the quantum mechanical quantity are more or less the same so that

$$\hbar l = b\mu v. \tag{6.29}$$

Now, the potential has a finite range, so for the particles to feel each others presence they must be closer than this range. If the distance is larger no interaction will occur. The potential range a gives an upper limit for the values for l that will contribute:

$$\hbar l \leq a\mu v. \tag{6.30}$$

This can be related to other properties like the temperature. The equipartition theorem relates the temperature to the speed as $\mu v^2 = 3k_B T$. One has $\mu v = \sqrt{3\mu k_B T}$, therefore only l-values satisfying

$$l \leq \frac{a\sqrt{3k_B \mu T}}{\hbar}, \tag{6.31}$$

will contribute to the scattering amplitude. This relation shows that a colder system requires less partial waves. To be specific consider lithium and helium atoms colliding with temperature $\sim$ 1mK. The reduced mass for this system is $\mu = 3661$a.u. If the potential range is $a = 15$a.u. then $l \leq 0.03$. Within a good approximation there is no relative orbital angular momentum between the atoms. Only the zeroth order partial wave contribute. This is called the s-wave and is the first term of the expansion in equation (6.14). Note that $P_0 = 1$ so the scattered s-wave is spherical for any potentials, or in other words: For very low energies the scattering is isotropic. This is a crude estimate but it shows that the partial wave expansion is useful for low temperatures. For ultracold collisions the s-wave contributes significantly. Considering only the s-wave scattering gives a good approximate description of the process.

Obtaining the phase shift

To find the phase shift one has to solve the Schrödinger equation in the interior region where the potential is present. Two types of wave functions (solutions) may exist: bound states and scattering states. Bound states have negative energy, and may exist if the potential well is deep enough. Scattering states are part of the continuous specter of states with positive energy. These are the states appropriate for describing the colliding system. Only the s-wave ($l = 0$) is calculated since the system is cold. In the exterior region the solution is given by equation (6.22). The zeroth order Bessel and Neumann functions are given in table 6.1.

Neumann	Bessel
$j_0(\rho) = \sin\rho/\rho$	$n_0(\rho) = -\cos\rho/\rho$

Table 6.1: Zeroth order Bessel and Neumann functions where $\rho = kr$.

The zeroth order phase shift denoted δ_0, is found by solving the radial equation (6.15). Once the solution is at hand, one must identify what the phase shift is. The radial equation is different for scattering and bound states due to different sign for the energy. In this case two equations are solved. For scattering states the radial equation becomes

$$\Big[\frac{d^2}{dr^2} - U(r) + k^2\Big]\psi_0(k,r) = 0. \tag{6.32}$$

According to equation (6.26) the potential has three different parts. The equation is solved separately for each. For $r < 0$ the potential is infinite so the solution is zero everywhere. For $L_0 \leq r \leq a$ the potential is equal a constant $-U_0$. This is the interior region and the solution is given by

$$\psi_0^{\text{int}}(k,r) = A\sin[k'(r - L_0)], \tag{6.33}$$

where $k'^2 = k^2 + U_0$ and A is a normalisation constant. The boundary condition at $r = L_0$ is satisfied because $\psi_0^{\text{int}}(k, L_0) = 0$. For $r > a$ the potential is zero. This is the exterior region and the solution is given by

$$\psi_0^{\text{ext}}(k,r) = B\sin(kr + \delta_0), \tag{6.34}$$

where B is a normalisation constant. The phase shift seems to suddenly appear here, but this is consistent with the more general form given in equation (6.22). To see this rewrite the solution for the exterior region:

$$\begin{aligned}\psi_0^{\text{ext}}(k,r) &= B\sin(kr+\delta_0)\\ &= B\sin(kr)\cos(\delta_0)+\cos(kr)\sin(\delta_0)\\ &= B\cos(\delta_0)[\sin(kr)+\tan(\delta_0)\cos(kr)]\\ &= C[\sin(kr)+\tan(\delta_0)\cos(kr)].\end{aligned}$$

Divide with r to return to the more general form given in equation (6.22):

$$\begin{aligned}R_0(k,r) = \frac{\psi_0(k,r)}{r} &= Ck[\frac{\sin(kr)}{kr}+\tan(\delta_0)\frac{\cos(kr)}{kr}]\\ &= B_0[j_0(kr)-\tan(\delta_0)n_0(kr)].\end{aligned} \tag{6.35}$$

The boundary conditions at $r=a$ must be satisfied. By joining the solution in the interior and the exterior region one finds that

$$\begin{aligned}\left.\frac{d\psi_0^{\text{ext}}/dr}{\psi_0^{\text{ext}}}\right|_{r=a} &= \left.\frac{d\psi_0^{\text{int}}/dr}{\psi_0^{\text{int}}}\right|_{r=a}\\ k\cot(ka+\delta_0) &= k'\cot[k'(a-L_0)]\\ \tan(ka+\delta_0) &= \frac{k}{k'}\tan[k'(a-L_0)].\end{aligned} \tag{6.36}$$

In equation (6.24) a more general relation was presented for the phase shift. That way of writing the phase shift may be more convenient. For the interior region one needs to determine $\gamma_0(k)$ from equation (6.23):

$$\begin{aligned}\gamma_0(k) &= \left.\frac{dR_0^{\text{int}}/dr}{R_0^{\text{int}}}\right|_{r=a}\\ &= \frac{k'\cos[k'(a-L_0)]/a-\sin[k'(a-L_0)]/a^2}{\sin[k'(a-L_0)]/a}\\ &= k'\cot[k'(a-L_0)]-1/a.\end{aligned} \tag{6.37}$$

In addition one needs the derivative of the Bessel and Neumann functions from equation (6.25):

$$j_0'(ka) = \frac{ka\cos(ka)-\sin(ka)}{k^2a}, \quad n_0'(ka) = \frac{ka\sin(ka)+\cos(ka)}{k^2a} \tag{6.38}$$

Expressed in the form given by equation (6.24), the phase shift can be written

$$\tan\delta_0 = \frac{k\tan[k'(a-L_0)]-k'\tan(ka)}{k'+k\tan(ka)\tan[k'(a-L_0)]}. \tag{6.39}$$

In addition equation (6.36) gives the explicit form of the phase shift

$$\delta_0 = -ka+\arctan\left(\frac{k}{\sqrt{k^2+U_0}}\tan[\sqrt{k^2+U_0}(a-L_0)]\right). \tag{6.40}$$

The phase shift is the desired result. This displays the potential interaction and the next step involves further investigation.

Investigation of the phase shift

The phase shift has certain physical implications. It is of interest to observe the behaviour of the phase shift δ_0 with respect to the potential depth U_0. The ranges of the potential is exemplified by the specific values: $L_0 = 8$a.u. and $a = 15$a.u.. With this ranges, the behaviour of δ_0 is plotted in figure 6.4. The

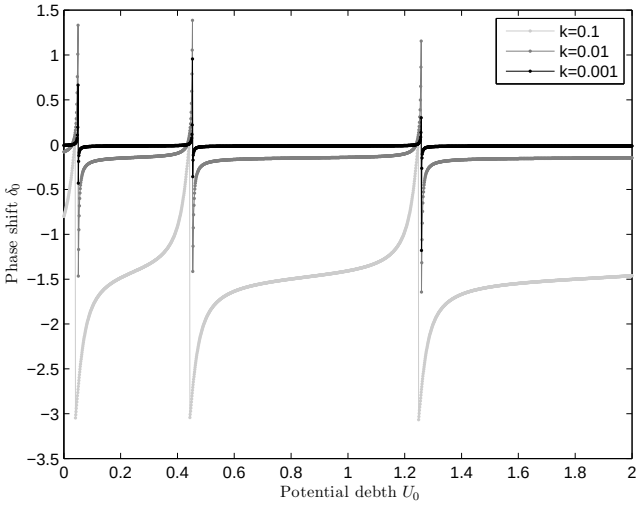

Figure 6.4: Variation of the phase shift δ_0 with respect to the potential depth U_0, with $L_0 = 8$ and $a = 15$. To get the absolute value of the phase shift follow the evolution from $U_0 = 0$ and for each divergence add $\pm\pi$ to the phase. Three different values of k are included.

periodic divergences are related to properties of the potential. If the potential depth increases it would allow more bound states to exist. Consider the partial wave amplitudes given in in equation (6.19). Adding π to the phase shift will not alter the amplitude because:

$$e^{i(\delta_0+\pi)} \sin(\delta_0 + \pi) = e^{i\delta_0} \sin\delta_0. \tag{6.41}$$

Defining the absolute phase shift to be zero when the potential is zero, the true value is obtained by following the evolution from $U = 0$ to $U = U_{\text{final}}$ and for each divergence add π, see figure 6.4. If the potential depth is $U_{\text{final}} = 1$, the phase shift for $k = 0.1$ is ≈ -1.5. However, the true value is $-1.5 + 2\pi$ because of the two divergences. The scattering amplitude is not dependent on the true value of the phase shift, but for the wave function this is not the case. To see this, consider ψ_0^{ext} from equation (6.34). Adding π changes the sign of the wave function, because $\sin(\delta_0 + \pi) = -\sin(\delta_0)$. If the wave function is of interest, the true value must be used as this ensures continuity.

An important feature of low-energy collisions is that the process is effectively described as a hard-sphere scattering process. This means that any interaction potential acts as a hard sphere with radius A_0. The radius A_0 is the so called

scattering length. This is defined in terms of the phase shift [8]

$$A_0 = -\lim_{k\to 0}\frac{\tan(\delta_0(k))}{k}. \tag{6.42}$$

There is not an unique scattering length for every potential, because different potentials can give the same scattering length. If the phase shift does not diverge for zero energy, the scattering length can be written as [8]

$$A_0 = -\lim_{k\to 0}\frac{\sin(\delta_0(k))}{k}. \tag{6.43}$$

One can find the total cross section from the scattering amplitude using equation (6.21). In the low energy limit (only $l = 0$ contributes) this is

$$\begin{aligned}\lim_{k\to 0}\sigma_{\text{tot}} &= \lim_{k\to 0}\frac{4\pi}{k^2}\sin^2\delta_l(k)\\ &= 4\pi A_0^2.\end{aligned} \tag{6.44}$$

This is four times the cross section of a sphere with radius A_0.

For the simple model potential the scattering length is found using equation (6.39):

$$\begin{aligned}A_0 &= -\lim_{k\to 0}\frac{\tan(\delta_0(k))}{k}\\ &= -\lim_{k\to 0}\frac{k'\tan(ka)/k - \tan[k'(a-L_0)]}{k' + k\tan(ka)\tan[k'(a-L_0)]}\\ &= a - \frac{\tan[\sqrt{U_0}(a-L_0)]}{\sqrt{U_0}}.\end{aligned} \tag{6.45}$$

The scattering length as a function of the potential depth U_0 is shown in figure 6.5. This also exhibits periodic divergences like the phase shift in figure 6.4.

For ultracold and dilute gases the effective potential interaction is proportional to the scattering length. In the limit $k \to 0$ one has [3]

$$V_{\text{eff}}(r) \propto A_0. \tag{6.46}$$

If the scattering length is negative ($A_0 < 0$) the overall effect is an attractive interaction. For positive scattering lengths ($A_0 > 0$) the overall effect is a repulsive interaction. According to figure 6.5, a slight change in the potential depth may result in a change from a repulsive to an attractive potential interaction. Consequently the sign of the phase shift changes.

The divergences in the scattering length are closely linked to the appearance of bound states in the potential. Each divergence corresponds to a possible bound state for the composite system. To see if any bound states can exist one must solve the Schrödinger equation. The radial equation (6.15) becomes

$$\Big[\frac{d^2}{dr^2} + U(r) - \xi^2\Big]\psi_0(\xi, r) = 0, \tag{6.47}$$

where $\xi^2 = 2\mu E_B/\hbar^2$ and the energy is negative $E = -E_B$. The solutions are:

$$\begin{aligned}R_B^{\text{int}}(k', r) &= A'\frac{\sin[k'(r-L_0)]}{r}\\ R_B^{\text{ext}}(\xi, r) &= B'\frac{e^{-\xi r}}{r}\end{aligned} \tag{6.48}$$

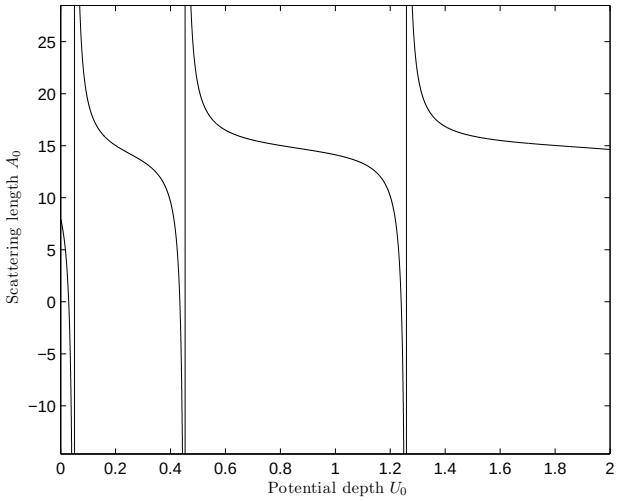

Figure 6.5: The scattering length A_0, for potentials with $L_0 = 8$ and $a = 15$, as a function of the potential depth U_0.

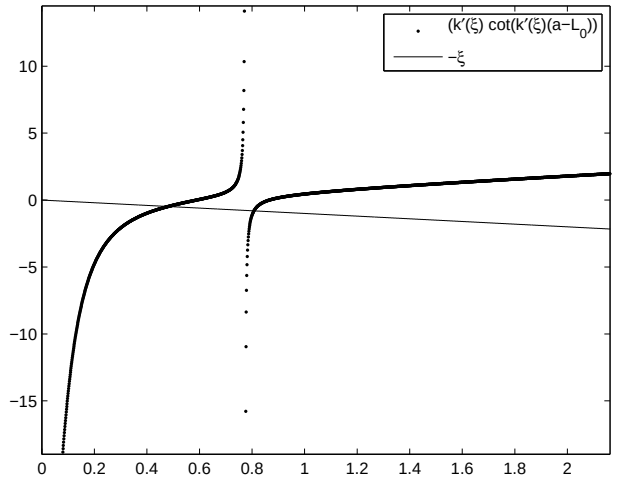

Figure 6.6: At each intersection the boundary conditions is satisfied. The potential depth is $U_0 = 0.8$ and equation 6.49 is satisfied only twice and thus restricting the possible states.

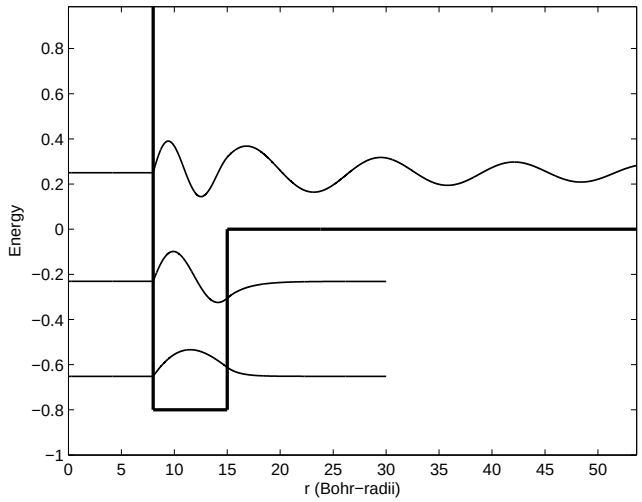

Figure 6.7: The wave functions (not normalised) for the two bound states and one scattering state with $k = 0.5$. Notice how the wave functions decay exponentially into the classically forbidden region.

where $k'^2 = -\xi^2 + U_0$ and A' and B' are normalisation constants. The subscript B labels bound states. The solution in the interior region are equal to the solution obtained for scattering states. But for the exterior region ($r > a$) the solution is different. Here the wave function decays exponentially into the classically forbidden region. Applying the boundary conditions at $r = a$ gives the following condition for bound states

$$k'(\xi)\cot[k'(\xi)(a - L_0)] = -\xi. \tag{6.49}$$

Fixing the potential depth U_0, the number of bound states should equal the number of times equation (6.49) are fulfilled. This is a transcendental equation solved graphically for ξ in figure 6.6, with a potential depth $U_0 = 0.8$. According to the scattering length shown in figure 6.5, the well should support only two bound states. This is consistent with figure 6.6 where the conditions for bound states are satisfied twice. The two points of intersection are

$$\begin{aligned} \xi_0 &= 0.4807 \\ \xi_1 &= 0.8072. \end{aligned} \tag{6.50}$$

Figure 6.7 displays the wave function for the two bound states and one scattering state. The normalisation constants A' and B', see equation (6.48), enables the continuity while equation (6.49) ensures continuity in the derivative. In addition the true value of the phase shift is employed to ensure continuity. If the system is in one of the bound states, the two atoms is called a molecule. The first bound state with the lowest energy corresponds to the ground state and the second bound state corresponds to an excited state of the molecule. This could be some vibrational energy level.

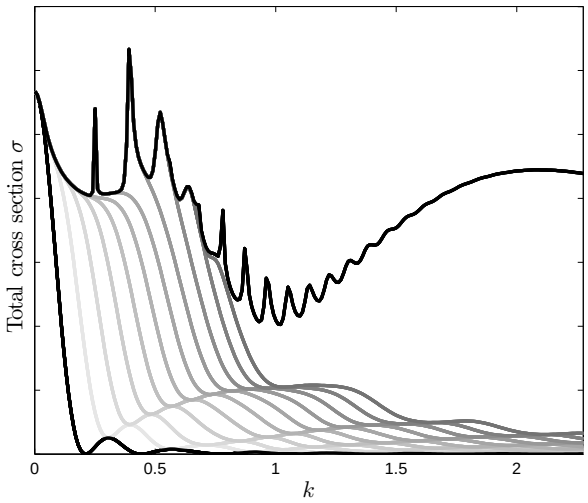

Figure 6.8: The figure displays the cross section σ as a function of k, and is understood as follows: The two black curves are the s-wave (down-left corner) and the complete scattering amplitude, within a convergence criteria. In between are the $1-10$ first terms of the scattering amplitude included. The partial waves for $l > 0$ are obtained numerically. For lower temperatures (lower k) the s-wave dominates.

The scattering amplitude

The reason for determining the phase shifts is to determine the scattering amplitude that is related to certain physical quantities. One important quantity is the total scattering cross section. This is connected to the scattering amplitude via the optical theorem given by:

$$\sigma_{\text{tot}} = \frac{4\pi}{k}\text{Im}[f(k,0)], \tag{6.51}$$

where $f(k,0)$ is the forward scattering amplitude (this is the scattering amplitude for $\theta = 0$). The phase shift for $l = 0$ gives the first term of the scattering amplitude equation (6.18). In the low temperature limit the scattering amplitude is approximately equal its first term, because the s-wave dominates. The forward scattering amplitude for s-wave scattering is therefore equal the zeroth order partial wave. From equation (6.19) one obtains:

$$\begin{aligned} f_0(k) &= \frac{1}{k}e^{i\delta_0(k)}\sin\delta_0(k) \\ &= \frac{1}{k}(\cos\delta_0(k)\sin\delta_0(k) - i\sin^2\delta_0(k)). \end{aligned} \tag{6.52}$$

Only considering the s-wave, the total cross section becomes

$$\sigma_{\text{tot}} = \frac{4\pi}{k^2}\sin^2\delta_0(k). \tag{6.53}$$

The total cross section is plotted in figure 6.8 as a function of k. Some higher order partial waves are included as well. The expansion in equation (6.18) is

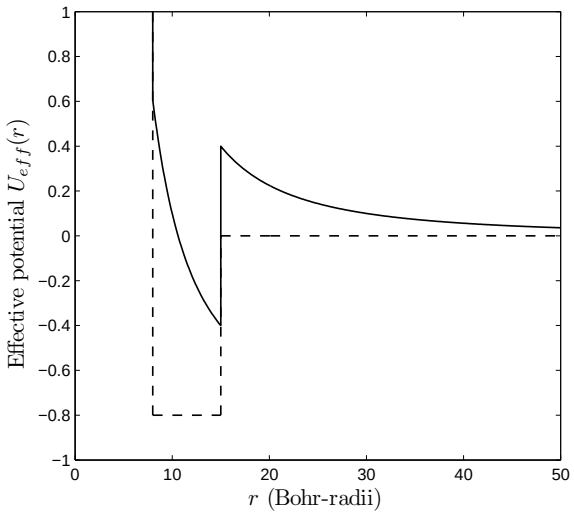

Figure 6.9: Effective potential for the 9'th partial wave with $l = 9$. The dashed line is the square well. This effective potential may allow quasi bound states to exist.

calculated numerically for $l = 1$ to $l = 10$. In addition the exact scattering amplitude is calculated. Exact means that the scattering amplitude is exact within a convergence criteria. The numerical procedure is discussed more in section 6.4. Starting with the s-wave down in the left corner, the following curves corresponds to one more partial wave added to the expansion in equation (6.18), until the exact amplitude (black curve). One can see from figure 6.8 that for low values of k the s-wave dominates the total cross section.

The total cross section with all partial waves included, exhibit a spike-like oscillating behaviour. These spikes are due to resonances. Resonances occur when a partial wave has the same energy as a bound state. This is not the bound states shown in figure 6.7, since the incident atoms have energy greater than zero. Rather so called quasibound states may exist. To see the origin of these, consider the potential term in equation (6.15). For $l > 0$ the effective potential for the radial equation is

$$U_{\text{eff}}(r) = \frac{l(l+1)}{r^2} + U(r), \tag{6.54}$$

where the first term is called the centrifugal term. Partial waves with orbital angular momentum $l \neq 0$ has an effective potential with a centrifugal barrier. This is illustrated in figure 6.9 for the ninth partial wave with $l = 9$. The square-well is drawn for comparison. This centrifugal barrier may allow quasibound states to exist. A resonance occur if the collision energy coincides with the energy of a quasibound state. These quasibound states are metastable. The particles are trapped in the effective potential and can only escape by tunneling through the potential barrier. Consequently the corresponding cross section for that given partial wave becomes very large. If the energy is low a small number of partial waves contributes and the resonant term contributes significantly to

the total cross section. For higher energies more partial waves must be included in the scattering amplitude. Therefore a large cross section due to a resonance for some partial wave contributes less to the total cross section. This is clearly displayed in 6.8. As the collision energy ($\propto k$) increases the spikes becomes less apparent, before they disappear.

6.3 Multichannel scattering

To describe collisions involving more realistic atoms and molecules the internal structure must be included. The basic equations discussed in section 6.1, are generalized. For the one channel elastic collision discussed in the preceding section, scalars were enough to describe the system. In an inelastic collision process the system is described with matrices. Off-diagonal elements can represent coupling between different internal structures before and after the collision.

The special case of a diatomic molecule colliding with an atom is discussed. This is general enough to also describe collisions involving only atoms. The collision can be inelastic, but no reactions are allowed. Reactions are processes where the final particles are different from the initial particles. There is not enough energy involved to ionize the atoms or split up the molecule since the system is cold. Thus the particles are the same after the collision. The equations are given in atomic units, where $\hbar = 1$.

Initially the system is specified by the internal state of the molecule and the collision energy. Projectile particles are described with initial channels, specified by a set of quantum numbers. These describe the relative orbital motion of the particles and the internal state of the molecule. Each projectile particle is in some initial state. This initial state can be a superposition of many channels since it depends on the relative motion of the colliding particles. Therefore the initial system is in various initial channels with a certain probability. The collision energy determines the number of possible collision events. If the collision energy allows N open channels, there is N different collision processes for an initial channel. The initial channels can be any of the open channels. Likewise the final channels can be any of the open channels. Since there are N initial channels there are N^2 different processes that may occur. In a calculation all these events must be described. A convenient way to express it, is the so called scattering matrix or the S-matrix. This is a $N \times N$ matrix where each element S_{ji} contains the relevant information connecting initial channel i with final channel j. From the S-matrix, certain collision properties like the forward scattering amplitude may be calculated.

The rigid rotator

The sodium molecule consists of two sodium atoms bound together. One assumes the separation between the atoms to be a fixed distance R. This way the molecule is treated as a rigid rotator. The Hamiltonian for the two atoms with masses m_1 and m_2, is

$$H = -\frac{1}{2m_1}\nabla_1^2 - \frac{1}{2m_2}\nabla_2^2, \tag{6.55}$$

where the potential term is zero. The two atoms are treated as free particles, only restricted by the fixed distance. According to equation (6.6), in the center

of mass frame, the Hamiltonian can be written as

$$H = -\frac{1}{2\mu}\nabla^2, \tag{6.56}$$

where μ is the reduced mass $\mu = m_1 m_2/(m_1 + m_2)$. The two atoms making up the molecule have equal masses $m_1 = m_2 = m$. The moment of inertia about an axis perpendicular to the internuclear axis, and through the center of mass is given by

$$I = \sum_i m_i r_i^2 = \frac{m}{2}R^2 = \mu R^2. \tag{6.57}$$

In spherical coordinates the Laplace operator is given by

$$\nabla^2 = \frac{1}{R^2}\frac{\partial}{\partial R}\Big(R^2\frac{\partial}{\partial R}\Big) - \frac{\mathbf{j}^2}{R^2}, \tag{6.58}$$

where $\mathbf{j}^2$ is the operator of the square of the rotational angular momentum. In the rigid rotator approximation, the derivation with respect to the radial coordinate vanish because the distance is fixed. Consequently the Schrödinger equation becomes

$$\frac{1}{2I}\mathbf{j}^2\chi = E\chi, \tag{6.59}$$

where χ describes the internal state of the molecule. The wave function describing the rotator must have cyclic boundary conditions. These conditions imply that the rotational energy is quantized.

The eigenfunctions for $\mathbf{j}^2$ are the spherical harmonics Y_{jm_j}. Therefore the Hamiltonian H_{int} describing the internal rotation of the rigid rotator has an eigenvalue given by

$$H_{\text{int}}Y_{jm_j} = \frac{1}{2I}j(j+1)Y_{jm_j}, \tag{6.60}$$

where $j = 0, 1, 2, \ldots$ is the rotational quantum number and $m_j = 0, \pm 1, \ldots, \pm j$ is the projection of the angular momentum along a quantization axis fixed in space. The rotational energy of the rigid rotator is given by

$$E_j = \frac{1}{2I}j(j+1). \tag{6.61}$$

This is dependent on j, but not on m_j, so for each energy E_j, $2j+1$ levels are possible.

To describe the molecule one must consider the translational movement of the center of mass in addition to the rotational movement. For $j = 0$ there is no rotation and the rotational energy is zero. For $j > 0$ the molecule rotates and has rotational energy.

The total wave function

The system is a diatomic molecule colliding with an atom. In the center of mass frame the collision process is described as a potential scattering by a rigid rotator. The total Hamiltonian in the center of mass frame is given by

$$H = -\frac{1}{2\mu}\nabla^2(\mathbf{r}) + H_{\text{int}} + V(\mathbf{r}, \mathbf{R}), \tag{6.62}$$

where μ is the reduced mass for the total system (atom+molecule), $V(\mathbf{r}, \mathbf{R})$ is the interaction potential between the projectile and the target particles and H_{int} describes the internal state of the molecule. The vectors specifying the system is given by

$$\begin{aligned} \mathbf{r} &= (r, \theta, \phi) \\ \mathbf{R} &= (R, \theta', \phi'), \end{aligned} \tag{6.63}$$

where r is the distance between the colliding particles, R is the fixed separation between the atoms in the molecule. The angles specifies the orientation of the system with respect to a coordinate system fixed in space.

The two sources of angular momentum is the relative orbital angular momentum $\mathbf{L}$ between colliding particles and the rotational angular momentum $\mathbf{j}$ of the molecule. The composite system has a total angular momentum $\mathbf{J}$. The latter is related to the others as

$$\mathbf{J} = \mathbf{j} + \mathbf{L}. \tag{6.64}$$

This is a sum of operators where the corresponding quantum numbers are J, j and l. No external torque acts on the system. Therefore, during the collision process the total angular momentum is conserved. The projection of the total angular momentum is also conserved

$$M_J = m_l + m_j, \tag{6.65}$$

where the quantized value of $\hat{J}_z$ is denoted M_J, and likewise for $\hat{L}_z$ and $\hat{j}_z$. The angular momentum operators has the following properties:

$$\begin{aligned} \mathbf{L}^2 Y_{lm_l}(\theta, \phi) &= l(l+1) Y_{lm_l}(\theta, \phi) \\ \mathbf{j}^2 Y_{jm_j}(\theta', \phi') &= j(j+1) Y_{jm_j}(\theta', \phi') \\ \mathbf{J}^2 \mathcal{Y}_{jlJM_J}(\theta, \phi, \theta', \phi') &= J(J+1) \mathcal{Y}_{jlJM_J}(\theta, \phi, \theta', \phi'), \\ \hat{J}_z \mathcal{Y}_{jlJM_J}(\theta, \phi, \theta', \phi') &= M_J \mathcal{Y}_{jlJM_J}(\theta, \phi, \theta', \phi'), \end{aligned} \tag{6.66}$$

where Y_{lm_l} are the spherical harmonics and $\mathcal{Y}_{jlJM_J}$ is an eigenfunction of the square of the total angular momentum and the projection of the total angular momentum. The composite system can be described with a state $|jm_j lm_l\rangle = Y_{lm_l} Y_{jm_j}$, where the labeled quantum numbers are well defined. It is more convenient to describe the system in terms of states specifying the total angular momentum J and projection M_J, since these are conserved. A change of representation to a basis where J, M_J, j and l are well defined, is given by

$$\mathcal{Y}_{jlJM_J}(\theta, \phi, \theta', \phi') = \sum_{m_l, m_j} \langle jm_j lm_l | JM_J \rangle \, Y_{lm_l}(\theta, \phi) Y_{jm_j}(\theta', \phi'), \tag{6.67}$$

where $\langle jm_j lm_l | JM_J \rangle$ are the Clebsch-Gordan coefficients. When combining states with different angular momenta, certain restrictions apply. These restrictions are included in the Clebsch-Gordan coefficients. Note that in this new basis the projection quantum numbers m_j and m_l are not well defined.

The function $\mathcal{Y}_{jlJM_J}$ is a simultaneous eigenfunction for $\mathbf{j}^2$ and $\mathbf{L}^2$. For the internal Hamiltonian from equation (6.60), one has

$$H_{\text{int}} \mathcal{Y}_{jlJM_J} = E_j \mathcal{Y}_{jlJM_J}. \tag{6.68}$$

The stationary scattering states (the wave function) $\psi(\mathbf{r}, \mathbf{R})$ describing the total system, fulfills the Schrödinger equation in the center of mass frame:

$$H\psi(\mathbf{r}, \mathbf{R}) = E\psi(\mathbf{r}, \mathbf{R}), \tag{6.69}$$

where H was given in equation (6.62) and E is the collision energy. The collision energy was introduced in equation (6.12). Since the molecule has rotational energy, the relative translational energy in the center of mass frame, is given by

$$E - E_j = \frac{k_j^2}{2\mu}, \tag{6.70}$$

where k_j is the wave vector describing the relative motion, and E_j is the rotational energy of the molecule with rotational quantum number j. The rotational state of the molecule is experimentally accessible, in the sense that one may prepare an ensemble of molecules where all has the same rotational state.

The wave function is an eigenfunction of the total angular momentum and its projection $\psi(\mathbf{r}, \mathbf{R}) = \psi_{JM_J}(\mathbf{r}, \mathbf{R})$, and are labeled with these quantum numbers. The wave function is expanded in terms of eigenstates of the total angular momentum:

$$\psi_{JM_J}(\mathbf{r}, \mathbf{R}) = \frac{1}{r}\sum_{jl} \phi_{jlJM_J}(r)\mathcal{Y}_{jlJM_J}(\theta, \phi, \theta', \phi'). \tag{6.71}$$

This expansion is similar to the one in equation (6.14). The wave function is separated into an angular part, and a part only depending on the distance r. The angular part is known, because the spherical harmonics are known and the Clebsch-Gordan coefficients are known. One is left with the radial part. Due to this separation of the wave function, the Schrödinger equation can be expressed in a form similar to the radial equation (6.15). This is the next step.

Obtaining the close-coupled equations

One can rewrite the Schrödinger equation (6.69) by inserting the wave function in equation (6.71). Then multiply with $\mathcal{Y}^*_{jlJM_J}$ and integrate over all the angles $d\Omega = d(\theta, \phi, \theta', \phi')$. The spherical harmonics are orthogonal, so

$$\int_0^{2\pi}\int_0^{\pi} Y^*_{lm_l}(\theta, \phi)Y_{l'm_{l'}}(\theta, \phi)\sin\theta d\theta d\phi = \delta_{ll'}\delta_{m_l m_{l'}}. \tag{6.72}$$

Integrating over the eigenfunctions for the total angular momentum, gives

$$\begin{aligned}
\int \mathcal{Y}^*_{jlJM_J}\mathcal{Y}_{j'l'J'M'_J}d\Omega &= \int d\Omega \sum_{m_l, m_j} \langle jm_j lm_l|JM_J\rangle\, Y_{lm_l}Y_{jm_j} \\
&\times \sum_{m_{l'}, m_{j'}} \langle j'm_{j'}l'm_{l'}|J'M_{J'}\rangle\, Y_{l'm_{l'}}Y_{j'm_{j'}} \\
&= \sum_{m_l, m_j}\sum_{m_{l'}, m_{j'}} \langle jm_j lm_l|JM_J\rangle\, \langle j'm_{j'}l'm_{l'}|J'M_{J'}\rangle \\
&\quad \times \delta_{ll'}\delta_{m_l m_{l'}}\delta_{jj'}\delta_{m_j m_{j'}} \\
&= \sum_{m_l, m_j} \langle jm_j lm_l|JM_J\rangle\, \langle jm_j lm_l|J'M_{J'}\rangle\, \delta_{ll'}\delta_{jj'} \\
&= \delta_{JJ'}\delta_{M_J M_{J'}}\delta_{ll'}\delta_{jj'},
\end{aligned} \tag{6.73}$$

where an orthogonality property for the Clebsch-Gordan coefficients is used before the last line.

Each term in the Hamiltonian in equation (6.62) is calculated separately. In spherical coordinates the Laplace operator is given by

$$\nabla^2 = \frac{1}{r^2}\frac{\partial}{\partial r}\Big(r^2\frac{\partial}{\partial r}\Big) - \frac{\mathbf{L}^2}{r^2}, \tag{6.74}$$

where $\mathbf{L}^2$ is the operator of the square of the orbital angular momentum. The Laplace operator acting on the wave function becomes:

$$\begin{aligned}
\int d\Omega \mathcal{Y}^*_{jlJM_J} \nabla^2 \psi(\mathbf{r},\mathbf{R}) &= \int d\Omega \mathcal{Y}^*_{jlJM_J} \frac{1}{r^2}\frac{\partial}{\partial r}\Big(r^2\frac{\partial}{\partial r}\Big)\frac{1}{r}\sum_{j'l'}\phi_{j'l'J'M'_J}(r)\mathcal{Y}_{j'l'J'M'_J} \\
&\quad - \int d\Omega \mathcal{Y}^*_{jlJM_J} \frac{\mathbf{L}^2}{r^2}\frac{1}{r}\sum_{j'l'}\phi_{j'l'J'M'_J}(r)\mathcal{Y}_{j'l'J'M'_J} \\
&= \sum_{j'l'}\int \mathcal{Y}^*_{jlJM_J}\mathcal{Y}_{j'l'J'M'_J} d\Omega \frac{1}{r^2}\frac{\partial}{\partial r}\Big(r^2\frac{\partial}{\partial r}\Big)\frac{1}{r}\phi_{j'l'J'M'_J}(r) \\
&\quad - \sum_{j'l'}\frac{1}{r^3}\phi_{j'l'J'M'_J}(r) l'(l'+1)\int \mathcal{Y}^*_{jlJM_J}\mathcal{Y}_{j'l'J'M'_J} d\Omega \\
&= \frac{1}{r}\frac{d^2}{dr^2}\phi_{jlJM_J}(r) - \frac{1}{r}\frac{l(l+1)}{r^2}\phi_{jlJM_J}(r).
\end{aligned}$$

In the last term the radial part of the Laplace-operator is given by

$$\begin{aligned}
\frac{1}{r^2}\frac{\partial}{\partial r}\Big(r^2\frac{\partial}{\partial r}\Big)\frac{\phi}{r} &= \frac{1}{r^2}\frac{\partial}{\partial r}\left\{r^2\Big(\frac{1}{r}\frac{d\phi}{dr} - \frac{\phi}{r^2}\Big)\right\} \\
&= \frac{1}{r^2}\frac{\partial}{\partial r}\left\{r\frac{d\phi}{dr} - \phi\right\} \\
&= \frac{1}{r^2}\left\{\frac{d\phi}{dr} + r\frac{d^2\phi}{dr^2} - \frac{d\phi}{dr}\right\} \\
&= \frac{1}{r}\frac{d^2\phi}{dr^2}.
\end{aligned}$$

For the internal Hamiltonian one has

$$\begin{aligned}
&\int \mathcal{Y}^*_{jlJM_J} H_{\text{int}} \frac{1}{r}\sum_{j'l'}\phi_{j'l'J'M'_J}(r)\mathcal{Y}_{j'l'J'M'_J} d\Omega \\
&\qquad = \frac{1}{r}\sum_{j'l'}\phi_{j'l'J'M'_J} E_{j'}\int \mathcal{Y}^*_{jlJM_J}\mathcal{Y}_{j'l'J'M'_J} d\Omega \\
&\qquad = \frac{1}{r}\phi_{jlJM_J}(r) E_j .
\end{aligned}$$

The energy term is simply:

$$\begin{aligned}
&\int \mathcal{Y}^*_{jlJM_J} E \frac{1}{r}\sum_{j'l'}\phi_{j'l'J'M'_J}(r)\mathcal{Y}_{j'l'J'M'_J} d\Omega \\
&\qquad = \frac{1}{r}\sum_{j'l'}\phi_{j'l'J'M'_J} E \int \mathcal{Y}^*_{jlJM_J}\mathcal{Y}_{j'l'J'M'_J} d\Omega \\
&\qquad = \frac{1}{r}\phi_{jlJM_J}(r) E.
\end{aligned}$$

One is left with the potential term. This is the interaction term that couple different states. Following the same procedure for this term one obtains:

$$\begin{aligned}\int d\Omega \mathcal{Y}^*_{jlJM_J} V(\mathbf{r},\mathbf{R}) \frac{1}{r} \sum_{j'l'} \phi_{j'l'J'M'_J}(r) \mathcal{Y}_{j'l'J'M'_J} \\ &= \frac{1}{r} \sum_{j'l'} \int \mathcal{Y}^*_{jlJM_J} V(\mathbf{r},\mathbf{R}) \mathcal{Y}_{j'l'J'M'_J} \phi_{j'l'J'M'_J}(r) d\Omega \\ &= \frac{1}{r} \sum_{j'l'} \langle jlJM_J | \, V(\mathbf{r},\mathbf{R}) \, | j'l'J'M'_J \rangle \, \phi_{j'l'J'M'_J}(r) \\ &= \frac{1}{r} \sum_{j'l'} \langle jlJM_J | \, V(\mathbf{r},\mathbf{R}) \, | j'l'JM_J \rangle \, \phi_{j'l'JM_J}(r).\end{aligned}$$

The bra-ket notation is used to denote the inner product. Putting all the terms together gives the Schrödinger equation in a new form:

$$\begin{aligned}-\frac{1}{2\mu}\left(\frac{1}{r}\frac{d^2}{dr^2}\phi_{jlJM_J}(r) - \frac{1}{r}\frac{l(l+1)}{r^2}\phi_{jlJM_J}(r)\right) + \frac{1}{r}E_j\phi_{jlJM_J}(r) \\ + \frac{1}{r}\sum_{j'l'} \langle jlJM_J | \, V(\mathbf{r},\mathbf{R}) \, | j'l'JM_J \rangle \, \phi_{j'l'J'M'_J}(r) = \frac{1}{r}E\phi_{jlJM_J}(r)\end{aligned}$$

Multiplying with $-2\mu r$ and rearranging some terms:

$$\begin{aligned}\left(\frac{d^2}{dr^2} - \frac{l(l+1)}{r^2} + 2\mu(E-E_j)\right)\phi_{jlJM_J}(r) \\ = 2\mu \sum_{j'l'} \langle jlJM_J | \, V(\mathbf{r},\mathbf{R}) \, | j'l'JM_J \rangle \, \phi_{j'l'JM_J}(r),\end{aligned}$$

one finally obtains the desired form

$$\begin{aligned}\left[\frac{d^2}{dr^2} + k_j^2 - \frac{l(l+1)}{r^2}\right]\phi_{jlJM_J}(r) \\ = 2\mu \sum_{j'l'} \langle jlJM_J | \, V \, | j'l'JM_J \rangle \, \phi_{j'l'JM_J}(r).\end{aligned} \tag{6.75}$$

This is a set of coupled equations, called the close-coupled (cc) equations. These are of the same form as the radial equation (6.15), except for the coupling via the potential. The close-coupled equations are solved numerically.

6.4 Numerical calculation of the scattering amplitude

The Schrödinger equation is solved numerically for all r. The multichannel Schrödinger equation is written on matrix form as

$$\left[\mathbb{1}\frac{d^2}{dr^2} + \mathcal{V}(r)\right]\boldsymbol{\psi}(r) = \mathbf{0}, \tag{6.76}$$

where $\boldsymbol{\psi}$ is a square matrix containing the solutions of the Schrödinger equation, and

$$\mathcal{V}(r) = 2\mu\Big[(E - E_j)\mathbb{1} - \mathbf{V}(r)\Big], \tag{6.77}$$

where E is the collision energy, E_j is the rotational energy of the molecule, $\mathbf{V}(r)$ is a potential matrix. The first term is a diagonal matrix with the collision energy and the rotational energy along the diagonal. The potential matrix includes the centrifugal term as diagonal elements and the potential coupling as off-diagonal elements. This is obtained from of the close-coupled equations (6.75). To see how this matrix can be constructed, consider a certain element: Let $j = 0$, $l = 2$ and $J = 2$ and let α label this particular state (channel) so that $|\alpha\rangle = |022M_J\rangle$. The quantum number M_J has no influence on the different elements. Another state coupling to $|\alpha\rangle$ is $|\beta\rangle = |112M_J\rangle$, because J is conserved in this case. The centrifugal term is zero since this is a off-diagonal element. The matrix element is given by

$$\langle\alpha|\,\mathbf{V}(r)\,|\beta\rangle = \langle 022M_J|\,V(r,\theta)\,|112M_J\rangle\,, \tag{6.78}$$

where the total angular momentum eigenstates are known from equation (6.67), and numbers are inserted for the potential. The potential must be known for the particular system. The angular part is integrated over. To construct the whole matrix, let α and β run through all the relevant states or channels in a systematic fashion, and calculate the matrix elements. When all the relevant matrix elements are calculated, the matrix $\mathbf{V}(r)$ is obtained. The dimension of this matrix is typically in the range 1000 to 5000.

In the interior region the interaction potential is present. For this region one defines the so called log-derivative matrix:

$$\mathbf{y}(r) = \frac{d\boldsymbol{\psi}(r)}{dr}\boldsymbol{\psi}(r)^{-1}. \tag{6.79}$$

Differentiation of this matrix and using the Schrödinger equation (6.76) gives

$$\mathbf{y}'(r) + \mathcal{V}(r) + \mathbf{y}^2(r) = \mathbf{0}, \tag{6.80}$$

where the prime means differentiation with respect to r. Let a denote the effective range of the potential. One is interested in obtaining the interior solution at the intersection $r = a$ between the interior and the exterior region, which is the log-derivative matrix evaluated at that point.

Algorithm

The algorithm is taken from [31]. The algorithm is a discreet integration routine over r until the final point at $r_N = a$. The total number of integration points is N and the steplength is h. The usual boundary condition for the wave function is given by $\boldsymbol{\psi}(0) = \mathbf{0}$. For the derivative the boundary condition must lead to linearly independent solutions. A convenient choice is $\boldsymbol{\psi}'(0) = \mathbb{1}$. Consequently the initial log-derivative matrix is diagonal with infinite elements. To represent an infinite number on a computer a very large number is used. For the initial matrix one can use

$$\mathbf{y}_0 = 10^{20}\mathbb{1}. \tag{6.81}$$

For step n the log-derivative matrix is given by

$$\mathbf{y}_n = (\mathbb{1} + h\mathbf{y}_{n-1})^{-1}\mathbf{y}_{n-1} - \frac{h}{3}w_n\mathbf{u}_n, \tag{6.82}$$

where

$$\mathbf{u}_n = \begin{cases} \mathcal{V}(r_n) & n = 0, 2, 4, \ldots, N, \\ [\mathbb{1} + (h^2/6)\mathcal{V}(r_n)]^{-1}\mathcal{V}(r_n) & n = 1, 3, 5, \ldots, N-1. \end{cases} \tag{6.83}$$

The weights w_n are given by

$$w_n = \begin{cases} 1 & n = 0, N, \\ 4 & n = 1, 3, 5, \ldots, N-1, \\ 2 & n = 2, 4, 6, \ldots, N-2. \end{cases} \tag{6.84}$$

The total number N of integration points must be odd. Only the final value $\mathbf{y}_N$ is of interest. The algorithm is such that only at this limit the value $\mathbf{y}_N$ is a good approximation to the exact value. The exact value $\mathbf{y}(r_N)$ for the last integration point is given by

$$\mathbf{y}(r_N) = \mathbf{y}_N + \mathbf{C}h^4 + \mathbf{O}(h^6), \tag{6.85}$$

where $\mathbf{y}_N$ is the obtained approximate value, $\mathbf{C}$ is some unknown constant matrix, $\mathbf{O}(h^6)$ is a matrix of order h^6. The truncation error varies as the fourth power of h.

S-matrix

One is interested in evaluating the wave function in the exterior region. In this region, where the potential interaction vanish, the wave function is a generalization of equation (6.22) given by [31]

$$\boldsymbol{\psi}(r) = \mathbf{J}(r) - \mathbf{N}(r)\mathbf{K}, \quad r \geq a \tag{6.86}$$

where $\mathbf{J}$ and $\mathbf{N}$ are diagonal matrices made up of known functions, $\mathbf{K}$ is called the reaction matrix and is unknown. This wave function describes both open and closed channels. For the open channels the elements of $\mathbf{J}$ and $\mathbf{N}$ are given by [31]

$$\begin{aligned} [\mathbf{J}(r)]_{ij} &= \delta_{ij}k_j^{-1/2}j_{l_j}(k_j r) \\ [\mathbf{N}(r)]_{ij} &= \delta_{ij}k_j^{-1/2}n_{l_j}(k_j r), \end{aligned} \tag{6.87}$$

where j_{l_j} (n_{l_j}) are the Bessel (Neumann) functions of order l_j. For the closed channels the elements are given by [31]

$$\begin{aligned} [\mathbf{J}(r)]_{ij} &= \delta_{ij}(k_j r)^{1/2}I_{l_j+1/2}(k_j r) \\ [\mathbf{N}(r)]_{ij} &= \delta_{ij}(k_j r)^{1/2}K_{l_j+1/2}(k_j r), \end{aligned} \tag{6.88}$$

where I and K are the modified spherical Bessel functions of the first and third kind. The matrix $\mathbf{K}$ contains information about the phase shifts. This matrix

has off-diagonal elements and takes care of the connection between the exterior and the interior region:

$$\mathbf{K} = -[\mathbf{y}(a)\mathbf{N}(a) - \mathbf{N}'(a)]^{-1} \cdot [\mathbf{y}(a)\mathbf{J}(a) - \mathbf{J}'(a)], \tag{6.89}$$

where the prime means differentiation with respect to r. This is a generalization of equation (6.24). The log-derivative matrix at the intersection is obtained numerically from the algorithm above $\mathbf{y}(a) \approx \mathbf{y}_N$. The K matrix can be written as an augmented matrix:

$$\mathbf{K} = \begin{bmatrix} \mathbf{K}_{\rm oo} & \mathbf{K}_{\rm oc} \\ \mathbf{K}_{\rm co} & \mathbf{K}_{\rm cc} \end{bmatrix}, \tag{6.90}$$

where $\mathbf{K}_{\rm oo}$, $\mathbf{K}_{\rm oc}$, $\mathbf{K}_{\rm co}$ and $\mathbf{K}_{\rm cc}$ are the open-open, open-closed, closed-open and closed-closed submatrices of $\mathbf{K}$.

The scattering matrix contains all the relevant information about the collision process, and is related to the K-matrix. The S-matrix is given in terms of the open-open submatrix of the K-matrix [31]:

$$\mathbf{S} = (\mathbb{1} + i\mathbf{K}_{\rm oo})^{-1}(\mathbb{1} - i\mathbf{K}_{\rm oo}). \tag{6.91}$$

The scattering amplitude

The atoms traveling out of the gas region along the incident direction is related to the forward scattering amplitude. This is obtained from the S-matrix. The forward scattering amplitude is given by [14]

$$\begin{aligned} f(jm_j j'm_j|\theta = 0) = \frac{1}{2i}\sum_J \sum_{ll'} \sqrt{\frac{(2l+1)(2l'+1)}{k_j k_{j'}}} \\ i^{l-l'} \left\langle jm_j l0|JM_J\right\rangle \left[S_{jl,j'l'} - \delta_{ll'}\delta_{jj'}\right] \left\langle j'm_j l'0|JM_J\right\rangle, \end{aligned} \tag{6.92}$$

where the brackets are Clebsch-Gordan coefficients. The S-matrix elements are given by $\langle jl|\, S\, |j'l'\rangle$, which relates channel $|jl\rangle$ and $|j'l'\rangle$.

For atom-atom scattering the rotational energy can be omitted and the forward scattering amplitude can be simplified. The rotational angular momentum $\mathbf{j}$ is zero so that $j = j' = 0$ and $m_j = m_{j'} = 0$. The projection of the total angular momentum is conserved, equation (6.65). Since $m_l = 0$ the total projection $m_J = 0$ for $m_j = m_{j'} = 0$. The Clebsch-Gordan coefficients becomes

$$\begin{aligned} \langle j'm_{j'}l'0|JM_J\rangle = \langle 00l'0|J0\rangle = \delta_{l'J} \\ \langle jm_j l0|JM_J\rangle = \langle 00l0|J0\rangle = \delta_{lJ}. \end{aligned} \tag{6.93}$$

For atom-atom scattering the forward scattering amplitude becomes

$$\begin{aligned} f(\theta = 0) &= \frac{1}{2i}\sum_J \sum_{ll'} \sqrt{\frac{(2l+1)(2l'+1)}{k_j k_{j'}}} i^{l-l'} \delta_{lJ}[S_{jl,j'l'} - \delta_{ll'}\delta_{jj'}]\delta_{l'J} \\ &= \frac{1}{2i}\sum_J \sum_l \frac{2l+1}{k}\delta_{lJ}[S_{ll} - 1] \\ &= \frac{1}{2ik}\sum_{l=0}^{\infty}(2l+1)(S_{ll} - 1). \end{aligned} \tag{6.94}$$

Comparing this relation to equation (6.19) one can identify $S_{ll} = e^{2i\delta_{ll}}$, where δ_{ll} is the phase shift.

A formula for the index of refraction is introduced in chapter 9. This formula depends on the forward scattering amplitude. To obtain the forward scattering amplitude one needs to know the potential interaction. This is the potential term in the Hamiltonian in equation (6.62). These interaction potentials are discussed in the next chapter.

Chapter 7

Interaction potentials

To determine the outcome of a collision process one needs to find the interaction between the involved particles. In collision processes the interactions between atom-atom and atom-molecule is described in terms of potentials. For atom-atom systems this potential is called the interatomic potential curve, and is only dependent on the distance between the nuclei. For atom-molecule systems a potential energy surface (PES) is needed to describe the interaction. This depends on the orientation of the molecule and on the distance between the molecule and the atom.

7.1 Interatomic potentials

For atom-atom collisions one must determine the potential curve U in equation (6.15). This curve is called the molecular potential energy curve and describes the potential energy between two atoms. Accurate determination of these curves are difficult due to electron-electron interactions. The potential curve for the lithium-helium system is obtained numerically. Performing a calculation one must choose a set of basis functions to represent the wave function for the system. This section emphasises that different choice of basis sets produce different results. Finding a good basis can be somewhat involved and this discussion is rather superficial.

Electronic structure calculation

One is interested in solving the time independent Schrödinger equation for a given configuration of the nuclei. Only two atoms participate and the configuration parameter is the distance between the nuclei. The Hamiltonian for the complete system contains the kinetic energy of the nuclei, the kinetic energy of the electrons and the interaction between them. Since the electronic mass is much smaller than the nuclear mass while their mutual forces are of the same magnitude, the kinetic energy of the nuclei is neglected. This is part of the Born-Oppenheimer approximation. More formally one separates the total wave function into an electronic part $\psi(\mathbf{x}; R)$ and a nuclear part ψ_N. The energy from the nuclear part, including the repulsion from the nuclei, is added as an extra term to the electronic energy. This assumption is usually valid for the ground state energy of the system. For excited states it is less reliable [1]. The

molecular system consists of n electrons moving in a static Coulomb potential set up by 2 nuclei at fixed locations. The energy is given by the Schrödinger equation

$$H\psi(\mathbf{x}; R) = E(R)\psi(\mathbf{x}; R), \tag{7.1}$$

where $\mathbf{x}$ contains all the spatial coordinates and spin coordinates for all the electrons. R is the distance between the two nuclei. The energy E depends only on this distance. The Hamilton operator, called the electronic Hamiltonian, in atomic units is

$$H = -\frac{1}{2}\sum_{i}^{n}\nabla_i^2 - \sum_{i}^{n}\sum_{I}^{2}\frac{Z_I}{r_{Ii}} + \sum_{i<j=1}^{n}\frac{1}{r_{ij}}, \tag{7.2}$$

where Z_I is the number of protons for nucleus I. The first term describes the kinetic energy for the n electrons. The second term is the electron-nucleus interaction between n electrons and the 2 nuclei. The last term represents the electron-electron interaction. Due to this term equation (7.1) is not separable into one-electron wave functions, and has no exact solution. Simplifying assumptions are made to find approximate solutions.

One approach is the Hartree-Fock method that finds an approximate wave function describing the ground state of the system. A detailed description of the Hartree-Fock method is found in e.g. Bransden [8]. The underlying assumption is that each electron moves in an effective central symmetric potential set up by the 2 nuclei and the other $n-1$ electrons in an average way. Each electron has its own wave function that includes the spatial state and the spin state, often called a spin-orbital. The one-electron wave function is written as $\psi_a(i)$, where i labels the electron and a includes all the relevant quantum numbers. The total wave function for the whole systems depends on all the one-electron wave functions. To be consistent with Pauli's exclusion principle this wave function is represented as a Slater determinant

$$\Phi = (n!)^{-1/2}\det|\psi_a(1), \psi_b(2), \ldots, \psi_c(n)|. \tag{7.3}$$

Each one-electron wave function is written as a linear combination of a given set of M different basis functions

$$\psi_l = \sum_{i=1}^{M} c_{il}\chi_i, \tag{7.4}$$

where c_{il} are constants and χ_i are the basis functions. One is interested in the energy in equation (7.1). According to the variational principle the energy from the trial wave function Φ, is higher than the true ground state energy E if the trial wave function is not exact:

$$E \leq \left[\langle\Phi| H |\Phi\rangle\right]_{\min}. \tag{7.5}$$

The Hartree-Fock method is a variational method and one is left to vary the constants in equation (7.4), in order to minimize the energy. To represent the one-electron wave functions exactly within the central field approximation, a complete basis should be used. In principle this means an infinite set of basis functions. This is not achievable from a computational point of view and one

must choose a finite set of basis functions. Due to this truncation of the basis the resulting energy deviates from the one obtained if the basis were complete. With only a finite number of basis functions at disposal, different basis sets will produce different results. This is the case for the lithium-helium system, and the choice of basis is briefly discussed.

The Hartree-Fock method excludes any correlation effects. Therefore the expectation value of the electronic Hamiltonian in equation (7.5) gives an energy higher than the true ground state energy. Several post-Hartree-Fock methods tries to include this correlation [1]. One method that compensates for the difference between the Hartree-Fock Hamiltonian and the exact electronic Hamiltonian is the Möller-Plesset perturbation theory. This method applies this difference as a perturbation and calculates the energy to different orders. It is denoted MP2 when the perturbation is applied to second order.

Numerical calculation of the potential curves for the LiHe-system

The potential curve for lithium and helium is calculated with GAMESS [48]. GAMESS is an acronym for General Atomic and Molecular Electronic Structure System. It is a program designed to perform quantum chemistry. Equation (7.1) is solved numerically and the solution procedure must be specified in an input file. In this calculation a restricted open Hartree-Fock (ROHF) method is used. This option puts some restraint on the one-electron wave functions: Electrons in a closed shell are forced to occupy the same spatial state. For lithium this means that the two innermost electrons would be forced to occupy the 1s state. MP2 is used to include the correlation effects. A set of basis functions is chosen. The names of the different basis functions used in this calculation are given in table 7.1. The only parameter specifying the geometry is the distance R from

	Official name	Reference
MIDI		[29]
ACC5	aug-cc-pCV5Z	[60]
CC5	cc-pCV5Z	[62]
CCD	cc-pCVDZ	[61]

Table 7.1: The different basis sets are given different names to characterize their properties.

equation (7.1). This equation is solved to find the energy $E(R)$ and the curve is obtained by calculating the energy for a whole range of distances. The different curves for different basis sets are given in figure 7.1.

The choice of basis in this discussion, is based upon properties of the electronic structure of the system. Consider each atom as a nucleus surrounded by an electronic distribution. If either atom is alone the choice of basis is less important. It is when they interact as a consequence of being placed near each other that some effects can occur. As the distance between the atoms decrease the electronic distribution for each atom may overlap. Electrons located somewhere between the nuclei can be bound to both and an electronic bond is formed. The lithium atom has three electrons, two electrons in the 1s state and the outermost electron in a 2s state. This valence electron is located further away

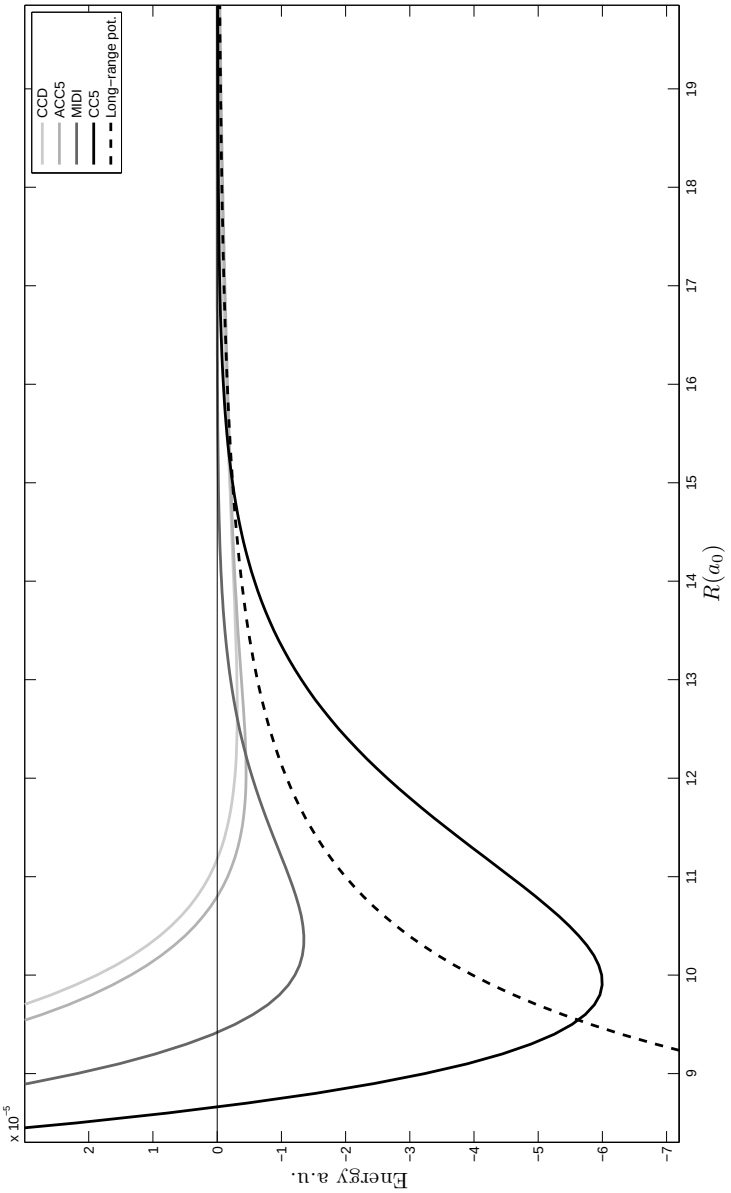

Figure 7.1: Different basis functions for the potential between lithium and helium. The long range potential curve is included (dashed line). The long-range potential must be connected to the other chosen curve to obtain the complete potential curve.

from the nucleus. Feeling the presence of other Coulomb interactions the charge distribution of the lithium atom is displaced due to this valence electron. The lithium atom is polarized and the valence electron may form a bond with the helium atom. This effect should be modeled properly by adjusting the degree of polarization in the basis set. By including diffuse orbitals, one models the possibility that the electron can be located far away from the nucleus.

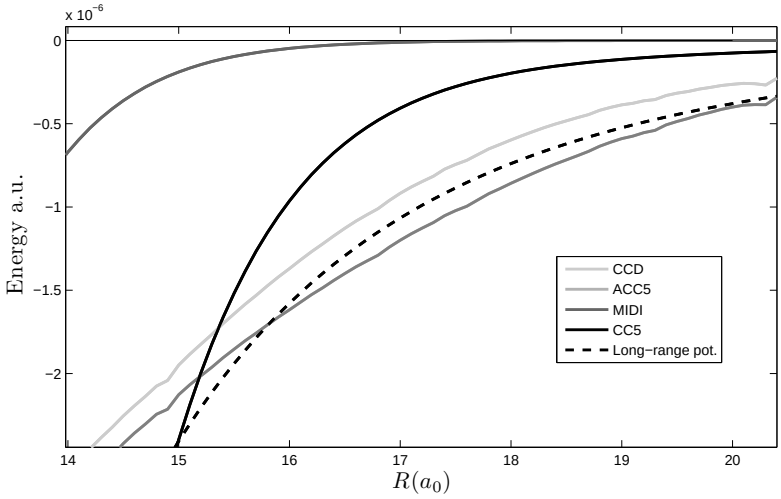

Figure 7.2: Different basis sets results in different potential curves. This figure illustrates the overlap with the long range potential curve (dashed line). The ACC5-basis agrees best with the long range potential.

The MIDI-basis is what is called a split valence basis set. This means that the outermost electron wave functions is represented by two basis functions. The inner-shell orbitals are represented by one basis function. This is believed to be the most inaccurate basis-set and is included to illustrate the implications of the basis set. The other basis-sets are denoted with the letter V indicating that the basis set are only valid for valence atoms, atoms with only one electron in the highest energy state. The letter D and the number 5 indicates amount of polarization. One basis set is denoted with aug (augmented) to point out that some diffuse functions are added to the basis set. The curves in figure 7.1 can be characterized by the depth and the position of the minimum point, called the equilibrium bond length. The lithium-helium system is weakly bound, meaning that the atoms are not likely to form a molecule. Therefore the potential curve is expected to be shallow. The deepest curve is obtained using the CC5-basis. The most accurate curve is believed to be the ACC5-basis with the diffuse orbitals. Also included is the long-range potential curve which describes the interaction at larger distances. The long-range potential takes the form

$$V(r) = -\frac{C_6}{r^6} - \frac{C_8}{r^8} - \frac{C_{10}}{r^{10}}, \tag{7.6}$$

where the coefficients are given in table 7.2. Comparison of the long-range curve and the other curves in the region where they are believed to be identical, gives

C_6	C_8	C_{10}
21.1	1059	80908

Table 7.2: Coefficients, in a.u., for the long range potential for Lithium-Helium taken from [6].

an indication of the accuracy of the curves, assuming the long range potential curve is known precisely. According to figure 7.2 the ACC5- and CCD-curves seem to agree best. The curve obtained from GAMESS is a discrete set of values for different distances. If one is interested in the potential curve for a continuous region, interpolation routines can be implemented. To obtain the potential curve from a few Bohr-radii and out to infinite distances, one needs to connect the long-range curve with the curve calculated with GAMESS. For cold collision processes the involved particles have low energies and are unlikely to come very close. Therefore the shape of the curve close to the nuclei is less important.

7.2 Potential energy surface PES

The interaction potential energy between a molecule and an atom is described in terms of a potential energy surface denoted PES. In this case the system consists of the diatomic sodium molecule Na_2 and the helium atom He. The PES is used to determine the outcome of a cold collision process. In this low temperature regime some simplifications are valid. The diatomic sodium molecule is treated as a rigid rotator with a fixed internuclear separation, called the equilibrium distance. In addition, the sodium molecule is in the electronic ground state with zero total electronic spin and zero angular momentum apart from rotation. The nuclear spin is also neglected. Within this assumption there is no fine structure and hyperfine structure that will influence the PES. The potential energy of the system depends only the distance r and on the orientation of the molecule relative to the atom, described in terms of the angle θ, see figure 7.3.

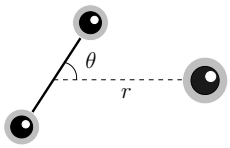

Figure 7.3: The orientation of the diatomic sodium molecule relative to the helium atom is described with an angle θ. The distance r is the distance between the atom and the center of mass for the diatomic molecule.

To find the energy for a given configuration one must solve the electronic Schrödinger equation. For interatomic systems this is equation (7.1) where the energy only depends on the distance R between the nuclei. For the molecule-atom system the same equation is solved, but the system is more complex. The energy depends on the distance r and the angle θ. The parameter R in equation (7.1) must therefore be generalised in order to describe the configuration of

all three nuclei. The PES is obtained by solving the electronic Schrödinger equation for the relevant orientations and distances. For this composite system the relevant angles is $\theta \in [0, 90°]$, because of the symmetry.

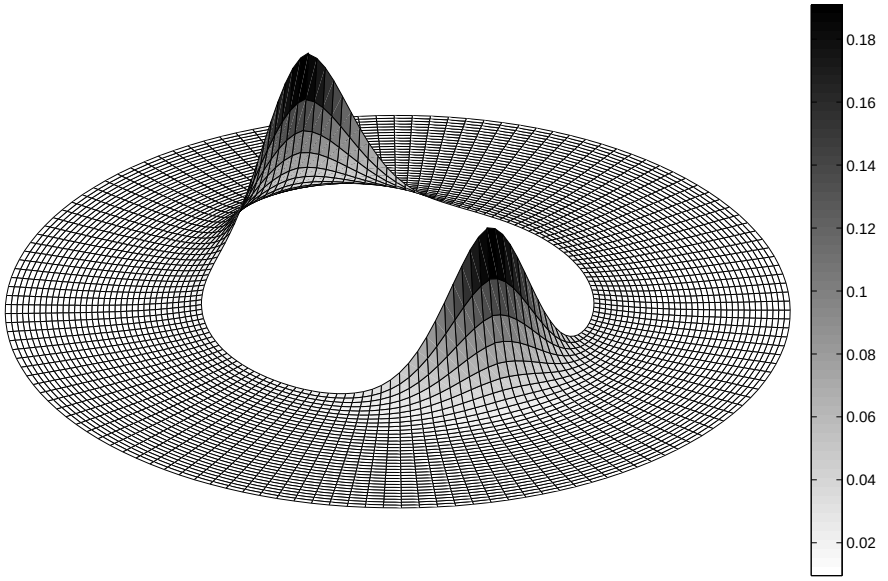

Figure 7.4: Polar plot of the PES for He-Na_2, for $r \in [5, 10]$a.u.. The energy scale to the right is in atomic units. The peaks corresponds to the location of the two nuclei. The molecule is oriented so that the angle $\theta = 0°$ at one of the peaks.

The PES for the He-Na_2 system is obtained numerically using GAMESS [48]. In the input file the configuration of the system is specified. The potential curve is obtained for distances $r \in [5, 25]$a.u. (Bohr-radii) with a resolution of 0.1a.u., and for angles $\theta \in [0, 90°]$ with an angular resolution of 1°. This means that 90 potential curves is calculated. As for the interatomic potential curve discussed in the preceding section, this calculation is performed with a ROHF molecular wave function. MP2 is used to include electron correlation effects. For the helium atom the aug-cc-pCVTZ basis set is used and for the sodium atoms the cc-pVTZ basis is used. Different basis sets are used on the different atoms while for the interatomic potential curve the same basis set was used for the composite system.

One obtains a set of potential curves that constitute the PES. The PES is plotted in two separate figures 7.4 and 7.5, because of the different orders of magnitude for the energy. Polar coordinates is used and $\theta \in [0, 360°]$. The figures are meant to illustrate the potential surface of the diatomic sodium molecule, as seen from the helium atom. In figure 7.4 the peaks corresponds to the location of the two nuclei of the sodium molecule. The angle θ is zero at one of the peaks (and $\theta = 180°$ at the other or vice versa). The PES is oriented

the same way in figure 7.5 so that $\theta = 0$ at one of the minima.

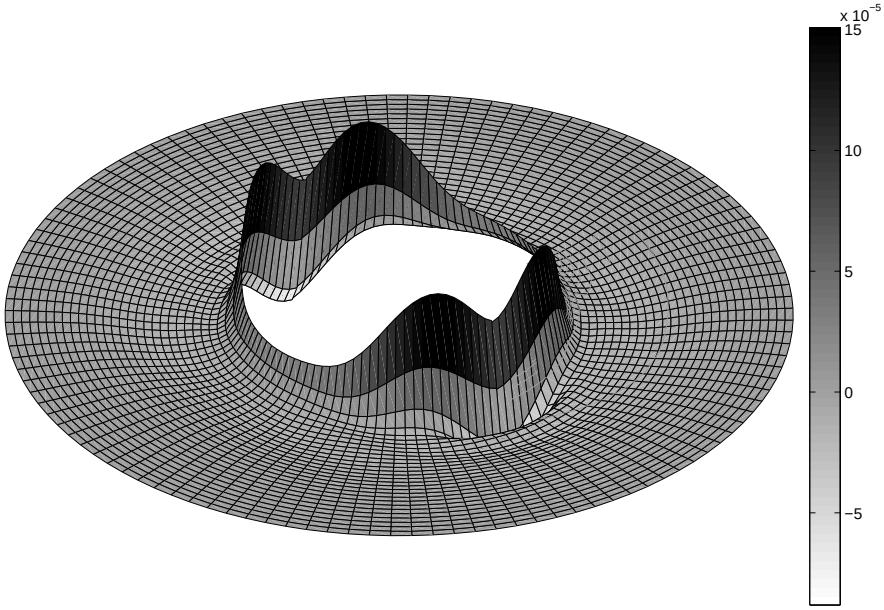

Figure 7.5: Polar plot of the PES for He-Na_2, for $r \in [10, 25]$a.u.. The energy scale to the right is in atomic units, note the different order of magnitude compared to figure 7.4. The PES is oriented the same way as in figure 7.4. The PES has attractive parts for r between 11a.u. and 12a.u. at $\theta = 0°$.

Figure 7.4 shows the PES for distances $r \in [5, 10]$a.u. and in this region the energy is large. Figure 7.5 shows the PES for distances $r \in [10, 25]$a.u. where the energy is much lower. In a cold collision process the involved particles have low energies (speed) and the colliding particles are not likely to come very close. Therefore the PES for shorter distances $r < 10$a.u. is less important. For larger distances $r > 10$a.u. the shape of the PES is of more interest, see figure 7.5 and 7.6. Figure 7.4 shows that the potential is most repulsive if the molecule is oriented so that $\theta = 0°$. But for r between 11 and 12a.u. the potential becomes attractive when $\theta = 0°$. This is clearly seen in figure 7.5 and 7.6. In figure 7.6 the geometry of the surface for $r \in [10, 25]$a.u. is illustrated more clearly.

The PES describes the short range interaction. In the long range region the interactions is described in terms of the Van der Waals coefficients. The long range part of the potential is important for cold collisions. The detailed form is given in [6], and the coefficients are believed to be accurately determined. Interpolation routines are used to join the PES and the long range part together.

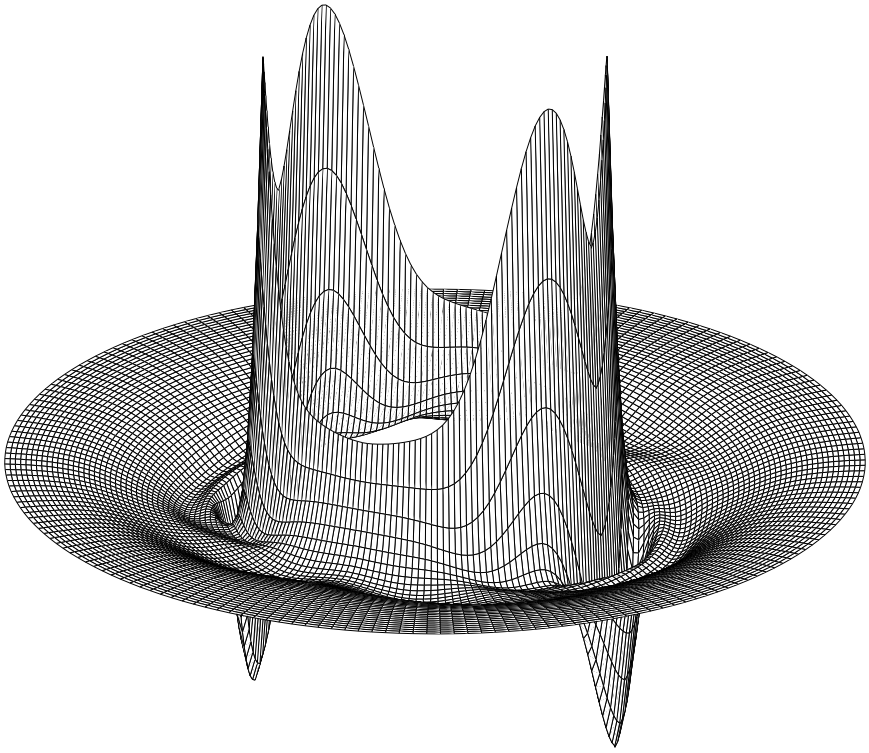

Figure 7.6: Polar plot of the PES for He-Na_2, for $r \in [10, 25]$. This is the same region plotted in figure 7.5, but with a different view to emphasise the geometry of the surface. The minima for the energy surface at $\theta = 0^\circ$ and $\theta = 180^\circ$ are attractive parts of the PES.

Chapter 8

Bound states

The potential curves for the lithium-helium (Li-He) system and the lithium-argon (Li-Ar) system, may allow bound states to exist. A numerical calculation investigates the number of bound states for the given potential curve.

The behaviour of the index of refraction, discussed in chapter 9, can give information about the number of bound states for the relevant potential. It is of interest to see if this behaviour is consistent with the calculated number of bound states.

For the Li-Ar system four bound states are found. For the Li-He system no bound states are found.

8.1 Algorithm

To determine the number of bound states one must solve the radial Schrödinger equation (6.15) for the s-wave with the given potential. In atomic units the radial equation for s-wave (corresponding to the ground state) scattering is given by

$$\Big[-\frac{d^2}{dr^2} + 2\mu V(r) \Big] u(r) = 2\mu E u(r), \tag{8.1}$$

where μ is the reduced mass for the system and E is the energy. The wave function must vanish for $r = 0$ and $r \to \infty$, and must therefore obey the boundary conditions:

$$\begin{aligned} u(0) &= 0 \\ u(\infty) &= 0. \end{aligned} \tag{8.2}$$

The radial equation (8.1) is solved numerically by approximating the second derivative using a Taylor expansion:

$$\frac{d^2}{dr^2} u(r) = \frac{u(r+h) - 2u(r) + u(r-h)}{h^2} + \mathcal{O}(h^2), \tag{8.3}$$

where h is the steplength. The discretized form is given by

$$-\frac{u_{i+1} - 2u_i + u_{i-1}}{h^2} + 2\mu V_i u_i = 2\mu E u_i, \tag{8.4}$$

where $u_{i+1} = u(r_i + h)$, $r_i = ih$ and $i = 0, 1, 2, \ldots n_{\max}$. The steplength is defined as $h = r_{\max}/n_{\max}$. This equation can be rewritten as a matrix eigenvalue problem. Define the diagonal elements:

$$d_i = 2/h^2 + V_i, \tag{8.5}$$

and the off diagonal elements:

$$e_i = -1/h^2. \tag{8.6}$$

With these expressions the radial equation (8.1) takes the following form

$$d_i u_i + e_{i-1} u_{i-1} + e_{i+1} u_{i+1} = \lambda u_i. \tag{8.7}$$

Written in matrix form:

$$\begin{bmatrix} \frac{2}{h^2} + V_1 & -\frac{1}{h^2} & & & \\ -\frac{1}{h^2} & \frac{2}{h^2} + V_2 & -\frac{1}{h^2} & & \\ & & \ldots & & \\ & \ldots & \ldots & -\frac{1}{h^2} & \\ & & -\frac{1}{h^2} & \frac{2}{h^2} + V_{n_{\max}} \end{bmatrix} \begin{bmatrix} u_1 \\ u_2 \\ \cdot \\ \cdot \\ u_{n_{\max}} \end{bmatrix} = 2\mu E \begin{bmatrix} u_1 \\ u_2 \\ \cdot \\ \cdot \\ u_{n_{\max}} \end{bmatrix}.$$

This is an eigenvalue matrix problem where the matrix on the left is tridiagonal. The tridiagonal form is a consequence of the boundary conditions given in equation (8.2). All elements except the diagonal- and the first off-diagonal elements are zero. One is interested in the eigenvalues for the vector $\mathbf{u} = (u_1, u_2, \ldots, u_{n_{\max}})$, corresponding to the energies E for the potential curve. To find the eigenvalues the routine named tqli ("Tridiagonal QL Implicit") [45] is applied. Only the eigenvalues are calculated since the eigenvectors are more computationally expensive to obtain and not very useful for the present discussion. The program is included in appendix A.

8.2 Results

Li-Ar system

The interatomic potential curve for the Li-He system is obtained by Cvetko *et al.* [16]. It has an analytical form that makes it convenient for calculations. It is also believed to be accurately determined. The reduced mass for the ^{6}Li^{40}Ar system is $\mu = 9530.314175$a.u.. The calculation is performed with $n_{\max} = 150000$ steps and maximum radial distance is $r_{\max} = 500$a.u.. This proved to be a stable choice. It gave the correct numbers when tested with a known system. In addition, the Li-Ar potential curve was approximated with a harmonic oscillator potential. The lowest bound state for the harmonic oscillator potential was consistent with the lowest bound state in the actual Li-Ar potential.

Four bound states (states with negative energy) are found. The values are given in table 8.1. Figure 8.1 shows the interatomic potential curve along with the energies of the bound states. From this calculation one can conclude that the Li-Ar potential curve holds three or four bound states. The uppermost bound state shown in figure 8.1 has a small bounding energy and may not be correct, due to possible numerical errors.

$E_1 =$	$-14.1927e-05$a.u.
$E_2 =$	$-6.46418e-05$a.u.
$E_3 =$	$-1.75282e-05$a.u.
$E_4 =$	$-0.03635e-05$a.u.

Table 8.1: Bound state energies obtained numerically, for the Cvetko potential [16] for Li-Ar.

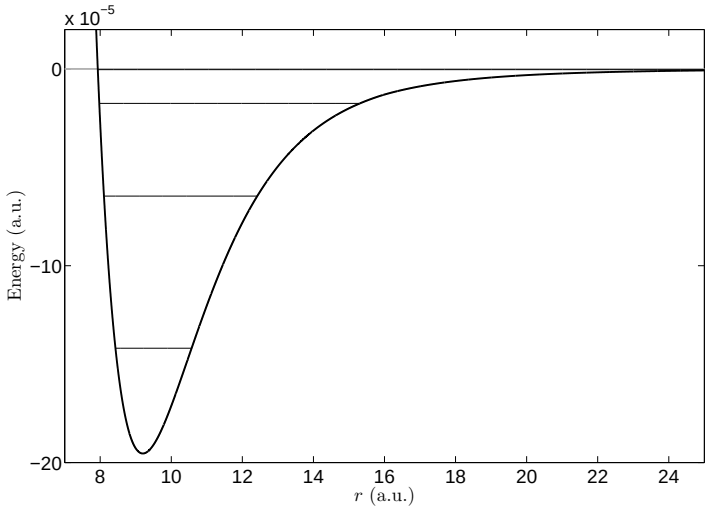

Figure 8.1: Bound states for the Li-Ar potential [16]. Notice the uppermost bound state close to the grey zero-asymptote.

In [37] a theoretical investigation of the $^7Li^{40}Ar$ found three vibrational levels. They reported that four vibrational levels have been observed experimentally. Their system has a different mass (^{7}Li) and is therefore not directly comparable, but it illustrates a point. It can be difficult to precisely determine the number of vibrational levels for a potential curve. In this connection an atom interferometer may provide valuable information. This is because the number of bound states can be revealed through the measured quantities, following the discussion in the preceding chapter.

Li-He system

The interatomic potential curve for the Li-He system is also obtained by Cvetko *et al.* [16], and has an analytical form. Cvetko *et al.* found their potential curve to be in agreement with previous experimental potentials and ab initio calculations [16]. This curve is shallow and is not expected to hold many bound states. Compared to the Li-Ar curve the Li-He curve is an order of magnitude shallower, see figure 8.2. The reduced mass of the Li-He system is $\mu = 3661.81995$a.u.. Performing a calculation on the Li-He system no bound states is found. Variation of the steplength and the maximum range gives the same result: no bound states.

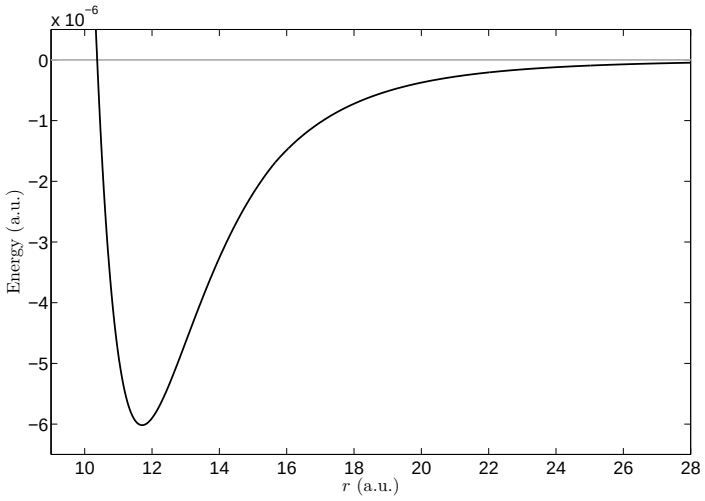

Figure 8.2: No bound states are found numerically for the Li-He potential [16]. This potential is shallow compared with the Li-Ar potential shown in figure 8.1, which is an order of magnitude deeper.

Chapter 9

Calculating the refractive index

The index of refraction provides a description of the situation when matter waves traverse a gas. It contains information about the phase shift and the attenuation of the matter waves. Both these quantities can be measured with an atom interferometer

A simple formula, from [12], for the index of refraction is presented. This depends on the speed of the incident particles and on the temperature of the target gas. The refractive index may provide information about atom-atom and atom-molecule interactions.

Atomic units are used in this chapter.

9.1 Formula for the index of refraction

In chapter 5 the macroscopic concept of the index of refraction was discussed. This section presents a formula for the index of refraction involving the scattering amplitude which origin is atomic collisions (discussed in chapter 6). In section 5.2 the imaginary part of the index of refraction was related to the attenuation of the traversing matter waves using Beer's law. The relation is given by

$$\mathrm{Im}[n-1] = \frac{\rho_t \sigma_{\mathrm{eff}}}{2k_p}, \tag{9.1}$$

where ρ_t is the density of the target gas, σ_{eff} is the effective cross section and k_p is the projectile wave vector. The notation follows from chapter 6 where subscripts t and p denote target and projectile particles respectively. The effective cross section as a function of the projectile velocity v_p is given by [12]

$$\sigma_{\mathrm{eff}}(v_p) = \sigma(v_r)\frac{v_r}{v_p}, \tag{9.2}$$

where v_r is the relative speed between the colliding particles. The relative speed is related to the target and projectile velocities as $v_r = |\mathbf{v}_p - \mathbf{v}_t|$, and describes the motion of the projectile in the center-of-mass frame. The target gas consists

of moving atoms and this is taken into account by averaging over the velocity distribution. The averaged value of the effective cross section is given by

$$\sigma_{\text{eff}}(v_p) \rightarrow \langle \sigma_{\text{eff}}(v_p) \rangle = \int P(\mathbf{v}_t)\sigma(v_r)\frac{v_r}{v_p}\mathrm{d}^3\mathbf{v}_t, \tag{9.3}$$

where $P(\mathbf{v}_t)$ is the speed distribution for the target atoms, discussed in section 9.3.

The cross section relates to the scattering amplitude that was introduced in equation (6.18). The scattering amplitude is a complex quantity and the cross section relates to the imaginary part via the optical theorem, from equation (6.51). The cross section as a function of the relative speed v_r, is given by

$$\sigma(v_r) = 4\pi\frac{\text{Im}[f(k_r, 0)]}{k_r}, \tag{9.4}$$

where k_r is the relative wave vector between colliding particles and $f(k_r, 0)$ is the forward scattering amplitude. The relative wave vector relates to the speed as $k_r = \mu v_r$, where μ is the reduced mass for the target and projectile particles. To shorten the notation the forward scattering amplitude is written $f(k_r, 0) = f(k_r)$. The effective cross section in terms of this is given by

$$\begin{aligned}\langle \sigma_{\text{eff}}(v_p) \rangle &= \int P(\mathbf{v}_t)\frac{v_r}{v_p}4\pi\frac{\text{Im}[f(k_r)]}{k_r}\mathrm{d}^3\mathbf{v}_t \\ &= 4\pi\Big\langle \frac{v_r}{k_r v_p}\text{Im}[f(k_r)]\Big\rangle \\ &= \frac{4\pi}{\mu}\frac{\langle \text{Im}[f(k_r)]\rangle}{v_p},\end{aligned} \tag{9.5}$$

where the brackets denote a thermal average. This expression for the effective cross section, can be related to the the imaginary part of the index of refraction using equation (9.1). Using the relation between the wave vectors and the speed $k_{p/t} = m_{p/t}v_{p/t}$, one obtains

$$\begin{aligned}\text{Im}[n-1] &= \frac{2\pi\rho_t m_p}{\mu}\frac{\langle \text{Im}[f(k_r)]\rangle}{k_p^2} \\ &= 2\pi\rho_t\frac{m_p + m_t}{m_t}\frac{\langle \text{Im}[f(k_r)]\rangle}{k_p^2}.\end{aligned} \tag{9.6}$$

This is in accordance with the more general relation given in [12]

$$n = 1 + 2\pi\rho_t\frac{m_p + m_t}{m_t}\frac{\langle f(k_r)\rangle}{k_p^2}. \tag{9.7}$$

It is reported in [12] that the derivation of this formula was very involved. Actually, several formulas relating the scattering amplitude to the index of refraction has been proposed throughout the literature. The various relations are discussed in [12]. Note that this relation connects the wave function in equation (5.2) to the microscopic collision theory via the scattering amplitude. The situation as matter waves traverse a gas is actually a coherent multiscattering process, that can be involved to describe. The formula for the refractive index therefore represents a simplification of the original multiscattering problem.

9.2 The ratio ρ

An atom interferometer can measure the phase shift and the attenuation of matter waves traversing a dilute gas. The phase shift is related to the real part of the index of refraction and the attenuation is related to the imaginary part, following the discussion in chapter 5. Both these two quantities can be determined from an interference pattern obtained with an atom interferometer, see section 3.5. From equation (5.2) the wave function after the gas region, is given by

$$\psi_{\text{gas}} = e^{-\text{Im}[n-1]k_p \cdot L} e^{i\text{Re}[n-1]k_p \cdot L} \psi_0, \tag{9.8}$$

where L is the length of the gas region and ψ_0 is the wave function if the gas is absent. Denote the phase shift $\Delta\phi = \text{Re}[n-1]k_p \cdot L$, and the attenuation of the amplitude $A = e^{-\text{Im}[n-1]k_p \cdot L}$. The primary variable to study is the ratio of the real and imaginary part $\rho(v_p)$ as a function of the projectile velocity, given by

$$\rho(v_p) = -\frac{\Delta\phi}{\ln A} = \frac{\text{Re}(n-1)}{\text{Im}(n-1)}. \tag{9.9}$$

The ratio is independent on the density ρ_t of the target gas:

$$\rho(v_p) = \frac{\langle \text{Re}[f(k_r)] \rangle}{\langle \text{Im}[f(k_r)] \rangle}. \tag{9.10}$$

This has the experimental advantage of being independent of the the pressure in the gas region, which is difficult to measure precisely [52]. This ratio is also studied in the literature and it is therefore easy to compare with experimental data where available.

9.3 Obtaining the ratio ρ

To obtain the ratio ρ, one must calculate the forward scattering amplitude. This is accomplished with the numerical procedure discussed in chapter 6. The forward scattering amplitude is calculated for velocities from $v_r = 0 \rightarrow v_r^{\max}$, where $v_r^{\max}$ is the maximum relative velocity for the colliding particles.

For high temperatures and projectile velocities, the relative speed may become high. In that case many partial waves need to be included for the scattering amplitude to converge.

The speed distribution in the center of mass frame determines which parts of the scattering amplitude that contribute for a given projectile velocity and target gas temperature. The target gas is assumed to be in thermodynamic equilibrium with a (normalised) Maxwell-Boltzmann distribution of the velocities given by

$$P(\mathbf{v}_t) d^3\mathbf{v}_t = \frac{1}{\pi^{3/2}\alpha^3} \exp\Big(-\frac{v_t^2}{\alpha^2} \Big) d^3\mathbf{v}_t, \tag{9.11}$$

where $\mathbf{v}_t$ is the speed of the target gas atoms and

$$\alpha = \sqrt{\frac{2k_B T}{m_t}}, \tag{9.12}$$

where T is the temperature of the target gas and k_B is the Boltzmann constant. The projectile velocity $\mathbf{v}_p$ is related to the target velocity as $\mathbf{v}_t = \mathbf{v}_p - \mathbf{v}_r$, where $\mathbf{v}_r$ is the relative velocity. The relative velocity distribution in the center of mass frame is obtained by replacing $\mathbf{v}_t$ with $\mathbf{v}_p - \mathbf{v}_r$ in the target gas distribution:

$$P(\mathbf{v}_p - \mathbf{v}_r)d^3\mathbf{v}_r = \frac{1}{\pi^{3/2}\alpha^3}\exp\Big[-\frac{(\mathbf{v}_p - \mathbf{v}_r)^2}{\alpha^2}\Big]d^3\mathbf{v}_r. \tag{9.13}$$

One is interested in the relative distribution in the center of mass frame, for a given projectile speed v_p. To obtain this the angular part is integrated over. The volume element is written as

$$d^3\mathbf{v}_r = v_r^2 \sin\theta dv_r d\theta d\phi, \tag{9.14}$$

where θ is the angle with the z-axis and ϕ is the azimuthal angle. The z-axis is directed along the projectile velocity $\mathbf{v}_p$. Using that $(\mathbf{v}_p - \mathbf{v}_r)^2 = v_p^2 + v_r^2 - 2v_p v_r \cos\theta$, and integrating over the angles gives

$$\begin{aligned} P(v_p - v_r)dv_r &= \frac{1}{\pi^{3/2}\alpha^3}\exp\Big(-\frac{v_p^2 + v_r^2}{\alpha^2}\Big) \\ &\quad \times \int_0^{2\pi} d\phi \int_0^{\pi} d\theta \sin\theta \exp\Big(\frac{2v_p v_r \cos\theta}{\alpha^2}\Big) v_r^2 dv_r \\ &= \frac{-2\pi v_r^2}{\pi^{3/2}\alpha^3}\exp\Big(-\frac{v_p^2 + v_r^2}{\alpha^2}\Big)\int_1^{-1}\exp\Big(\frac{2v_p v_r u}{\alpha^2}\Big)du dv_r \\ &= \frac{2v_r^2}{\pi^{1/2}\alpha^3}\exp\Big(-\frac{v_p^2 + v_r^2}{\alpha^2}\Big)\frac{\alpha^2}{v_r v_p}\sinh\Big(\frac{2v_r v_p}{\alpha^2}\Big)dv_r. \end{aligned} \tag{9.15}$$

The relative speed distribution as seen from a projectile particle with velocity v_p is given by

$$P(v_p - v_r)dv_r = \frac{2v_r}{\pi^{1/2}\alpha v_p}\exp\Big(-\frac{v_p^2 + v_r^2}{\alpha^2}\Big)\sinh\Big(\frac{2v_r v_p}{\alpha^2}\Big)dv_r. \tag{9.16}$$

This distribution is normalised so that $\int_0^\infty P(v_p - v_r)dv_r = 1$.

To obtain the ratio ρ for a given projectile speed v_p, one must calculate the expectation value of the forward scattering amplitude for the relevant distribution. The distribution is specified by the projectile velocity v_p and the temperature T of the target gas. The average $\langle f(k_r)\rangle$ is given by

$$\langle f(k_r)\rangle = \int_0^\infty f(k_r)P(v_p - v_r)dv_r. \tag{9.17}$$

This integral is calculated for selected temperatures and the relevant projectile velocities. The relative speed distribution for different temperatures T and different projectile velocities v_p, is shown in figure 9.1. The ratio ρ is given by

$$\rho(v_p) = \frac{\int_0^\infty \mathrm{Re}[f(k_r)]P(v_p - v_r)dv_r}{\int_0^\infty \mathrm{Im}[f(k_r)]P(v_p - v_r)dv_r}. \tag{9.18}$$

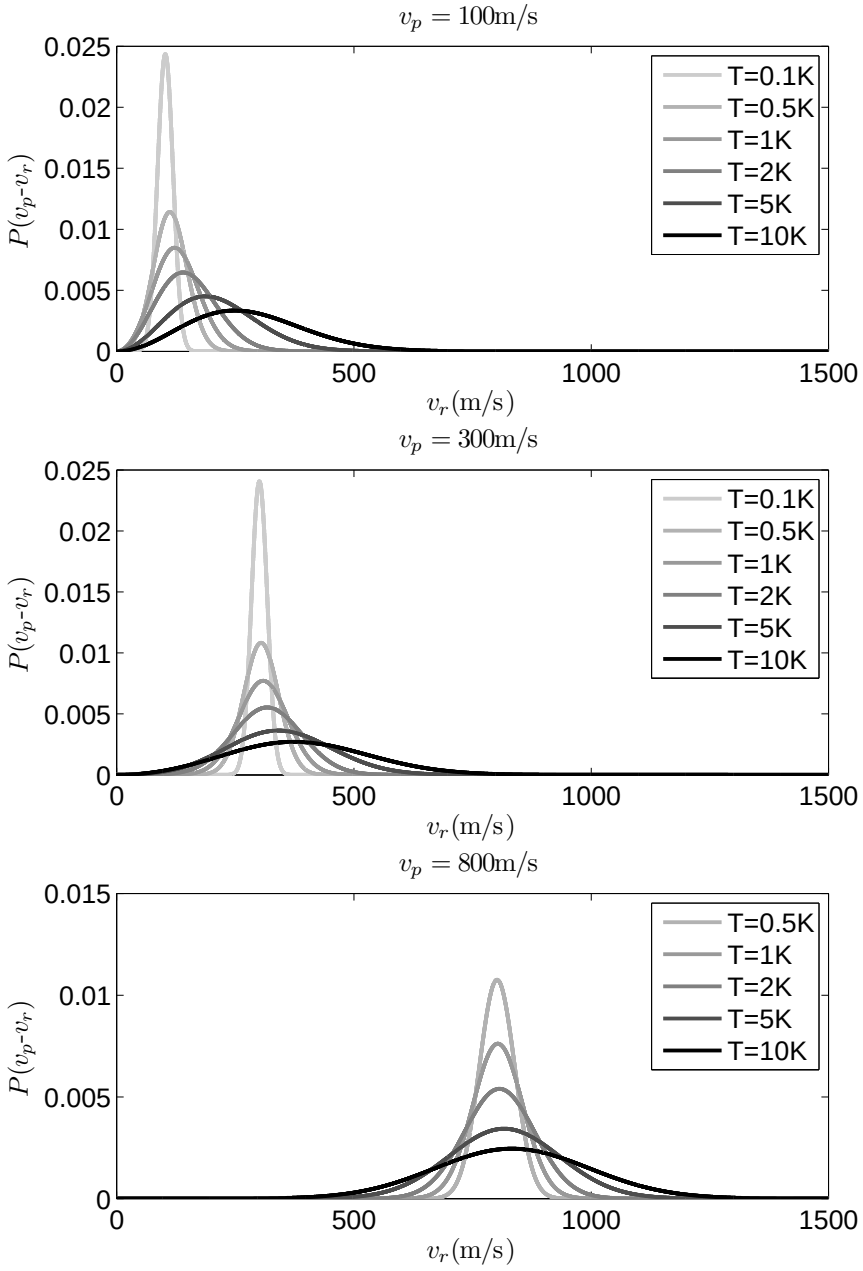

Figure 9.1: The relative speed distribution $P(v_p - v_r)$ for three different projectile speeds $v_p = 100, 300, 800$m/s, and selected temperatures T. The distribution depends on both the projectile speed and the temperature. The bottom plot is for 5 temperatures only, since the coldest distribution becomes very high. For low projectile velocities and temperatures T, the detailed features of the scattering amplitude and consequently the refractive index become more apparent.

9.4 Properties of the ratio ρ

Observing the behaviour of $\rho(v_p)$ as a function of the projectile velocity v_p, may provide valuable information regarding atomic and molecular properties.

The ratio $\rho(v_p)$ may oscillate when the interatomic potential has capacity for at least one bound state. This behaviour is named glory oscillations and the number of maxima may serve as a 'counter' of bound states, see Bernstein [4,5]. The correspondence is not one-to-one since bound states may exist without being revealed through an oscillation. Bernstein [5] proposed the following rule: *The observation of m maxima in the elastic atom-atom impact spectrum implies existence of at least m discrete levels of zero angular momentum for the composite system.* The term atom-atom impact spectrum is an alternative way to express the total elastic cross section, which relates to the forward scattering amplitude. The ratio $\rho(v_p)$ exhibit the same behaviour. Glory oscillations in $\rho(v_p)$ were first measured by Roberts *et al.* [46] for sodium matter waves.

For low temperatures ρ may oscillate rapidly. This behaviour is called resonances and are due to the appearance of quasibound states in the effective potential. These resonances are discussed in section 6.2, see figure 6.8. For low temperatures only a small number of partial waves contributes to the scattering amplitude. An estimate for this number was found in section 6.2

$$l_{\max} \propto a\sqrt{\mu T}, \tag{9.19}$$

where a is the effective range of the potential, μ is the reduced mass, and T is the temperature. Resonances are therefore more likely to be observed in the low energy region.

Schmiedmayer *et al.* [55] have calculated ρ for a long range attractive van der Waals interaction $V_{\mathrm{vdW}}(r) = -r^{-6}$. They used a semi classical approximation and found that $\rho \approx 0.72$. At low temperatures too few partial waves contributes to use a semi classical approximation, but for higher energies this value can give an indication of the long range part of the potential. If the value of ρ is close to 0.72 this signals that the long range part of the potential dominates.

As the results show, the sign of ρ varies with the projectile speed v_p and the temperature of the target gas. It is stated in [53] that the sign of ρ separates between an attractive (positive sign) and a repulsive (negative sign) potential interaction. The imaginary part of the refractive index is never negative. This is seen by considering the partial wave amplitudes given in equation (6.19). If the imaginary part is negative this should correspond to a negative cross section, which corresponds to amplification instead of attenuation according to Beer's law equation (5.6). Therefore, the sign of ρ is determined by the sign of the phase shift $\Delta\phi$. (The sign of ρ is opposite to $\Delta\phi$, see equation (9.9)). In the low energy limit where $k_r \to 0$, the s-wave phase shift δ_0 dominates. If this changes sign, the real part of the scattering amplitude also changes sign, because

$$f(k_r) \propto \sin 2\delta_0. \tag{9.20}$$

Consequently, $\mathrm{Re}(n-1)$ changes sign. However, the other way around is not so simple. If $\mathrm{Re}(n-1)$ changes sign it does not necessarily mean that the phase shift δ_0 changes sign. The sign of the sine may change even if the argument does not. Therefore it is difficult to draw conclusions based on the sign of the ratio ρ.

Chapter 10

Results

The index of refraction is calculated for lithium atoms through a helium gas, lithium atoms through an argon gas and diatomic sodium molecules through a helium gas. The results are expressed in terms of the ratio $\rho(v_p)$ as a function of the projectile velocity v_p. The sensitivity of the index of refraction upon changes in the different potentials is investigated.

10.1 The Li-He system

The refractive index for lithium matter waves through a helium gas is calculated. Helium is chosen as target gas, since it can be cooled to very low temperatures.

Interatomic potential curves for Li-He

The lithium-helium (Li-He) system is weakly interacting. Therefore the potential curve describing the interaction is shallow and may not hold any bound states. The index of refraction for the Li-He system has been calculated with three different potential curves.

Cvetko *et al.* [16] have obtained a potential curve for Li-He. This potential is determined from density functional calculations of the free atom electron densities. The curve depends on the van der Waals coefficients C_6, C_8 and C_{10}, that was introduced in equation (7.6). The potential is written on an analytical form and is therefore convenient to implement (into a computer program). Cvetko *et al.* report that their potential curve agrees with experimental data [16]. This potential curve is referred to as the 1(LiHe) potential.

A modified potential curve is obtained from the analytical form given by Cvetko *et al.* [16]. Different van der Waals coefficients C_6, C_8 and C_{10} are used. These are obtained from an ab initio calculation in [6]. This potential curve is referred to as the 2(LiHe) potential.

The final potential curve is obtained with the quantum chemistry package GAMESS [48]. This curve was discussed in more detail in section 7.1, and is referred to as the 3(LiHe) potential.

All three potentials curves are shown in figure 10.1.

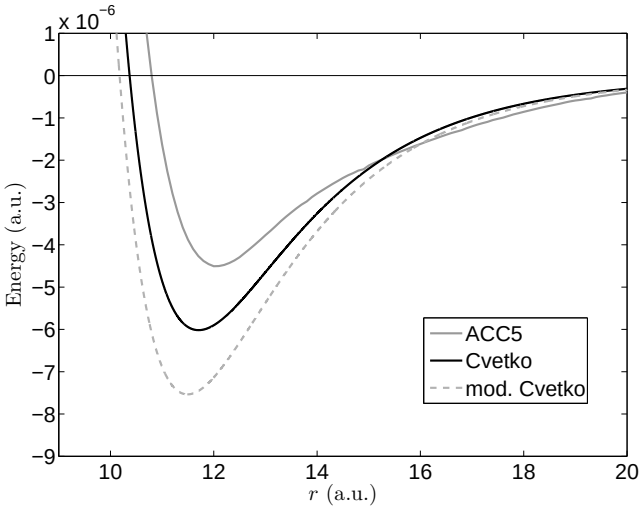

Figure 10.1: Interatomic potential curves for the Li-He system. The black curve is the Cvetko potential curve 1(LiHe). This is believed to be the most accurate. The dashed grey curve is a modified Cvetko curve 2(LiHe) with different van der Waals coefficients. The uppermost grey curve is the ACC5-potential 3(LiHe) obtained with GAMESS.

Results Li-He

The ratio $\rho(v_p)$ as a function of the projectile velocity v_p is calculated for the 1(LiHe) potential, which is believed to be the most accurate. Various temperatures of the target gas are used and the results are presented in figure 10.2.

The function $\rho(v_p)$ behaves smoothly with perhaps one resonance or a glory oscillation, as the temperature of the target gas approaches ultracold. A calculation has been performed with the 1(LiHe) potential curve, see chapter 8. This calculation found no bound states for this potential curve. Based on this, the observed oscillation of $\rho(v_p)$ is a resonance and probably not a glory oscillation.

In [53] it is stated that for light gases with a weak interaction, the ratio ρ is very sensitive to changes in the potential curve. The Li-He system is both weakly interacting and light (low mass). The function $\rho(v_p)$ has been calculated for the two other potential curves 2(LiHe) and 3(LiHe). Three different temperatures for the target gas are used. The results are given in figure 10.3 together with the results from the 1(LiHe) potential curve.

As shown in figure 10.3, the ratio ρ is sensitive to changes in the potential curve for low temperatures and low projectile velocities. Grey areas displays the uncertainty due to the different potential curves. The 1(LiHe) potential (black curve) which is believed to be the most accurate, resides in the grey areas bounded by the 2(LiHe) and the 3(LiHe) potentials. The 3(LiHe) potential represents the upper bound, while the 2(LiHe) potential represents the lower bound. Actually, the grey areas probably overestimates the error as the 2(LiHe) potential may be too deep and the 3(LiHe) potential too shallow. In any case, the grey areas give reasonable bounds for the ratio $\rho(v_p)$ due to inaccuracies in the potential curves.

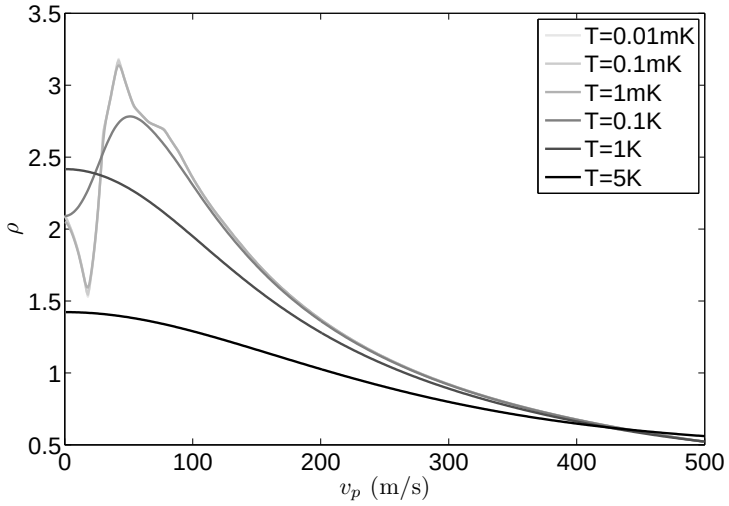

Figure 10.2: The ratio $\rho(v_p)$ as a function of the projectile velocity for the 1(LiHe) potential. Various temperatures T on the target gas, are plotted with different shades of grey (see the box). For low temperatures the function $\rho(v_p)$ exhibit an oscillation.

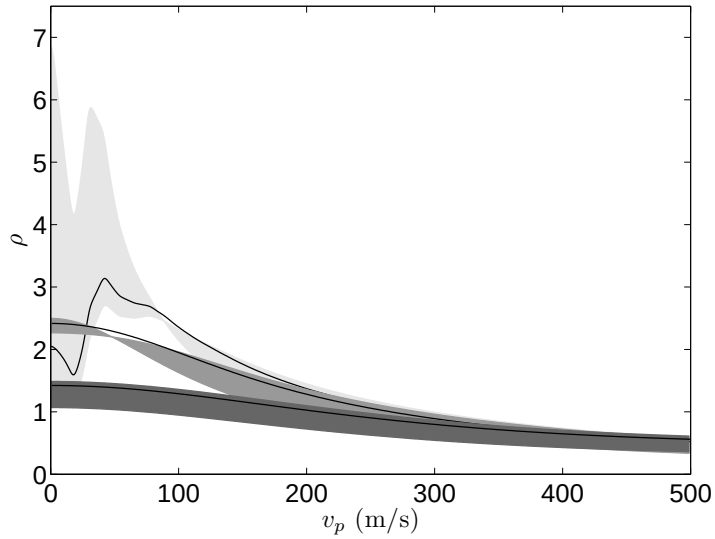

Figure 10.3: The ratio $\rho(v_p)$ for three different temperatures. From the top 1mK, in the middle 1K and the lowest is 5K. The black continuous curves are calculated with the 1(LiHe) potential that is believed to be the most accurate. The boundaries of the shaded areas are the ratios for the 2(LiHe) (lower) and 3(LiHe) (upper) potentials.

Due to the large area of uncertainty it is difficult to conclude whether the behaviour of ρ is due to a resonance or reveals a bound state for the Li-He system. The oscillating behaviour only happens at $T = 1$mK. For the higher temperatures no such oscillation occur. In the cold regime experimental data may provide valuable information regarding accuracy of the interatomic potentials.

Figure 10.3 shows that ρ is positive for all the temperatures and projectile velocities. This is consistent with an attractive potential. However, the function ρ is far from the value $\rho = 0.72$ obtained from a long range potential of the form $-r^{-6}$ (section 9.4). This suggests that the interaction is mostly dependent on the short range part of the potential.

10.2 The Li-Ar system

The refractive index for lithium matter waves through an argon gas is calculated. The calculations for the lithium-argon (Li-Ar) system are motivated by a recent experiment by Jacquey *et al.* [30].

Interatomic potential curves for Li-Ar

The Li-Ar system is heavier and has a deeper potential curve than the Li-He system. The ratio ρ has been calculated with two different potential curves.

Brühl *et al.* [10] have obtained a potential curve for the Li-Ar system. This curved is obtained empirically from high-resolution laser spectroscopy and is written as an analytical function. This potential curve is referred to as the 1(LiAr) potential.

Again a curve obtained by Cvetko *et al.* [16] is used for the Li-Ar system. As for the LiHe-potential, this curve is obtained from density functional calculations of the free atom electron densities. It is represented by an analytical function. This potential curve is referred to as the 2(LiAr) potential.

Both potential curves are shown in figure 10.4.

Results Li-Ar

The ratio $\rho(v_p)$ as a function of the projectile velocity v_p is calculated for the 1(LiAr) potential for different temperatures of the target gas. The results are shown in figure 10.5. The function ρ exhibit three glory oscillations. As the temperature increases the glory oscillations become less prominent, but are easily observed for the temperatures included in figure 10.5. These three glory oscillations indicates that the 1(LiAr) potential holds at least three bound states. Additional glory oscillations may also occur at higher projectile velocities. Resonances due to quasibound states are observed for temperatures $T < 1$K, and for projectile velocities below 500m/s.

The ratio ρ oscillates around the value 0.72 obtained from an attractive long range potential on the form $-r^{-6}$. This might suggest that the long range part of the potential is important.

A recent (2007) atom interferometer experiment [30] measured the ratio $\rho(v_p)$ for the Li-Ar system with a projectile velocity $v_p = 1075$m/s. Their experiment was carried out with a target gas at $T = 298$K. This is a higher

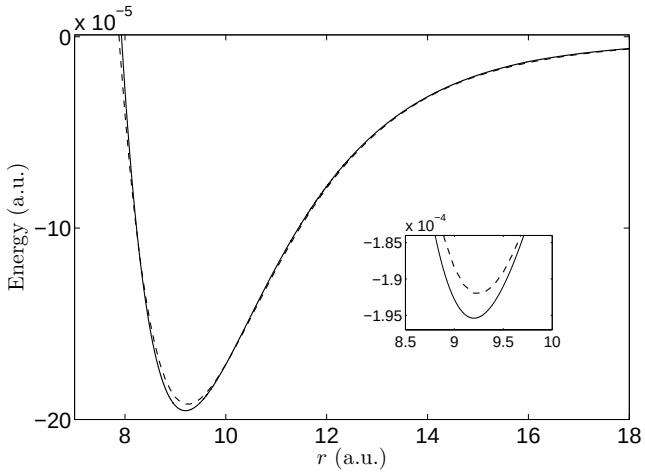

Figure 10.4: The two potential curves for the Li-Ar system. The solid line is the potential 1(LiAr), obtained by Brühl *et al.* [10] and the dashed line is the potential 2(LiAr), obtained by Cvetko *et al.* [16]. The insert shows the differences around the equilibrium bond length (minimum point).

temperature then for the present calculations, but the ratio ρ seems less dependent on the target gas temperature for projectile speeds $v_p > 500$ m/s. The measured value of ρ is included in figure 10.5. The theoretical values of ρ is in agreement with the measured value.

The ratio ρ is also calculated for the 2(LiAr) potential curve. A calculation found three or four bound states for this potential curve, see chapter 8. This is consistent with the behaviour of ρ which exhibit three glory oscillations, as shown in figure 10.6.

Comparison between the 1(LiAr) and the 2(LiAr) are displayed in figure 10.6. The grey area is meant to illustrate how sensitive ρ is to changes in the interatomic potential curve. As shown in figure 10.6 the discrepancies are small. The number of glory oscillations is the same for both potential curves. Only at low projectile velocities and low temperatures, resonances are sensitive to changes in the potential curve. It is expected that experiments and theory should be in agreement for the Li-Ar system.

The sign of ρ becomes negative around $v_p \sim 50$m/s for $T \leq 1$K. If ρ is negative the phase shift for the matter wave is positive. It is difficult to conclude regarding the potential interaction based upon this change of sign.

Effective cross section for Li-Ar

Jacquey *et al.* [30] have measured the ratio ρ for lithium matter waves through a gas of argon at $T = 298$K. They report that measurements at low temperatures should provide more information regarding accuracy of the different potential curves. However, there is some difficulties in the low energy regime: Cooling of gases can be complicated. In addition, low projectile velocities and low temperatures, gives a large attenuation. This makes it difficult to obtain interference fringes with a good visibility, because the detected signal becomes weak. There-

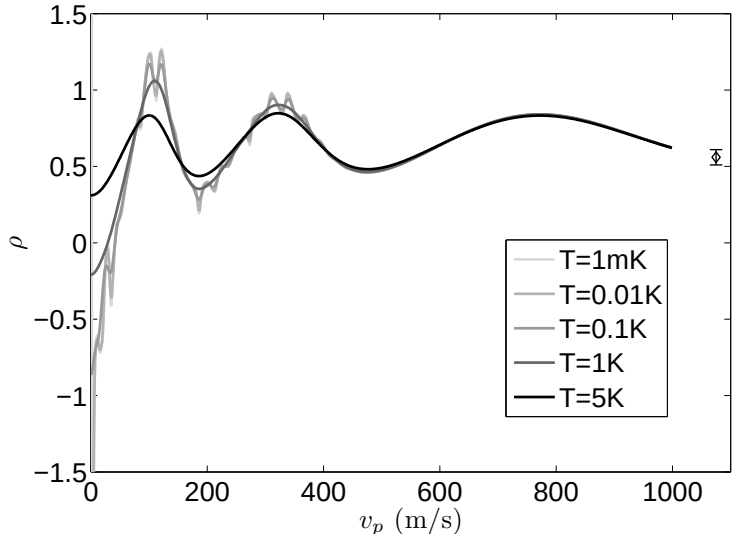

Figure 10.5: The ratio $\rho(v_p)$ as a function of the projectile velocity v_p is calculated with the 1(LiAr) potential curve. Various temperatures T on the target gas, are plotted with different shades of grey (see the box). The experimental value of ρ is taken from [30] and agrees with the theory.

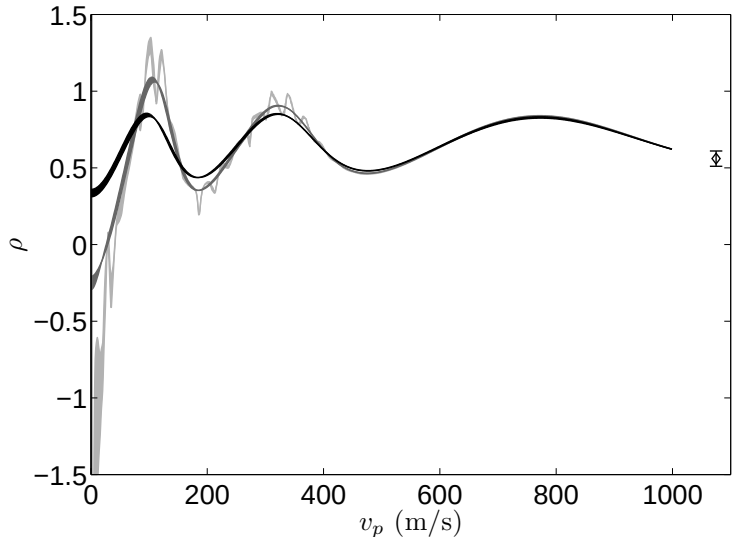

Figure 10.6: The ratio ρ for both potential curves. The shaded areas represents differences in ρ due to differences in the potential curve. The experimental value of ρ is taken from [30]. The black curve corresponds to a target gas temperature of 5K, the dark grey 1K and the light grey 1mK.

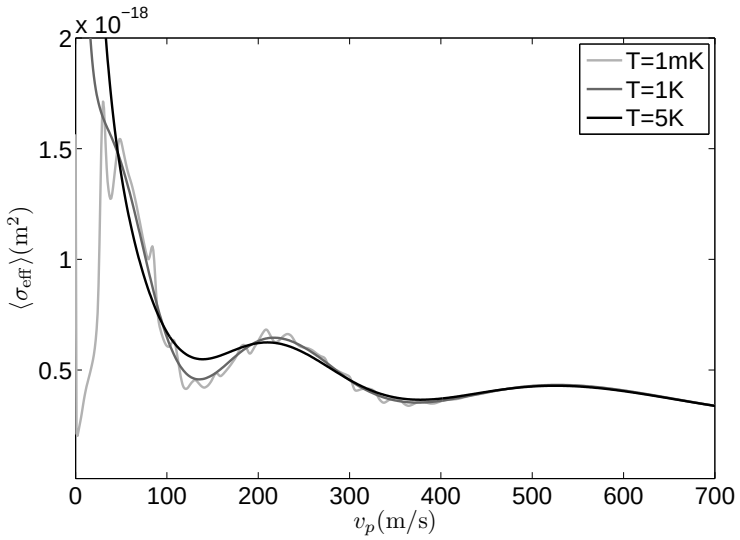

Figure 10.7: The effective cross section for the Li-Ar system as a function of the projectile velocity v_p. Calculations are performed with three different temperatures for the target gas. Note that for a target gas temperature $T = 1\text{mK}$ and low projectile velocities, the effective cross section is small.

fore, an intense source of matter waves is required. The most intense signals are produced by sources using thermal atom beams, while sources producing cold atoms usually are less intense, see section 3.2.

The attenuation of the intensity I/I_0 is given by Beer's law equation (5.6):

$$\frac{I}{I_0} = e^{-\rho_t \langle \sigma_{\text{eff}} \rangle L}, \tag{10.1}$$

where ρ_t is the density of the target gas, L is the length of the gas region and $\langle \sigma_{\text{eff}} \rangle$ is the effective cross section. To obtain a good visibility on the detected interference fringes, the cross section should be as small as possible.

The effective cross section is obtained from the forward scattering amplitude, and is given by equation (9.5):

$$\langle \sigma_{\text{eff}}(v_p) \rangle = \frac{4\pi}{\mu} \frac{\langle \text{Im}[f(k_r)] \rangle}{v_p}, \tag{10.2}$$

where μ is the reduced mass for the colliding system. This has been calculated for the Li-Ar system. The results are given in figure 10.7. For low temperatures and low projectile velocities, the general trend is that the cross section becomes large. However, for $T = 1\text{mK}$ and projectile velocities $v_p < 50\text{m/s}$ the corresponding cross section is small. This result motivates the possibility for an interferometric measurement at low energies.

10.3 The Na_2-He system

An interferometer using Na_2-molecules as projectiles has been demonstrated by Chapman *et al.* [13]. They measured the ratio ρ for Na_2-molecules through a gas of neon atoms. The system considered here is Na_2-molecules through a gas of helium atoms. Again, helium is chosen as target gas since it can be cooled to low temperatures.

Potential energy surface for Na_2-He

The potential energy surface (PES) describing the interaction between the Na_2-molecule and the helium atom is discussed in section 7.2.

Results Na_2-He

The diatomic sodium molecule is in the molecular ground state and does not have any orbital or electronic angular momentum. However, the Na_2-molecule is treated as a rigid rotator with a mechanical rotation. This rotation is quantized and the rotational quantum number is denoted j, see equation (6.61). The first three rotational levels are considered $j = 0, 1, 2$.

The ratio ρ as a function of the projectile velocity v_p is calculated for the different rotational quantum numbers $j = 0, 1, 2$. The results are presented in figure 10.8. Note that the different y-axes are not equally scaled in this figure. From figure 10.8 it is observed that ρ depends quite heavily on the rotational quantum number j. As the value of j increases, the ratio $\rho = \mathrm{Re}(n-1)/\mathrm{Im}(n-1)$ decreases. The function ρ obtained from different temperatures, only differ significantly at low projectile velocities.

All the calculated ratios of ρ have one maximum for $v_p \in [0, 1000]$m/s. This behaviour indicates that the PES supports at least one bound state for $l = 0$ (s-wave). For $j = 0$ the function ρ exhibit some resonances at low velocities. When the molecule has rotational energy corresponding to $j = 1$ and $j = 2$, more resonances occur. If the temperature of the helium gas is low, resonances for $j = 1, 2$, are observed for velocities all the way up to 1000m/s. These resonance structures are due to the effective potential. Consider the total angular momentum $\mathbf{J}$ for the composite system, given by

$$\mathbf{J} = \mathbf{L} + \mathbf{j}, \tag{10.3}$$

where $\mathbf{j}$ is the rotational angular momentum and $\mathbf{L}$ is the relative orbital angular momentum. The associated quantum numbers are J, l and j, and the effective potential depends on these. For $j = 1, 2$ the effective potential holds more quasibound states and this explains the resonance structures.

At higher projectile velocities the value of ρ is in the range $0.80 - 1.00$ for $j = 0, 1$. This is rather close to the value 0.72 for an attractive potential of the form $-1/r^6$. This indicates that the long range part of the PES is important.

Chapman *et al.* [13] have measured the ratio ρ for Na_2-molecules through a gas of neon atoms, and found that $\rho = 1.43$. In their experiment the projectile speed was 1000m/s and the gas was kept at room temperature. Their value for ρ is larger than the one obtained from the present calculation with the Na_2-He system. However, in [54] it seems that using neon as a target gas gives a higher value for ρ. This is seen by comparing Na-He and Na-Ne in [54].

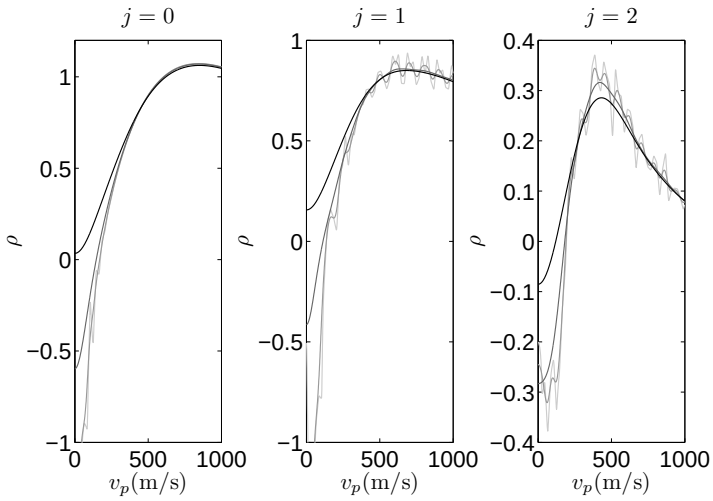

Figure 10.8: The ratio ρ for the Na_2-He system, at four different temperatures and three different rotational levels $j = 0, 1, 2$. Note the different scales for the y-axes. Different shades of grey indicate the different temperatures used: 4K,1K,0.1K and 1mK. The black curves corresponds to $T = 4$K, and the lighter shaded grey curves are colder. The different panels correspond to different rotational levels for the Na_2 molecule.

It is interesting to observe the sensitivity of ρ with respect to changes in the PES. The functional form is kept, but the the refractive index is calculated with the PES 20% deeper, and 20% more shallow. This gives a quantitative estimate of the uncertainties in the obtained results due to inaccuracies in the calculated PES. The calculated ratios for the adjusted PESs are expected to yield reasonable bounds for measurements. The results are shown in figure 10.9.

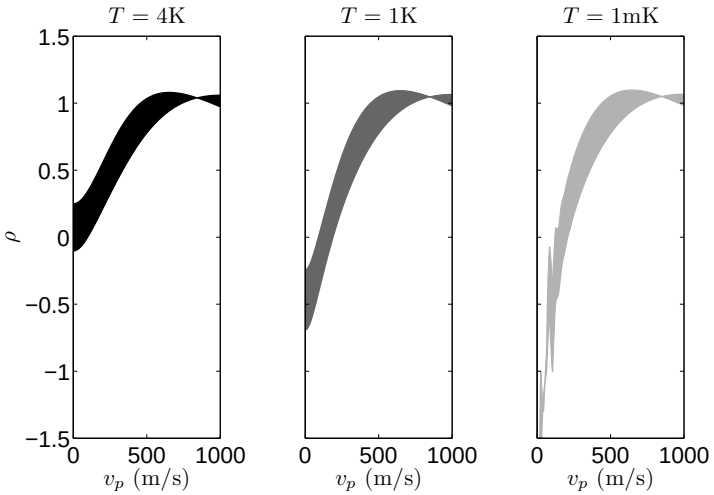

Figure 10.9: Estimate of the uncertainties in the calculated ratios ρ for three different temperatures. The shaded areas are bounded by the curves ρ obtained with potential energy surfaces that deviate within $\pm 20\%$ from the calculated PES. The PES is discussed in section 7.2.

Chapter 11

Concluding remarks

The index of refraction of gases for matter waves is a macroscopic concept based on atomic collisions. This quantity has been calculated for matter waves traveling through various cold noble gases. As the results show, it is for low energies that the characteristics of the refractive index is most evident. These are very sensitive to changes in the interparticle potentials describing the interactions between the involved particles.

Measurements of the index of refraction for matter waves, are only accessible through an atom interferometry experiment. Experimental data is only available where the target gas is at room temperature. It has been stated by several authors [7, 30], that in this region, many features of the refractive index are washed out due to thermal averaging. Therefore, a measurement in the cold regime could provide new access to information regarding the accuracy of different potentials.

The refractive index for the lithium-helium system depends quite heavily on the different potentials. Experimental data combined with theoretical values may be able to favour certain potentials for this system.

For the lithium-argon system it is expected that theory and measurements should be in agreement. The uncertainties in the potential curves are small. In addition, an experimental value from [30], agrees with the theoretical values. Scattering resonances are observed at low temperatures. These are very sensitive to changes in the potentials. Experimental observation of a resonance structure could therefore provide a stringent test of the theoretical model used to calculate the index of refraction.

The refractive index for diatomic sodium molecules through a helium gas has also been calculated. This calculation is based upon a rigid rotator approximation for the molecule. The results show that the refractive index depends significantly on the rotational state of the molecule. Therefore, experimental data may provide a conclusion regarding the validity of the rigid rotator approximation.

To obtain a detectable signal in an interferometry experiment, enough atoms must reach the detector. If the attenuation is large, this requires an intense source. For cold atoms the sources are usually less intense. The cross section for the lithium-argon system shows that selected temperatures and projectile velocities give a small attenuation. This motivates the possibility for an atom interferometric experiment in the low energy regime.

Appendix A

Program for calculating bound states

```
#include <cmath>
#include <iostream>
#include <fstream>
#include <iomanip>
#include "lib.cpp"//Householders algorithm, tqli
using namespace std;

double potential(double h, int i);
void initialise(int *n_steps, double *rho_max);
void householder(int n_steps, double **A, double rho_max);

int main(){
  int n_steps;
  double rho_max;
  initialise(&n_steps, &rho_max);

  //Konstrurere matrise
  double  **A;

  //HOUSEHOLDER
  householder(n_steps, A, rho_max);
}

double potential(double h, int i){
//  //SQUARE-WELL
//    double v_i;
//    double a=15;
//    double L=8;
//    //v_i = -(h*i)*(h*i);//(hi)^2 harmonic oscillator
//    if(h*i<=L)
//      v_i=1e10;
//    else if(h*i>L && h*i<=a)
//      v_i=-.8;
//    else if(h*i>a)
//      v_i=0;
```

```
  double r=h*i;
  double v_i;

  //CVetko Li-Ar
  double mu=9530.314175;
  double a=1620;
  double b=1.04;
  double r_stop=16.6/b;
  double C6=175;
  double Q = 7.40;
  double Qb= 7.70;
  double chi = (14.6+0.918*pow(Qb,2))/(1-pow(Qb/16.6,2));
  if(r<=r_stop){
    v_i = (C6/120)*pow((b/3.0),6)*(a*exp(-b*r) -chi*exp
        (-(2.0/3.0)*b*r)-exp((-1.0/3.0)*b*r));
    v_i=2*mu*v_i;
    //cout<<r<<" "<<v_i<<endl;
  }
  else if(r>r_stop){
    v_i = (C6/120)*pow((b/3.0),6)*a*exp(-b*r)-C6/(pow(r,6)-Q*Q
        *pow(r,4));
    v_i=2*mu*v_i;
    //cout<<r<<" "<<v_i<<endl;
  }

  // //CVetko Li-He
//    double mu=3661.81995;
//    //double C6 = 22.5;
//    double C8 = 1059;
//    double C10= 80900;
//    //double Q =  pow((C8*C10/C6/C6),(1.0/6.0));
//    double b = 1.06;
//    double a = 4700;
//    //double Qb = Q*b;
//    //double chi = (14.6+0.918*Qb*Qb)/(1-(Qb/16.6)*(Qb/16.6))
    ;

//    double C6 = 21.1;
//    double Q = 7.0;
//    double Qb = 7.42;
//    double chi = (14.6+0.918*Qb*Qb)/(1-(Qb/16.6)*(Qb/16.6));

//    double r_stop=16.6/b;
//    if(r<=r_stop){
//      v_i = (C6/120)*pow((b/3.0),6)*(a*exp(-b*r) -chi*exp
    (-(2.0/3.0)*b*r)-exp((-1.0/3.0)*b*r));
//      v_i=2*mu*v_i;
//      //cout<<r<<" "<<v_i<<endl;
//    }
//    else if(r>r_stop){
//      v_i = (C6/120)*pow((b/3.0),6)*a*exp(-b*r)-C6/(pow(r,6)-
    Q*Q*pow(r,4));
//      v_i=2*mu*v_i;
```

```
//      //cout<<r<<" "<<v_i<<endl;
//    }

  return v_i;
}


void initialise(int *n_steps, double *rho_max){
  cout << "Number of steps n_steps= ";
  cin >> *n_steps;
  cout << "rho_max = ";
  cin >> *rho_max;
  return;
}

void householder(int n_steps, double **A, double rho_max){
  double *diag, *off_diag;
  diag = new double[n_steps];
  off_diag = new double[n_steps];
  double h = rho_max/(n_steps);

  for(int i=0; i < n_steps; i++){
    diag[i] = (2.0)/(h*h) + potential(h,i+1);//diagonal
        elements
    off_diag[i] = (-1.0)/(h*h);//off diagonal = -1/h^2
  }
  off_diag[0] = 0;

  tqli(diag, off_diag, n_steps, A);
  sort(diag,diag + n_steps);

  double mu=9530.314175;
  //double mu=3661.81995;
  //double mu =.5;
  for(int i=0; i<10; i++){
    cout <<diag[i]/(2*mu)<<endl;
  }
}
```

Bibliography

[1] P. Atkins and R. Friedman, *Molecular Quantum Mechanics*, Dover Publications, fourth ed., 2007.

[2] K. G. H. Baldwin, Contemporary Physics, 46 (2005), pp. 105–120.

[3] M. L. Bellac, *Quantum Physics*, Cambridge University Press, first ed., 2006.

[4] R. B. Bernstein, J. Chem. Phys., 37 (1962), p. 1880.

[5] ——, J. Chem. Phys., 38 (1963), p. 2599.

[6] H. Bjørgen, M. Lysebo, and L. Veseth, *Index of refraction for lithium- and diatomic sodium matter waves traveling through cold noble gases*, To be published, (2010).

[7] S. Blanchard, D. Civello, and R. C. Forrey, Phys. Rev. A, 67 (2003), p. 013604.

[8] B. H. Bransden and C. J. Joachain, *Physics of Atoms and Molecules*, Prentice Hall, second ed., 2003.

[9] B. Brezger, L. Hackermüller, S. Uttenhaler, J. Petschinka, M. Arndt, and A. Zeilinger, Phys. rev. Lett., 88 (2002), p. 100404.

[10] R. Brühl and D. Zimmermann, J. Chem. Phys., 115 (2001), p. 7892.

[11] M. Cadoret, E. D. Mirandes, P. Clade, F. Nez, and L. Julien, Eur. Phys. J. Special Topics, 172 (2009), pp. 121–136.

[12] C. Champenois, M. Jacquey, S. Lepoutre, M. Buchner, G. Trenec, and J. Vigue, Phys. Rev. A, 77 (2008), p. 013621.

[13] M. S. Chapman, C. R. Ekstrom, T. D. Hammond, R. A. Rubenstein, J. Schmiedmayer, S. Wehinger, and D. E. Pritchard, Phys. Rev. Lett., 74 (1995), pp. 4783–4786.

[14] M. S. Child, *Molecular Collision Theory*, Academic Press London and New York, 1974.

[15] A. D. Cronin, J. Schmiedmayer, and D. E. Pritchard, arXiv:0712.3703v1, (2008).

[16] D. Cvetko, A. Lausi, A. Morgante, F. Tommasini, P. Cortona, and M. G. Dondi, J. Chem. Phys., 100 (1994), p. 2052.

[17] S. Dürr and G. Rempe, Advances in Atomic, Molecular and Optical Physics, 42 (2000).

[18] C. R. Ekstrom, J. Schmiedmayer, M. S. Chapman, T. D. Hammond, and D. E. Pritchard, Phys. Rev. A, 51 (1995), p. 3883.

[19] M. Fattori, G. Lamporesi, T. Petelski, J. Stuhler, and G. M. Tino, Phys. Lett. A, 318 (2003), pp. 184–191.

[20] C. J. Foot, *Atomic physics*, Oxford University Press, first ed., 2005.

[21] M. Fox, *Quantum Optics An Introduction*, Oxford University Press, first ed., 2006.

[22] R. H. Garstang, The Astrophysical Journal, 447 (1995), pp. 962–965.

[23] R. M. Godun, M. B. D'Arcy, G. S. Summy, and K. Burnett, Contemporary Physics, 42 (2001), pp. 77–95.

[24] D. J. Griffiths, *Introduction To Quantum Mechanics*, Pearson Education International, second ed., 2005.

[25] ——, *Introduction To Electrodynamics*, Pearson Benjamin Cummings, third ed., 2008.

[26] T. L. Gustavson, A. Landragin, and M. A. Kasevich, Class. Quantum Grav, 17 (2000), pp. 2385–2398.

[27] P. C. Hemmer, *Kvantemekanikk*, Tapir akademisk forlag, fifth ed., 2005.

[28] W. F. Holmgren, M. C. Revelle, V. P. A. Lonij, and A. D. Cronin, arXiv:1001.3888v1, (2010).

[29] S. Huzinaga, J. Andzelm, M. Klobukowski, E. Radzio-Andzelm, Y. Sakai, and H. Tatewaki, *Gaussian basis sets for molecular calculations*, Elsevier, (1984).

[30] M. Jacquey, M. Büchner, G. Trenec, and J. Vigue, Phys. Rev. Lett., 98 (2007), p. 240405.

[31] B. R. Johnson, Journal of Comp. Phys, 13 (1973), pp. 445–449.

[32] K. Johnson, J. H. Thywissen, N. H. Dekker, K. K. Berggren, A. P. Chu, R. Younkin, and M. Prentiss, Science, 280 (1998), pp. 1583–1586.

[33] W. Just, C. S. Schneider, R. Ciszewski, and C. G. Schull, Phys. Rev. B, 7 (1973), pp. 4142–4145.

[34] M. Kasevich and S. Chu, Phys. Rev. Lett., 67 (1991), pp. 181–184.

[35] ——, Appl. Phys. B, 54 (1992), pp. 321–332.

[36] D. W. Keith, C. R. Ekstrom, Q. A. Turchette, and D. E. Pritchard, Phys. Rev. Lett., 66 (1991), p. 2693.

[37] I. Kerkines and A. Mavridis, Journal of Chemical Physics, 116 (2002), p. 9305.

[38] J. M. Leinaas, *Non-Relativistic Quantum Mechanics*, 2008.

[39] A. Miffre, M. Jacquey, M. Büchner, G. Trénec, and J. Vigué, arXiv:quant-ph/0507279v2, (2008).

[40] R. W. Molof, H. L. Schwartz, T. M. Miller, and B. Bederson, Phys. Rev. A, 10 (1974), pp. 1131–1140.

[41] T. Müller, T. Wendrich, M. Gilowski, C. Jentsch, E. M. Rasel, and W. Ertmer, Phys. rev. A, 76 (2007), p. 063611.

[42] O. Nairz, M. Arndt, and A. Zeilinger, Am. J. Phys., 71 (2003), pp. 319–325.

[43] O. Nairz, B. Brezger, M.Arndt, and A. Zeilinger, Phys. Rev. Lett, 87 (2001), p. 160401.

[44] A. Peters, K. Y. Chung, and S. Chu, Metrologia, 38 (2001), pp. 25–61.

[45] W. H. Press, S. A. Teuklosky, W. T. Vetterling, and B. P. Flannery, *Numerical Recipes*, Cambridge University Press, third ed., 2007.

[46] T. D. Roberts, A. D. Cronin, D. A. Kokorowski, and D. E. Pritchard, Phys. Rev. Lett, 89 (2002), p. 200406.

[47] J. J. Sakurai, *Modern Quantum Mechanics*, Addison-Wesley, revised ed., 1994.

[48] M. W. Schmidt, K. K. Baldridge, J. A. Boatz, S. T. Elbert, M. S. Gordon, J. H. Jensen, S. Koseki, N. Matsunaga, K. A. Nguyen, S. J. Su, T. L. Windus, M. Dupuis, and J. A. Montgomery, J. Comput. Chem., 14 (1993), pp. 1347–1363.

[49] J. Schmiedmayer, J. M. Chapman, C. R. Ekstrom, T. D. Hammond, D. Kokorowski, A. Lenef, R. R. Rubenstein, E. Smith, and D. E. Pritchard, *Atom Interferometry*, Academic Press, San Diego, 1997, p. 20.

[50] ——, *Atom Interferometry*, Academic Press, San Diego, 1997, p. 52.

[51] ——, *Atom Interferometry*, Academic Press, San Diego, 1997, p. 45.

[52] ——, *Atom Interferometry*, Academic Press, San Diego, 1997, p. 43.

[53] ——, *Atom Interferometry*, Academic Press, San Diego, 1997, p. 49.

[54] ——, *Atom Interferometry*, Academic Press, San Diego, 1997, p. 50.

[55] J. Schmiedmayer, M. S. Chapman, C. R. Ekstrom, T. D. Hammond, S. Wehinger, and D. E. Pritchard, Phys. Rev. Lett, 74 (1995), p. 1043.

[56] C. S. Schneider and C. G. Schull, Phys. Rev. B, 3 (1971), pp. 830–835.

[57] M. Sigel and J. Mlynek, Physics World, (1993), pp. 36–42.

[58] P. Storey and C. Cohen-Tannoudji, J. Phys. II France, 4 (1994), pp. 1999–2027.

[59] D. J. Tannor, *Introduction To Quantum Mechanics A Time Dependent Perspective*, University Science Books, first ed., 2007.

[60] D. E. Woon and T. Dunning, J. Chem. Phys., 100 (1994), p. 2975.

[61] ——, J. Chem. Phys., 103 (1995), p. 4572.

[62] D. E. Woon and K. Peterson, J. Chem. Phys., 117 (2002), p. 10548.